Karlsruhe Institute of Technology

Wave phenomena

Polychromatic T-Matrix: Group-Theoretical Derivation and Applications

Zur Erlangung des akademischen Grades eines
Doktors der Naturwissenschaften (Dr. rer. nat.)
von der KIT-Fakultät für Physik
des Karlsruher Instituts für Technologie (KIT)
angenommene DISSERTATION
von

M. Sc. Maxim Vavilin

Tag der mündlichen Prüfung:	09. Februar 2024
Referent:	Prof. Dr. Carsten Rockstuhl
Korreferent:	Prof. Dr. Gabriel Molina-Terriza
Betreuender Mitarbeiter:	Dr. Ivan Fernandez-Corbaton

Erklärung zur Selbstständigkeit

Ich versichere, dass ich diese Arbeit selbstständig verfasst habe und keine anderen als die angegebenen Quellen und Hilfsmittel benutzt habe, die wörtlich oder inhaltlich übernommenen Stellen als solche kenntlich gemacht und die Satzung des KIT zur Sicherung guter wissenschaftlicher Praxis in der gültigen Fassung vom 05. Oktober 2021 beachtet habe.

Karlsruhe, 08.01.2024

. . . . . .

(M. Sc. Maxim Vavilin)

Acknowledgments

First and foremost, I would like to thank my family for supporting me and being my constant source of strength. In particular, I am thankful to my mother, who recognized the value of good education and ensured I was provided with the best possible opportunities.

I want to warmly thank Prof. Carsten Rockstuhl for creating such a group of competent and genuinely kind individuals. I am grateful for the opportunity to be a part of this group, which has been a conducive environment for learning and growth.

A very special thanks goes to Dr. Ivan Fernandez-Corbaton, my scientific advisor. His flawless supervision and guidance have created an ideal atmosphere for conducting research. His introduction to group-theoretical methods has been a turning point in my academic journey, for which I am profoundly thankful. Additionally, his invaluable comments and insights have significantly enriched my dissertation.

I am deeply grateful for the financial support provided by the CRC SFB "Wave Phenomena" and the Deutsche Forschungsgemeinschaft (DFG, German Research Foundation) under Project-ID 258734477 – SFB 1173.

I warmly thank my love Nigar for being with me and helping with proofreading the text of my dissertation.

Abstract

This dissertation presents theoretical advancements in the study of linear light-matter interactions, emerging from the enhancement of the well-established T-matrix method through the application of group representation theory.

The main contributions are threefold. Firstly, the monochromatic T-matrix method is expanded into the polychromatic domain, enabling the description of linear interactions between pulses and objects, both at rest and moving with relativistic velocities. Numerical simulations demonstrate the theory's applicability, particularly in computing the transfer of energy and momentum between the pulse and a moving object.

The second contribution focuses on the description of the object's chirality. The challenge of differentiating between enantiomers is addressed with a novel quantity called chirality signature. This measure, for the first time, captures the infinite-dimensional nature of chirality, allowing for the continuous distinction between any pair of enantiomers. Additionally, its conformal invariance is established.

The third contribution introduces a novel method of describing linear light-matter interactions by representing a scatterer's action as a sum of symmetry transformations. The coefficient of this decomposition, named the scattering function, is defined on the symmetry group manifold and is bijectively connected to the T-matrix. It has been shown that the scattering function's values can reflect the positions of objects within a cluster. This insight opens up two promising avenues for advancement: the first involves the use of the scattering function in imaging and inverse object design, and the second suggests progress in understanding the Rayleigh hypothesis. Unlike the T-matrix, the scattering function is not constrained by the sphere circumscribing the object.

Contents

List of Figures

Nomenclature

$\boldsymbol{\mathcal{B}}(\boldsymbol{r}, t)$	Real-valued magnetic field
$\boldsymbol{\mathcal{E}}(\boldsymbol{r}, t)$	Real-valued electric field
$\boldsymbol{\nabla}$	Nabla operator
$\boldsymbol{A}(\boldsymbol{r}, t)$	Complex-valued vector potential
$\boldsymbol{B}(\boldsymbol{r}, t)$	Complex-valued magnetic field
$\boldsymbol{E}(\boldsymbol{r}, t)$	Complex-valued electric field
$\boldsymbol{F}_{\pm}(\boldsymbol{r}, t)$	Riemann-Silberstein fields
$\boldsymbol{k}$	Wave vector
$\langle f \vert$	Dirac bra
$\delta(x)$	Dirac delta
δ_{im}	Kroneker delta
ϵ_0	Vacuum permittivity
$\hat{\boldsymbol{e}}_\lambda(\hat{\boldsymbol{k}})$	Polarization vector
$\hbar$	Reduced Planck constant
$\mathfrak{I}$	Imaginary part
κ	Optical extinction coefficient
$\vert f \rangle$	Dirac ket
λ	Helicity
$\mathfrak{R}$	Real part
ξ	Rapidity
c	Speed of light in vacuum
$C^{j_3 m_3}_{j_1 m_1; j_2 m_2}$	Clebsch-Gordan coefficient
$D^{j}_{mn}(\alpha, \beta, \gamma)$	Wigner matrix of Euler angles in zyz-convention

$d^j_{mn}(\beta)$	Small Wigner matrix
j	Quantum number of total angular momentum
k	Wavenumber
$L_{\hat{\boldsymbol{n}}}(\xi)$	Lorentz boost in $\hat{\boldsymbol{n}}$-direction
m	Quantum number of angular momentum around z-axis
n	Refractive index
$x^\mu y_\mu$	Scalar product with respect to $(-+++)$ Minkowski metric
$\begin{pmatrix} j_1 & j_2 & j_3 \\ m_1 & m_2 & m_3 \end{pmatrix}$	Wigner 3j-symbol

1 Introduction

Interaction between electromagnetic radiation and matter represents an example of a physical phenomenon that surrounds us in nearly every aspect of our lives. Advancements that we experience daily, from fast telecommunications and efficient capturing of the solar power, to the progress in medical imaging, are possible because of our increasing understanding of this physical phenomenon.

One of the well-established methods to describe a large class of linear light-matter interactions is the T-matrix formalism, developed by Waterman [1]. It provides an accurate and efficient numerical method to describe electromagnetic scattering by means of a linear operator. Given an incident illumination, the T-matrix of an object or a cluster of objects produces the corresponding scattered field. Usually, the incident field is expanded in the regular multipolar fields, while the scattered field is decomposed into the irregular outgoing multipolar fields. The T-matrix maps between these two sets of coefficients but is independent of the specific incident field. This formalism has proven to be a powerful method that continues to inspire a wide range of applications [2, 3].

Despite its advantages, the T-matrix method has limitations, such as the questionable validity of the expansion of scattered fields inside the smallest encompassing sphere of an object [4, 5, 6, 7, 8, 9, 10]. This hinders the description of scattering by clusters of objects, whose circumscribing spheres intersect. Another limitation concerns the monochromatic character of formalism: it has been defined and systematically developed only for monochromatic fields, with equal frequency for both incident and scattered fields. The present dissertation addresses this particular limitation. The linearity of Maxwell's equations allows to represent the incident and the scattered fields in their most general polychromatic form as a superposition of monochromatic fields with different frequencies. Here, the first systematic development of the polychromatic T-matrix formalism is presented, which extends the range of its application to new classes of problems.

First, this is the direct description of objects interacting with electromagnetic pulses, which has significant practical applications in various fields such as pulsed optical tweezers [11], control of matter magnetization [12], and refractive index measurements [13]. The second class of problems includes linear light-matter interactions, where the frequency of the scattered field is not identical to the frequency of the incident field. For example, the interaction of a monochromatic light with a constantly moving object produces a polychromatic scattered field that includes frequencies not present in the incident illumination. The polychromatic T-matrix allows one to solve such a problem directly by applying the Lorentz boost transformation to the operator. Another example is Raman scattering, where the action of the internal vibrations of the object adds or subtracts energy from the incident field, thereby changing its frequency.

My work is guided by the ideas from group representation theory, a subject that studies symmetry transformations of physical systems [14]. One of its core ingredients, relevant for

the T-matrix, is the concept of irreducible representations of a group of transformations. Its meaning for the scattering that can be understood by decomposing the field into the irreducible parts. The T-matrix then can be seen as an operator connecting these simplest elements of the field. Peterson and Ström [15] used these ideas to show that the monochromatic T-matrix acts between irreducible representations of the symmetry group of the 3D Euclidean space. This group consists of spacial rotations and translations, the irreducible representations of whose allowed to conveniently formulate the transformation laws of the T-matrix under these transformations, as well as to compute T-matrices of composite objects.

However, the 3D Euclidean group does not provide the group-theoretical ground for the most general polychromatic electromagnetic fields. As it was shown by Wigner [16], physical fields describing elementary particles such as electrons and photons arise from the irreducible representations of the Poincaré group, which is the group of isometries of the 4D Minkowski spacetime. This group consists of the 3D Euclidean group together with time translations and Lorentz transformations, also called Lorentz boosts. The latter describe changes from the stationary reference frame to the one moving with constant velocity. They also change the frequency content of the field, as exemplified by the Doppler effect. In addition to providing simple formulations of transformation laws for the electromagnetic field, the group-theoretical perspective allows one to introduce the unique scalar product of two arbitrary fields [17], with the defining property that the value of such scalar product is invariant under all actions of the Poincaré group (and even under a larger group, the group of conformal transformations [17]). The scalar product allows one to represent electric fields as states in a Hilbert space and gives access to the convenient Dirac bra-ket notation. In this setting, one may benefit from the simple formulas for fundamental quantities [18, §9, Chap. 3], such as energy and momentum, contained in the field, as well as their conservation laws in scattering [19].

The decomposition of the regular electromagnetic field into irreducible parts with respect to the Poincaré group was first studied by Moses [20], and here his results are further generalized to the case of irregular fields, which are necessary for the description of outgoing and incoming electromagnetic fields. Motivated by the simple group-theoretical arguments, this dissertation introduces new definitions for the polychromatic multipolar fields, the defining property of which is the unitary behavior under all actions of the Poincaré group, including the Lorentz boosts. For the first time, the closed-form expression for the Lorentz boosts in multipolar basis is derived, which allows to relativistically describe scattering by moving objects, formulated within the new polychromatic T-matrix method [21]. This approach is applicable to general objects, given their T-matrix at rest, while previous developments were limited to the relativistic motion of spherical objects [22, 23]. Since the polychromatic domain encompasses electromagnetic fields of arbitrary time-dependence, the polychromatic T-matrix formalism presents a new theoretical method of describing time-dependent scattering, complementing existing approaches [24, 25].

The T-matrix contains the complete information of an object that can be accessed via light-matter interactions. This fact, combined with the framework of symmetry groups, provides a powerful language for studying complex attributes of matter, such as chirality. The concept of chirality describes the phenomenon that all objects in the world fall into two categories: objects that can be superimposed into their mirror images, and those that

can not. Entities from the latter category are called chiral and they exist in pairs, called enantiomers: an object and its mirror version.

Chirality is a fundamental concept influencing a broad range of phenomena, from the left-right asymmetry of the weak interaction in particle physics to the chiral magnetic fields of galaxies. In pharmacy, it is crucial to select a particular molecular enantiomer from a chemical reaction, and to discard its undesired counterpart, since they are typically simultaneously produced in the same reaction. Theoretical challenges in the field of chirality analysis are related to the quantification of chirality. If an object is chiral, can one assign a quantity that describes how chiral it is? Given two enantiomers, how can one label them and distinguish one from the other? The idea of chirality has been transferred to the context of light-matter interactions, and formulated with the help of the T-matrix formalism in [26]. The new property, called electromagnetic chirality (em-chirality), was introduced in relation to the difference between an object's interaction with fields of opposite polarization handedness. The scalar measure of em-chirality as a function of the T-matrix $\hat{\chi}(T)$ was introduced as well, which can take values between $[0, 1]$ with 0 standing for electromagnetically achiral objects and 1 for maximally em-chiral objects.

In this thesis, a further development of [26] is presented, which solves the question of labeling both enantiomers of a chiral object. It is well-known, that despite their widespread adoption, the terms 'left-handed' and 'right-handed' are not universally applicable to all chiral objects [27, 28]. The reason is that a sufficiently complex chiral object can undergo a continuous transformation into its mirror image while maintaining its chiral nature throughout the transformation process [29]. This phenomenon is known as the chiral connectedness property. It presents the main challenge for the differentiation of enantiomers: any one-dimensional label that is introduced to continuously label the handedness of an object will encounter a chiral object without a well-defined handedness. This phenomenon stems from the infinite-dimensional nature of chirality [27]. In this manuscript, the first quantitative description of chirality is introduced, which captures its infinite-dimensional nature entirely. The introduced quantity is called the chirality signature, and it solves the problem of differentiating between any pair of enantiomers.

Another advancement in understanding electromagnetic scattering from the group-theoretical point of view is presented in the last chapter of this dissertation. There, a novel description of linear electromagnetic scattering is introduced, formulated with the help of a complex-valued function, called the scattering function. This new function is defined on a manifold of symmetry transformations and contains the same information as the T-matrix, being bijectively connected to it. Its physical role manifests through the decomposition of the T-matrix into the actions of the corresponding symmetry group, such as rotations and translations. Remarkably, the profile of the scattering function reflects the geometry of the cluster, which highlights its potential value in inverse design and image reconstruction applications.

The dissertation is structured as follows. Chapter 2 introduces the relevant concepts of the group theory, Chapter 3 provides a detailed group-theoretical view on regular electromagnetic fields, and Chapter 4 generalizes it to irregular fields. In Chapter 5, the theory of polychromatic T- and S-matrices is presented. Chapter 6 discusses its applications to the transfer of physical quantities between electromagnetic fields and objects, both at rest and moving with constant speed. Chapter 7 is devoted to electromagnetic chirality

and to the solution of the problem of enantiomeric differentiation with the introduction of the chirality signature. Chapter 8 presents a new approach to scattering based on the decomposition of the T-matrix into actions of symmetry transformations.

2 Relevant aspects of group representation theory

One of the fundamental elements of this thesis is the theory of group representations. While this manuscript is written to be accessible for people without prior knowledge of this theory, readers who seek a deeper understanding are referred to the book by Wu-Ki Tung [14]. It provides a pedagogical introduction with a focus on applications in physics.

2.1 Projection into irreducible components

The primary aim of this section is to familiarize the reader with the idea of decomposing a function into irreducible parts with respect to the actions of a given transformation group. This method is best illustrated with the help of some elementary examples.

Consider an arbitrary function $f : \mathbb{R} \to \mathbb{R}$. A well-known procedure is to decompose such function into even and odd parts:

$$f = f_+ + f_- \tag{2.1}$$

with

$$f_+(x) = \frac{f(x) + f(-x)}{2} \tag{2.2}$$

$$f_-(x) = \frac{f(x) - f(-x)}{2}, \tag{2.3}$$

such that the new parts change under the parity transformation I_p in an elementary manner

$$I_p f_+ = f_+ \tag{2.4}$$

$$I_p f_- = -f_-. \tag{2.5}$$

In terms of the identity operator $\mathbb{1}$ and the parity operator, the decomposition may be also written as

$$f_+ = \left(\frac{1}{2}\mathbb{1} + \frac{1}{2}I_p\right)f = \Pi_+ f \tag{2.6}$$

$$f_- = \left(\frac{1}{2}\mathbb{1} - \frac{1}{2}I_p\right)f = \Pi_- f. \tag{2.7}$$

In the context of group representation theory, this decomposition is called projection into irreducible components for the group of transformations $\{\, \mathbb{1}, I_p \,\}$. Note that expressions in

the brackets do not depend on f or on the space where f is defined. They would be the same if the same parity decomposition would be conducted, say, for a three-dimensional vector field.

The generalization of this procedure to the case of more complex transformations than parity is one of the important tasks of the group representation theory. The core ingredient here is the abstract group of transformations (defined solely by group multiplication law), while the spaces where it may be represented may be different. It means that one may use well-studied groups, in particular their projectors Π, and apply them to the distinct systems. One of the beneficial results of such application is the access to the elementary building blocks that have the simplest possible transformation laws under given transformations.

Two following examples illustrate how the representation theory of the same group may lead to a variety of results, depending on the spaces where its action is considered.

For the group of rotations $SO(2)$ parametrized by a single rotation angle α, the projectors are known to be

$$\Pi_m = \frac{1}{2\pi}\int_0^{2\pi} d\alpha\, e^{im\alpha} R(\alpha), \tag{2.8}$$

with integer m and $R(\alpha)$ being rotation by α in a given representation space. The form of the projector is general, while the action of $R(\alpha)$ depends on the representation space (or, equivalently, on physical context) and has to be defined or postulated additionally.

First, consider a representation space that consists of functions f defined on a circle, with rotations acting as

$$R(\alpha) f(\phi) \coloneqq f(\phi - \alpha). \tag{2.9}$$

The application of a projector gives

$$\begin{aligned}
\Pi_m f(\phi) &= \frac{1}{2\pi}\int_0^{2\pi} d\alpha\, e^{im\alpha} R(\alpha) f(\phi) \\
&= \frac{1}{2\pi}\int_0^{2\pi} d\alpha\, e^{im\alpha} f(\phi - \alpha) \\
&= -\frac{1}{2\pi}\int_{\phi}^{\phi-2\pi} d\alpha\, e^{im(\phi-\alpha)} f(\alpha) \\
&= e^{im\phi}\frac{1}{2\pi}\int_0^{2\pi} d\alpha\, e^{-im\alpha} f(\alpha) \\
&=: e^{im\phi} a_m,
\end{aligned} \tag{2.10}$$

where the substitution $\phi - \alpha \mapsto \alpha$ and the periodicity of the circle were used. The resulting projection consists of two parts: one is the function $e^{im\phi}$ that transforms in a 'simplest' manner under Eq. (2.9) — the rotation for it is just multiplication by a complex number, — and the other is the decomposition coefficient. The sum of all projected parts gives the initial function, as in Eq. (2.1), producing the well-known Fourier series:

$$f(\phi) = \sum_{m=-\infty}^{\infty} \Pi_m f(\phi) = \sum_{m=-\infty}^{\infty} e^{im\phi} a_m. \tag{2.11}$$

For the second example consider a space of complex functions analytical on some annulus, with rotation acting via

$$R(\alpha)f(z) \coloneqq f(e^{-i\alpha}z). \tag{2.12}$$

Now application of the projector gives

$$\begin{aligned}\Pi_m f(z) &= \frac{1}{2\pi}\int_0^{2\pi} d\alpha\, e^{im\alpha} R(\alpha) f(z) \\ &= \frac{1}{2\pi}\int_0^{2\pi} d\alpha\, e^{im\alpha} f(e^{-i\alpha}z).\end{aligned} \tag{2.13}$$

Parametrization of a complex curve $\xi = e^{-i\alpha}$ allows to write the last expression as a contour integral over the unit circle (note the first integration is clockwise):

$$\begin{aligned}\Pi_m f(z) &= \frac{1}{2\pi} i \oint_{|\xi|=1} \frac{d\xi}{\xi}\, \xi^{-m} f(\xi z) \\ &= \frac{1}{2\pi i}\oint_{|\xi|=1} d\xi\, \xi^{-m-1} f(\xi z).\end{aligned} \tag{2.14}$$

Substituting $\xi z \mapsto \xi$ gives

$$\begin{aligned}\Pi_m f(z) &= \frac{1}{2\pi i}\oint_{|\xi|=|z|} \frac{d\xi}{z}\left(\frac{z}{\xi}\right)^{m+1} f(\xi) \\ &= z^m \frac{1}{2\pi i}\oint d\xi\, \frac{f(\xi)}{\xi^{m+1}} \\ &=: z^m c_m,\end{aligned} \tag{2.15}$$

where the integral value is the same for any simple closed curve in the annulus. Again, z^m transforms in an elementary way under rotation Eq. (2.12) and the sum of all components provides the decomposition of the function in the Laurent series:

$$f(z) = \sum_{m=-\infty}^{\infty} \Pi_m f(z) = \sum_{m=-\infty}^{\infty} z^m c_m. \tag{2.16}$$

Numerous well-known decompositions in physics, such as those involving Bloch waves or multipolar fields, have a similar interpretation in terms of group theory. Establishing a connection between a physical theory and the theory of group representations can provide new and insightful perspectives. This dissertation focuses on the transformation of electromagnetic fields under the group of 4D space-time symmetries, also called the Poincaré group. The decomposition of the electromagnetic field into irreducible components with respect to this group was first explored by Harry Moses [20]. This manuscript builds on his work and that of others, to enhance and generalize some of the existing methods relevant to the study of electromagnetic scattering.

2.2 Poincaré group

All transformations of the Minkowski space-time that leave the scalar product $x^\mu y_\mu = -x^0 y^0 + \boldsymbol{x}\cdot\boldsymbol{y}$ invariant constitute the 10-parameter Poincaré group. 3 of its parameters are responsible for translations in space, 1 for translation in time, 3 for rotations in space, and another 3 for Lorentz boosts. The latter relativistically describe the change of the reference frame to the one that moves the a constant speed. The next section provides a brief overview of Lorentz boosts.

2.2.1 Lorentz boosts

First, it is important to distinguish between the transformation of the reference frame and the transformation of the object. In the first case, the transformation is called active, and in the second it is called passive. Throughout the article, unless stated otherwise, transformations are assumed to be active.

Active Lorentz boosts provide a relativistic description of an object in uniform motion with velocity $\boldsymbol{v}$, possibly close to the speed of light c. A 4-vector of a point in Minkowski space-time is transformed under a Lorentz boost in the z-direction via [14, Chap. 10]

$$x^\mu = \begin{pmatrix} ct \\ x^1 \\ x^2 \\ x^3 \end{pmatrix} \mapsto L_z(\xi)^\mu{}_\nu\, x^\nu = \begin{pmatrix} \cosh(\xi) & 0 & 0 & \sinh(\xi) \\ 0 & 1 & 0 & 0 \\ 0 & 0 & 1 & 0 \\ \sinh(\xi) & 0 & 0 & \cosh(\xi) \end{pmatrix} \begin{pmatrix} ct \\ x^1 \\ x^2 \\ x^3 \end{pmatrix}, \tag{2.17}$$

where the boost parameter is called rapidity and is connected to the velocity via $\xi = \operatorname{arctanh}(v/c)$. Rapidity provides a natural parametrizaation of boosts, making a lot of formulas more compact, compared with formulation with $\boldsymbol{v}$. However, the speed of the boost will be also used in this text.

A general Lorentz boost in an arbitrary direction $\hat{\boldsymbol{n}}$ can be expressed as a composition of a boost in the z-direction and spacial rotations:

$$L_{\hat{\boldsymbol{n}}}(\xi) = R(\phi,\theta,0) L_z(\xi) R^{-1}(\phi,\theta,0). \tag{2.18}$$

Here the direction of the boost $\hat{\boldsymbol{n}}$ is parametrized by polar angle $\theta = \arccos\left(k_z/|\boldsymbol{k}|\right)$ and azimuthal angle $\phi = \operatorname{atan2}\left(k_y, k_x\right)$, with the rotations R parametrized via Euler angles in zyz-convention.

For a massless 4-wave vector k^μ with $k^\mu k_\mu = 0$, or $k^0 = |\boldsymbol{k}| =: k$, the z-direction boost implies

$$k^\mu = \begin{pmatrix} |\boldsymbol{k}| \\ k_x \\ k_y \\ k_z \end{pmatrix} \mapsto \begin{pmatrix} \cosh(\xi)|\boldsymbol{k}| + \sinh(\xi) k_z \\ k_x \\ k_y \\ \sinh(\xi)|\boldsymbol{k}| + \cosh(\xi) k_z \end{pmatrix} = \tilde{k}^\mu. \tag{2.19}$$

The angles and the wave number of the boosted wave vector can be written in terms of the old ones via $\tilde{\phi} = \phi$ and

$$\cos(\tilde{\theta}) = \frac{\cos(\theta)\cosh(\xi) + \sinh(\xi)}{\cosh(\xi) + \cos(\theta)\sinh(\xi)} = \frac{\cos(\theta) + \tanh(\xi)}{1 + \cos(\theta)\tanh(\xi)} \tag{2.20}$$

$$\tilde{k} = k(\cosh(\xi) + \cos(\theta)\sinh(\xi)). \tag{2.21}$$

The transformation properties of electric and magnetic fields do not follow from the transformation rules of the points in space-time, but they have to be defined additionally. Specifically, the active Lorentz boost with velocity $\boldsymbol{v}$ of real-valued electromagnetic fields is defined as [30, Sec.11.10]

$$\widetilde{\boldsymbol{\mathcal{E}}}(\boldsymbol{r}, t) = \gamma\boldsymbol{\mathcal{E}}(\tilde{\boldsymbol{r}}, \tilde{t}) - \gamma\boldsymbol{v} \times \boldsymbol{\mathcal{B}}(\tilde{\boldsymbol{r}}, \tilde{t}) - \frac{\gamma^2\boldsymbol{v}}{(\gamma+1)c^2}\boldsymbol{v} \cdot \boldsymbol{\mathcal{E}}(\tilde{\boldsymbol{r}}, \tilde{t}) \tag{2.22}$$

$$\widetilde{\boldsymbol{\mathcal{B}}}(\boldsymbol{r}, t) = \gamma\boldsymbol{\mathcal{B}}(\tilde{\boldsymbol{r}}, \tilde{t}) + \frac{1}{c^2}\gamma\boldsymbol{v} \times \boldsymbol{\mathcal{E}}(\tilde{\boldsymbol{r}}, \tilde{t}) - \frac{\gamma^2\boldsymbol{v}}{(\gamma+1)c^2}\boldsymbol{v} \cdot \boldsymbol{\mathcal{B}}(\tilde{\boldsymbol{r}}, \tilde{t}) \tag{2.23}$$

with inversely transformed space-time point $\begin{pmatrix} c\tilde{t} \\ \tilde{\boldsymbol{r}} \end{pmatrix} = L^{-1}(\xi)\begin{pmatrix} ct \\ \boldsymbol{r} \end{pmatrix}$ and $\gamma = (1 - v^2/c^2)^{-1/2}$. The passive version of the Lorentz boost, i.e. the boost of the reference frame instead of the field, differs from Eqs. (2.22-2.23) by the substitution $\boldsymbol{v} \longrightarrow -\boldsymbol{v}$ and should not be confused with the active version.

3 Electromagnetic fields: wave function and Hilbert space formalism in the plane wave basis

In the frequency domain, Maxwell's equations for the electric field $\tilde{\boldsymbol{E}}(\boldsymbol{r}, k)$ and magnetic field $\tilde{\boldsymbol{B}}(\boldsymbol{r}, k)$ in vacuum, written in SI units, are

$$\boldsymbol{\nabla} \times \tilde{\boldsymbol{E}}(\boldsymbol{r}, k) = ick\tilde{\boldsymbol{B}}(\boldsymbol{r}, k), \qquad \boldsymbol{\nabla} \times \tilde{\boldsymbol{B}}(\boldsymbol{r}, k) = -\frac{ik}{c^2}\tilde{\boldsymbol{E}}(\boldsymbol{r}, k), \tag{3.1}$$

$$\boldsymbol{\nabla} \cdot \tilde{\boldsymbol{E}}(\boldsymbol{r}, k) = 0, \qquad \boldsymbol{\nabla} \cdot \tilde{\boldsymbol{B}}(\boldsymbol{r}, k) = 0, \tag{3.2}$$

where $c = 1/\sqrt{\epsilon_0 \mu_0}$ is the speed of light in vacuum and for convenience the frequency is expressed in terms of the absolute value of the wave vector $k = \sqrt{\boldsymbol{k} \cdot \boldsymbol{k}} = |\boldsymbol{k}| = \omega/c$. Since the magnetic field is entirely determined by the electric field, our focus will be solely on the latter.

It is convenient to start from the complex-valued electric field in the space-time domain. It is defined by setting the components of negative frequency in the Fourier decomposition of the field to zero:

$$\boldsymbol{E}(\boldsymbol{r}, t) = \frac{1}{\sqrt{2\pi}} \int_0^\infty dk\, e^{-ikct}\, \tilde{\boldsymbol{E}}(\boldsymbol{r}, k). \tag{3.3}$$

Then the real-valued electric field can be restored via

$$\boldsymbol{\mathcal{E}}(\boldsymbol{r}, t) = \boldsymbol{E}(\boldsymbol{r}, t) + \boldsymbol{E}^*(\boldsymbol{r}, t) = 2\Re[\boldsymbol{E}(\boldsymbol{r}, t)]. \tag{3.4}$$

3.1 Plane waves $|\mathrm{k}\lambda\rangle$ and wave function $f_\lambda(\mathrm{k})$

One can express the electric field as a sum of plane waves of right-handed circular polarization, helicity $\lambda = -1$, and of left-handed circular polarization, helicity $\lambda = 1$, using polarization vectors as defined in [31] (Sec. 1.1.4)

$$\boldsymbol{e}_\lambda(\hat{\boldsymbol{k}}) := -\frac{1}{\sqrt{2}}(\lambda \boldsymbol{e}_\theta(\hat{\boldsymbol{k}}) + i\boldsymbol{e}_\phi(\hat{\boldsymbol{k}})) \tag{3.5}$$

$$= \frac{1}{\sqrt{2}} \begin{pmatrix} -\lambda \cos\phi \cos\theta + i \sin\phi \\ -\lambda \sin\phi \cos\theta - i \cos\phi \\ \lambda \sin\theta \end{pmatrix}, \tag{3.6}$$

where $\boldsymbol{e}_\theta$, $\boldsymbol{e}_\phi$ are spherical basis vectors, $\hat{\boldsymbol{k}}$ is the unit vector along the direction of the wave vector, with $\theta = \arccos(k_z/|\boldsymbol{k}|)$ and $\phi = \text{atan2}\left(k_y, k_x\right)$ being its polar and azimuthal angles.

The vectors $\boldsymbol{e}_\lambda(\hat{\boldsymbol{k}})$, $\lambda = \pm 1$ together with $\boldsymbol{e}_0(\hat{\boldsymbol{k}}) := \hat{\boldsymbol{k}}$ form a local orthonormal basis at $\boldsymbol{k}$. They serve as eigenvectors of the helicity operator $\Lambda = \frac{i\hbar \boldsymbol{k}\times}{k}$:

$$\frac{i\hbar \boldsymbol{k}\times}{k} \boldsymbol{e}_\lambda(\hat{\boldsymbol{k}}) = \lambda \hbar \boldsymbol{e}_\lambda(\hat{\boldsymbol{k}}) \,, \qquad \text{for } \lambda = -1, 0, 1. \tag{3.7}$$

The basis vectors with helicity $\lambda = \pm 1$ are suitable for decomposing transverse fields into components of definite circular polarizations, as the $\lambda = 0$ fields have zero curl and do not occur in $k > 0$ Maxwell fields. To achieve the decomposition, the first step involves performing the 3D Fourier transform of the complex electric field

$$\boldsymbol{E}(\boldsymbol{r}, t) = \frac{1}{\sqrt{(2\pi)^3}} \int d^3\boldsymbol{k}\, \bar{\boldsymbol{E}}(\boldsymbol{k})\, e^{-ikct} e^{i\boldsymbol{k}\cdot\boldsymbol{r}}, \tag{3.8}$$

with the absolute value of wave vector $k = |\boldsymbol{k}| = \omega/c$. The next step is to project the polarization vectors of helicity $\lambda = \pm 1$ onto $\bar{\boldsymbol{E}}(\boldsymbol{k})$, using dimensional constants chosen for future convenience:

$$f_\lambda(\boldsymbol{k}) = \sqrt{2} \sqrt{\frac{\epsilon_0}{c\hbar}}\, \boldsymbol{e}_\lambda(\hat{\boldsymbol{k}})^* \cdot \bar{\boldsymbol{E}}(\boldsymbol{k}), \tag{3.9}$$

resulting in $\bar{\boldsymbol{E}}(\boldsymbol{k}) = \sqrt{\frac{c\hbar}{2\epsilon_0}} \sum_{\lambda=\pm1} f_\lambda(\boldsymbol{k}) \boldsymbol{e}_\lambda(\hat{\boldsymbol{k}})$. This leads to the decomposition:

$$\boldsymbol{E}(\boldsymbol{r}, t) = \sqrt{\frac{c\hbar}{2\epsilon_0}} \frac{1}{\sqrt{(2\pi)^3}} \sum_{\lambda=\pm1} \int \frac{d^3\boldsymbol{k}}{k} f_\lambda(\boldsymbol{k})\, k\, \boldsymbol{e}_\lambda(\hat{\boldsymbol{k}})\, e^{i(\boldsymbol{k}\cdot\boldsymbol{r} - ckt)}, \tag{3.10}$$

where the coefficients $f_\lambda(\boldsymbol{k})$ follow the transformation laws of a photon wave function according to [20].

The independent helicity $\lambda = \pm 1$ components of the electric field, representing left- and right-handed polarization, are described by the two complex Riemann-Silberstein vectors:

$$\boldsymbol{F}_\lambda(\boldsymbol{r}, t) = \left(\boldsymbol{E}(\boldsymbol{r}, t) + i\lambda c \boldsymbol{B}(\boldsymbol{r}, t)\right)/\sqrt{2}, \tag{3.11}$$

which can be written in terms of the wave function coefficients as

$$\begin{aligned}
\boldsymbol{F}_\lambda(\boldsymbol{r}, t) &= \frac{1}{\sqrt{(2\pi)^3}} \int d^3\boldsymbol{k}\, \frac{\bar{\boldsymbol{E}}(\boldsymbol{k}) + i\lambda c \bar{\boldsymbol{B}}(\boldsymbol{k})}{\sqrt{2}} e^{i(\boldsymbol{k}\cdot\boldsymbol{r} - ckt)} && (3.12)\\
&= \frac{1}{\sqrt{2}} \frac{1}{\sqrt{(2\pi)^3}} \int d^3\boldsymbol{k} \left(\bar{\boldsymbol{E}}(\boldsymbol{k}) + i\lambda \frac{\boldsymbol{k}\times}{k} \bar{\boldsymbol{E}}(\boldsymbol{k})\right) e^{i(\boldsymbol{k}\cdot\boldsymbol{r} - ckt)} && (3.13)\\
&= \sqrt{\frac{c\hbar}{\epsilon_0}} \frac{1}{\sqrt{2}} \frac{1}{\sqrt{(2\pi)^3}} \int d^3\boldsymbol{k}\, \frac{1}{\sqrt{2}} \Big(f_+(\boldsymbol{k}) \boldsymbol{e}_+(\hat{\boldsymbol{k}}) + f_-(\boldsymbol{k}) \boldsymbol{e}_-(\hat{\boldsymbol{k}}) \\
&\qquad + \lambda f_+(\boldsymbol{k}) \boldsymbol{e}_+(\hat{\boldsymbol{k}}) - \lambda f_-(\boldsymbol{k}) \boldsymbol{e}_-(\hat{\boldsymbol{k}}) \Big) e^{i(\boldsymbol{k}\cdot\boldsymbol{r} - ckt)} \\
&= \sqrt{\frac{c\hbar}{\epsilon_0}} \frac{1}{\sqrt{(2\pi)^3}} \int \frac{d^3\boldsymbol{k}}{k} f_\lambda(\boldsymbol{k}) \boldsymbol{e}_\lambda(\hat{\boldsymbol{k}})\, k\, e^{i(\boldsymbol{k}\cdot\boldsymbol{r} - ckt)}. && (3.14)
\end{aligned}$$

Here, the Maxwell equation in the wave vector space $\boldsymbol{k} \times \bar{\boldsymbol{E}}(\boldsymbol{k}) = ck\bar{\boldsymbol{B}}(\boldsymbol{k})$ is used in the second line of Eq. (3.14). Given that the complex-valued form of electric and magnetic fields is considered, the two Riemann-Silberstein vectors, $\boldsymbol{F}_-$ for waves of the right-handed circular polarization and $\boldsymbol{F}_+$ for the left-handed, are independent and together provide the complete description of the electromagnetic field.

The proposed definition for the electromagnetic plane wave is

$$\boxed{\begin{aligned} |\boldsymbol{k}\,\lambda\rangle &\equiv \boldsymbol{Q}_\lambda(\boldsymbol{k},\boldsymbol{r},t) && (3.15)\\ &= \sqrt{\frac{c\hbar}{\epsilon_0}}\,\frac{1}{\sqrt{2}}\,\frac{1}{\sqrt{(2\pi)^3}}\,k\,\boldsymbol{e}_\lambda(\hat{\boldsymbol{k}})e^{-ikct}e^{i\boldsymbol{k}\cdot\boldsymbol{r}}, && (3.16)\end{aligned}}$$

so the decomposition of the electromagnetic field can be written compactly as

$$\boldsymbol{E}(\boldsymbol{r},t) = \sum_{\lambda=\pm1}\int \frac{d^3\boldsymbol{k}}{k}\, f_\lambda(\boldsymbol{k})\,\boldsymbol{Q}_\lambda(\boldsymbol{k},\boldsymbol{r},t). \tag{3.17}$$

The factor k in the definition of the plane wave in Eq. (3.16) is significant. This factor arises from the transition in Eq. (3.10) from the integration measure $d^3\boldsymbol{k}$ of the 3D Fourier transform, to the Lorentz-invariant integration measure in he light cone $\frac{d^3\boldsymbol{k}}{k}$ [32, Eq. (2.5.15)][14, Sec. 10.4.6]. This change introduces a factor of k in the definition of the plane wave in Eq. (3.16). As demonstrated in Sec. 3.5, this specific factor of k ensures that $\boldsymbol{Q}_\lambda(\boldsymbol{k},\boldsymbol{r},t)$ and $f_\lambda(\boldsymbol{k})$ transform as massless unitary irreducible representations of the Poincaré group with helicity $\lambda = \pm1$. These transformation properties align with the requirements for the photon wave function according to Wigner's classification [16]. The transformation rules are provided in [14, Eqs. (10.4-23), (10.4-24)]:

$$T(a^\mu)\,|\boldsymbol{k}\,\lambda\rangle = |\boldsymbol{k}\,\lambda\rangle\, e^{-ia^\mu k_\mu} \tag{3.18}$$

$$R(\alpha,\beta,\gamma)\,|\boldsymbol{k}\,\lambda\rangle = |\tilde{\boldsymbol{k}}\,\lambda\rangle\, e^{-i\lambda\psi}, \qquad \tilde{\boldsymbol{k}} = R(\alpha,\beta,\gamma)\boldsymbol{k} \tag{3.19}$$

$$L_z(\xi)\,|\boldsymbol{k}\,\lambda\rangle = |\boldsymbol{k}'\,\lambda\rangle\,, \qquad \boldsymbol{k}' = L_z(\xi)\boldsymbol{k} \tag{3.20}$$

where $T(a^\mu)$ is a 4D translation in Minkowski space-time with metric signature $(-+++)$, so $a^\mu k_\mu = -a^0|\boldsymbol{k}| + \boldsymbol{a}\cdot\boldsymbol{k}$. The operator $R(\alpha,\beta,\gamma) = R_z(\alpha)R_y(\beta)R_z(\gamma)$ stands for rotation with corresponding Euler angles. The angle ψ satisfies $R(0,0,\psi) = R(\tilde{\phi},\tilde{\theta},0)^{-1}R(\alpha,\beta,\gamma)R(\phi,\theta,0)$, where $\tilde{\phi},\tilde{\theta}$ are spherical angles of the rotated wave vector $\tilde{\boldsymbol{k}} = R(\alpha,\beta,\gamma)\boldsymbol{k}$). Operator $L_z(\xi)$ is a Lorentz boost (App.2.2.1) along the z-axis with rapidity ξ. Since a boost along an arbitrary direction can be decomposed into rotations and a boost in the z-direction with Eq. (2.18), only the boost along the z-direction is explicitly considered.

In this representation, plane waves undergo transformations under parity and time reversal[1] as follows:

$$I_s\,|\boldsymbol{k}\lambda\rangle = |-\boldsymbol{k}\;-\lambda\rangle \tag{3.21}$$

$$I_t\,|\boldsymbol{k}\lambda\rangle = |-\boldsymbol{k}\,\lambda\rangle\,. \tag{3.22}$$

[1]The time reversal is represented anti-unitarily by an operator I_t satisfying $\langle I_t\phi|I_t\psi\rangle = \langle\phi|\psi\rangle^* = \langle\psi|\phi\rangle$.

The integration measure $\int \frac{d^3\boldsymbol{k}}{k}$ is invariant under the actions of the Poincaré group, which enables the formulation of field transformations via transforming the coefficients $f_\lambda(\boldsymbol{k})$ in a way similar to transforming the basis vectors [14, Secs. 7.6 and 10.5.1]. For example, for a boost in the z-direction Eq. (3.20), the invariance of the measure implies that

$$\int \frac{d^3\boldsymbol{k}}{|\boldsymbol{k}|} = \int \frac{d^3 L_z^{-1}(\xi)\boldsymbol{k}}{|L_z^{-1}(\xi)\boldsymbol{k}|}. \tag{3.23}$$

This, combined with the linearity of the boost operator and Eq. (3.20), leads to:

$$\begin{aligned} L_z(\xi)\,|f\rangle &= \sum_{\lambda=\pm1} \int \frac{d^3\boldsymbol{k}}{k} f_\lambda(\boldsymbol{k})\ |L_z(\xi)\boldsymbol{k}\,\lambda\rangle \\ &= \sum_{\lambda=\pm1} \int \frac{d^3 L_z^{-1}(\xi)\boldsymbol{k}}{|L_z^{-1}(\xi)\boldsymbol{k}|} f_\lambda(L_z^{-1}(\xi)\boldsymbol{k})\ |\boldsymbol{k}\lambda\rangle \\ &= \sum_{\lambda=\pm1} \int \frac{d^3\boldsymbol{k}}{k} f_\lambda(L_z^{-1}(\xi)\boldsymbol{k})\ |\boldsymbol{k}\lambda\rangle\,. \end{aligned} \tag{3.24}$$

The complete list of transformation rules for the coefficients $f_\lambda(\boldsymbol{k})$ is as follows:

$$T(a^\mu) f_\lambda(\boldsymbol{k}) = f_\lambda(\boldsymbol{k}) e^{-ia^\mu k_\mu}, \tag{3.25}$$

$$R(\alpha,\beta,\gamma) f_\lambda(\boldsymbol{k}) = f_\lambda(\tilde{\boldsymbol{k}}) e^{-i\lambda\psi}, \qquad \tilde{\boldsymbol{k}} = R^{-1}(\alpha,\beta,\gamma)\boldsymbol{k} \tag{3.26}$$

$$L_z(\xi) f_\lambda(\boldsymbol{k}) = f_\lambda(\boldsymbol{k}'), \qquad \boldsymbol{k}' = L_z^{-1}(\xi)\boldsymbol{k}. \tag{3.27}$$

Here, ψ is determined from $R(0,0,\psi) = R(\phi,\theta,0)^{-1} R(\alpha,\beta,\gamma) R(\tilde{\phi},\tilde{\theta},0)$, where $\tilde{\phi},\tilde{\theta}$ correspond to the wave vector $\tilde{\boldsymbol{k}} = R^{-1}(\alpha,\beta,\gamma)\boldsymbol{k}$. The transformations under parity and time reversal are expressed as:

$$I_s f_\lambda(\boldsymbol{k}) = f_{-\lambda}(-\boldsymbol{k}) \tag{3.28}$$

$$I_t f_\lambda(\boldsymbol{k}) = f_\lambda^*(-\boldsymbol{k}). \tag{3.29}$$

The transformation properties of the defined plane waves and coefficients in the decomposition Eq. (3.17) validate the representation of the electric field as a ket:

$$|f\rangle = \sum_{\lambda=\pm1} \int \frac{d^3\boldsymbol{k}}{k} f_\lambda(\boldsymbol{k})\ |\boldsymbol{k}\lambda\rangle\,. \tag{3.30}$$

3.2 Scalar product in plane wave basis

The coefficients $f_\lambda(\boldsymbol{k})$ are associated with a Hilbert space of states with finite norm with respect to the scalar product

$$\langle f|g\rangle = \sum_{\lambda=\pm1} \int \frac{d^3\boldsymbol{k}}{k} f_\lambda^*(\boldsymbol{k}) g_\lambda(\boldsymbol{k}). \tag{3.31}$$

Wave functions that possess infinite norms are not physical, since they correspond to fields with an infinite number of photons. Because of the additional dimensional factors in Eq. (3.9), the coefficient function $f_\lambda(\boldsymbol{k})$ has the units of length: $[f_\lambda(\boldsymbol{k})] = \mathrm{m}$. The scalar product Eq. (3.31) is consequently dimensionless, aligning with the physical interpretation of $\langle f|f\rangle$ as the number of photons [33] that are contained in the field described by $|f\rangle$. The integral in [33, Eq. (1)] offers a distinct representation of the same scalar product, as can be seen by comparing Eq. (3) and Eq. (6) in [17].

This scalar product also serves as a tool to quantify fundamental quantities carried by the field, such as energy, linear momentum, and angular momentum, through the evaluation of expectation values $\langle f|\Gamma|f\rangle$, where Γ stands for the self-adjoint generator of the corresponding symmetry transformation: time translation for energy, spatial translation for linear momentum and rotation for angular momentum.

It is well-established [17] that the scalar product in Eq. (3.31) remains invariant under the conformal group, which stands as the largest group of invariance of Maxwell equations [34]. This group encompasses the Poincaré group and includes special conformal transformations and dilations.

In the next section, it is discussed how the same analysis done in this section for the electric field may be applied to the formulation in terms of the electromagnetic vector potential. In particular, why the plane waves for decomposing the vector potential do not feature the extra factor of k.

3.3 Representation of vector potential

The transverse part of the vector potential determines the transverse electric field as follows:

$$\boldsymbol{E}(\boldsymbol{r},t) = -\frac{\partial \boldsymbol{A}^\perp(\boldsymbol{r},t)}{\partial t}, \tag{3.32}$$

independently of the gauge [35, Eq. B.26]. In the wave vector space, one consequently finds

$$\bar{\boldsymbol{A}}^\perp(\boldsymbol{k}) = \frac{-i\bar{\boldsymbol{E}}(\boldsymbol{k})}{ck}, \tag{3.33}$$

and the decomposition analogous to Eq. (3.10) can be expressed as

$$\boldsymbol{A}^\perp(\boldsymbol{r},t) = \sqrt{\frac{\hbar}{c\epsilon_0}}\frac{1}{\sqrt{2}}\frac{-i}{\sqrt{(2\pi)^3}}\sum_{\lambda=\pm1}\int \frac{d^3\boldsymbol{k}}{k}\, f_\lambda(\boldsymbol{k})\ \boldsymbol{e}_\lambda(\hat{\boldsymbol{k}})\, e^{i(\boldsymbol{k}\cdot\boldsymbol{r}-ckt)}, \tag{3.34}$$

where the coefficients of the decomposition $f_\lambda(\boldsymbol{k})$ are the same as those of the corresponding electric field. To maintain the invariant measure $\frac{d^3\boldsymbol{k}}{k}$, the decomposition in Eq. (3.34) gives rise to a definition of plane waves for the vector potential that differs from one of the electric plane waves by the factor of ik/c:

$$\boldsymbol{Q}_\lambda^{A^\perp}(\boldsymbol{k},\boldsymbol{r},t) = -i\sqrt{\frac{\hbar}{c\epsilon_0}}\,\frac{1}{\sqrt{2}}\frac{1}{\sqrt{(2\pi)^3}}\,\boldsymbol{e}_\lambda(\hat{\boldsymbol{k}})e^{-ikct}e^{i\boldsymbol{k}\cdot\boldsymbol{r}}. \tag{3.35}$$

Plane waves of the vector potential are ruled by the same transformation laws Eqs. (3.18-3.20) and Eq. (3.21), with the exception of time reversal. In time reversal, the presence of the imaginary unit i introduces an additional factor of (-1) on the right-hand side of Eq. (3.22). The differentiation $\frac{\partial}{\partial t}$ in Eq. (3.32) also hints at the difference in time-reversal transformation properties. The factor of k exactly compensates for the different way that $\boldsymbol{A}^{\perp}(\boldsymbol{r},t)$ and $\boldsymbol{E}(\boldsymbol{r},t)$ transform under Lorentz boosts, namely as the space component of a four-vector, and as the space-time component of an anti-symmetric tensor, respectively.

3.4 On basis states and the Hilbert space

The Hilbert space is defined to contain states $|f\rangle$ that possess finite norm

$$\langle f|f\rangle < \infty. \tag{3.36}$$

A plane basis state $|\boldsymbol{k}\lambda\rangle$ is not in the Hilbert space, because its wave function contains the Dirac delta distribution

$$|\boldsymbol{k}\lambda\rangle = \sum_{\lambda'=\pm1} \int \frac{d^3\boldsymbol{k}'}{k'}\, \delta_{\lambda\lambda'}\, k\, \delta^{(3)}(\boldsymbol{k}'-\boldsymbol{k})\, |\boldsymbol{k}'\boldsymbol{\lambda}'\rangle\,, \tag{3.37}$$

and its norm is infinite:

$$\langle \boldsymbol{k}\lambda|\boldsymbol{k}\lambda\rangle = \sum_{\lambda'=\pm1} \int \frac{d^3\boldsymbol{k}'}{k'} \left[\delta_{\lambda\lambda'}\, k\, \delta^{(3)}(\boldsymbol{k}'-\boldsymbol{k})\right]^* \delta_{\lambda\lambda'}\, k\, \delta^{(3)}(\boldsymbol{k}'-\boldsymbol{k}) \tag{3.38}$$

$$= k\, \delta^{(3)}(0). \tag{3.39}$$

This makes it physically unrealizable and not belonging to the Hilbert space. Similar issues arise for states from any continuous spectrum, as opposed to the discrete spectrum. This reflects the well-known fact that the Hilbert space formalism is not sufficient to describe Dirac's bra-ket notation for operators with continuous spectrum. A mathematically complete treatment of the Dirac formalism involves the construction called rigged Hilbert space, also known as Gel'fand triplet, which is a triad of spaces: a Hilbert space, a space of distributions, and a space of test functions. A short pedagogical introduction to this topic is given in [36].

In the current work, the Dirac formalism is only used as a convenient way of writing and proving formulas that work for physically realizable states. Distributions arise only in intermediate steps before being eliminated by integration to produce a finite result.

3.5 Lorentz boost of plane waves

Here, the transformation of $\boldsymbol{Q}_\lambda(\boldsymbol{k},\boldsymbol{r},t)$ under an active boost in the z-direction with rapidity ξ is explicitly derived. First, one notes that the Riemann-Silberstein vectors in Eq. (3.12) transform under active Lorentz boosts as:

$$\widetilde{\boldsymbol{F}}_\lambda(\boldsymbol{r},t) = \gamma \boldsymbol{F}_\lambda(\tilde{\boldsymbol{r}},\tilde{t}) + \frac{i\lambda\gamma}{c}\boldsymbol{v}\times\boldsymbol{F}_\lambda(\tilde{\boldsymbol{r}},\tilde{t}) - \frac{\gamma^2\boldsymbol{v}}{(\gamma+1)c^2}\boldsymbol{v}\cdot\boldsymbol{F}_\lambda(\tilde{\boldsymbol{r}},\tilde{t}). \tag{3.40}$$

The transformation rule for general electromagnetic fields in [30, Eq. (11.149)] is used to derive the action of the boost (see also Eq. (3.40)):

$$\begin{aligned}\boldsymbol{Q}_\lambda(\boldsymbol{k},\boldsymbol{r},t) &= \gamma \boldsymbol{Q}_\lambda(\boldsymbol{k},\tilde{\boldsymbol{r}},\tilde{t}) + \frac{i\lambda\gamma}{c}\boldsymbol{v}\times\boldsymbol{Q}_\lambda(\boldsymbol{k},\tilde{\boldsymbol{r}},\tilde{t}) - \frac{\gamma^2\boldsymbol{v}}{(\gamma+1)c^2}\boldsymbol{v}\cdot\boldsymbol{Q}_\lambda(\boldsymbol{k},\tilde{\boldsymbol{r}},\tilde{t}) \\ &\equiv \Big(\gamma\mathbb{1} + \frac{i\lambda\gamma}{c}\boldsymbol{v}\times - \frac{\gamma^2\boldsymbol{v}}{(\gamma+1)c^2}\boldsymbol{v}\cdot\Big)\boldsymbol{Q}_\lambda(\boldsymbol{k},\tilde{\boldsymbol{r}},\tilde{t}),\end{aligned} \tag{3.41}$$

where in Eq. (3.41) $\boldsymbol{Q}_\lambda$ is factored out and, leaving the sum of three linear operators $\mathbb{1}$, $\boldsymbol{v}\times$, and $\boldsymbol{v}\,\boldsymbol{v}\cdot$ in brackets. Here $\boldsymbol{v} = v\boldsymbol{e}_z = c\tanh(\xi)\boldsymbol{e}_z$, $\gamma = (1 - v^2/c^2)^{-1/2} = \cosh(\xi)$, $\gamma v = c\sinh(\xi)$ and space-time coordinates are inversely transformed via

$$\begin{pmatrix} c\tilde{t} \\ \tilde{\boldsymbol{r}} \end{pmatrix} = L_z^{-1}(\xi)\begin{pmatrix} ct \\ \boldsymbol{r} \end{pmatrix} = \begin{pmatrix} \cosh(\xi) & 0 & 0 & -\sinh(\xi) \\ 0 & 1 & 0 & 0 \\ 0 & 0 & 1 & 0 \\ -\sinh(\xi) & 0 & 0 & \cosh(\xi) \end{pmatrix}\begin{pmatrix} ct \\ x \\ y \\ z \end{pmatrix}. \tag{3.42}$$

It is crucial to distinguish between the passive and active versions of the Lorentz boost. In the passive version, where the reference frame is boosted instead of the field, Eqs. (3.41-3.42) incorporate $-\boldsymbol{v}$ in place of $\boldsymbol{v}$ (and, equivalently, $-\xi$ instead of ξ).

The helicity basis vectors $\boldsymbol{e}_\sigma(\hat{\boldsymbol{k}})$ can be obtained by rotation of the reference helicity basis vector pointing in the z-direction: $\boldsymbol{e}_\sigma(\hat{\boldsymbol{k}}) = R(\phi,\theta,0)\boldsymbol{e}_\sigma(\hat{\boldsymbol{z}})$, in particular

$$R(\alpha,\beta,\gamma)\,\boldsymbol{e}_\lambda(\hat{\boldsymbol{k}}) = \sum_{\sigma=\pm1,0} D^1_{\sigma\lambda}(\alpha,\beta,\gamma)\,\boldsymbol{e}_\sigma(\hat{\boldsymbol{k}}). \tag{3.43}$$

Here $D^j_{mn}(\alpha,\beta,\gamma) = e^{-im\alpha}d^j_{mn}(\beta)e^{-in\gamma}$ are Wigner matrices and $d^j_{mn}(\beta)$ are small Wigner matrices, as defined in [14], Sec. 7.3. Continuing the derivation:

$$\begin{aligned}&\Big(\gamma\mathbb{1} + \frac{i\lambda\gamma}{c}\boldsymbol{v}\times - \frac{\gamma^2\boldsymbol{v}}{(\gamma+1)c^2}\boldsymbol{v}\cdot\Big)\,k\,\boldsymbol{e}_\lambda(\hat{\boldsymbol{k}}) \\ &= \Big(\cosh(\xi)\mathbb{1} + i\lambda\sinh(\xi)\boldsymbol{e}_z\times - \frac{\sinh^2(\xi)\boldsymbol{e}_z}{\cosh(\xi)+1}\boldsymbol{e}_z\cdot\Big)\sum_{\sigma=-1,0,1} D^1_{\sigma\lambda}(\phi,\theta,0)\,k\,\boldsymbol{e}_\sigma(\hat{\boldsymbol{z}}) \\ &= \sum_{\sigma=-1,0,1} D^1_{\sigma\lambda}(\phi,\theta,0)\Big(\cosh(\xi) + \lambda\sigma\sinh(\xi) - \frac{\sinh^2(\xi)\delta_{0\sigma}}{\cosh(\xi)+1}\Big)\,k\,\boldsymbol{e}_\sigma(\hat{\boldsymbol{z}}) \qquad (3.44) \\ &= \sum_{\sigma=-1,0,1} e^{-i\phi\sigma}\,d^1_{\sigma\lambda}(\theta)\Big(\sigma\lambda\sinh(\xi) + \frac{\cosh(\xi)+\cosh^2(\xi)-\sinh^2(\xi)\delta_{0\sigma}}{\cosh(\xi)+1}\Big)\,k\,\boldsymbol{e}_\sigma(\hat{\boldsymbol{z}}) \\ &= \sum_{\sigma=-1,0,1} e^{-i\phi\sigma}\,d^1_{\sigma\lambda}(\tilde{\theta})\,\tilde{k}\,\boldsymbol{e}_\sigma(\hat{\boldsymbol{z}}) \qquad (3.45) \\ &= \tilde{k}\,\boldsymbol{e}_\lambda(\hat{\tilde{\boldsymbol{k}}}). \qquad (3.46)\end{aligned}$$

For the step leading to Eq. (3.44) one uses $\boldsymbol{e}_z\times\boldsymbol{e}_\sigma(\hat{\boldsymbol{z}}) = -i\sigma\boldsymbol{e}_\sigma(\hat{\boldsymbol{z}})$ and $\boldsymbol{e}_z\big(\boldsymbol{e}_z\cdot\boldsymbol{e}_\sigma(\hat{\boldsymbol{z}})\big) = \delta_{0\sigma}\boldsymbol{e}_\sigma(\hat{\boldsymbol{z}})$ for $\sigma = -1, 0, 1$. Eq. (3.45) follows from the transformation rules for the wave vector $\boldsymbol{k}$ as

discussed in Sec.2.2.1:

$$\tilde{k}\, d^1_{0\lambda}(\tilde{\theta}) = \frac{\lambda\tilde{k}}{\sqrt{2}}\sin(\tilde{\theta}) = \frac{\lambda k}{\sqrt{2}}\sin(\theta) = k\, d^1_{0\lambda}(\theta) \tag{3.47}$$

that holds for $\lambda = \pm 1$, $\sigma = 0$. In case $\lambda = \pm 1$, $\sigma = \pm 1$, the following holds:

$$\begin{aligned}
\tilde{k}\, d^1_{\sigma\lambda}(\tilde{\theta}) &= \frac{\tilde{k}}{2}\big(1 + \sigma\lambda\cos(\tilde{\theta})\big) && (3.48)\\
&= \frac{k\big(\cosh(\xi) + \cos(\theta)\sinh(\xi)\big)}{2}\left(1 + \sigma\lambda\frac{\cos(\theta)\cosh(\xi) + \sinh(\xi)}{\cosh(\xi) + \cos(\theta)\sinh(\xi)}\right)\\
&= \frac{k}{2}\big(\cosh(\xi) + \cos(\theta)\sinh(\xi) + \sigma\lambda(\cos(\theta)\cosh(\xi) + \sinh(\xi))\big)\\
&= \frac{k}{2}\big(1 + \sigma\lambda\cos(\theta)\big)\big(\cosh(\xi) + \sigma\lambda\sinh(\xi)\big)\\
&= k\, d^1_{\sigma\lambda}(\theta)\big(1 + \sigma\lambda\sinh(\xi)\big). && (3.49)
\end{aligned}$$

The final step follows from the fact that Lorentz boosts L preserves the norm of the 4-vectors:

$$e^{-ik^\mu (L^{-1}x)_\mu} = e^{-i(Lk)^\mu x_\mu}, \tag{3.50}$$

which implies Eq. (3.20):

$$\boxed{\left(\gamma\mathbb{1} + \frac{i\lambda\gamma v}{c}\boldsymbol{e}_z \times -\frac{\gamma^2 v^2 \boldsymbol{e}_z}{(\gamma+1)c^2}\boldsymbol{e}_z \cdot \right)\boldsymbol{Q}_\lambda(\boldsymbol{k}, \tilde{\boldsymbol{r}}, \tilde{t}) = \boldsymbol{Q}_\lambda(\tilde{\boldsymbol{k}}, \boldsymbol{r}, t).} \tag{3.51}$$

This derivation relies on the extra factor of k in the definition Eq. (3.16), and the plane wave would not transform according to the unitary representation in Eq. (3.20) without it.

4 Electromagnetic fields: wave function and Hilbert space formalism in the angular momentum basis

The multipolar fields play a central role in the scattering formalism: they constitute the convenient basis with respect to which the fields are expanded. Opposite to the plane wave fields, the multipolar basis fields are labeled with discrete indices, which makes them convenient entities to use in numerical approaches. In the beginning, the regular multipolar basis is discussed, which is unitarily connected to the plane wave basis, and then the irregular basis is introduced, derived in relation to its regular counterpart.

4.1 Regular fields

4.1.1 Angular momentum basis for regular fields $|kjm\lambda\rangle$

There are multiple types of bases in which states $|f\rangle$ can be expanded. Apart from the plane wave basis that has been discussed so far, the angular momentum basis constitutes a useful type of basis as well. The connection between the latter and the former is well known [14, Sec. 8.4.1]:

$$|kjm\lambda\rangle = \sqrt{\frac{2j+1}{4\pi}} \int_0^{2\pi} d\phi \int_{-1}^{1} d(\cos\theta)\, D^j_{m\lambda}(\phi,\theta,0)^* \, |\boldsymbol{k}\lambda\rangle \tag{4.1}$$

$$|\boldsymbol{k}\lambda\rangle = \sum_{j=1}^{\infty} \sum_{m=-j}^{j} \sqrt{\frac{2j+1}{4\pi}} D^j_{m\lambda}(\phi,\theta,0)\, |kjm\lambda\rangle\,. \tag{4.2}$$

The corresponding connection between coefficients in the angular momentum and the plane wave basis is written as

$$f_{jm\lambda}(k) = \sqrt{\frac{2j+1}{4\pi}} \int_0^{2\pi} d\phi \int_{-1}^{1} d(\cos\theta)\, D^j_{m\lambda}(\phi,\theta,0)\, f_\lambda(\boldsymbol{k}) \tag{4.3}$$

$$f_\lambda(\boldsymbol{k}) = \sum_{j=1}^{\infty} \sum_{m=-j}^{j} \sqrt{\frac{2j+1}{4\pi}} D^j_{m\lambda}(\phi,\theta,0)^*\, f_{jm\lambda}(k). \tag{4.4}$$

and follows from the orthogonality and completeness relations of the Wigner matrices:

$$\sum_{j=1}^{\infty}\sum_{m=-j}^{j}\frac{2j+1}{8\pi^2}D^{j}_{m\lambda}(\alpha_1,\beta_1,\gamma_1)D^{j}_{m\lambda}(\alpha_2,\beta_2,\gamma_2)^{*}=\delta(\alpha_1-\alpha_2)\delta(\cos\beta_1-\cos\beta_2)\delta(\gamma_1-\gamma_2) \tag{4.5}$$

$$\int_0^{2\pi}d\alpha\int_{-1}^{1}d\cos\beta\int_0^{2\pi}d\gamma\,\frac{2j+1}{8\pi^2}\,D^{j_1}_{m_1n_1}(\alpha,\beta,\gamma)D^{j_2}_{m_2n_2}(\alpha,\beta,\gamma)^{*}=\delta_{j_1j_2}\delta_{m_1m_2}\delta_{n_1n_2}. \tag{4.6}$$

The labels of basis vectors $|kjm\lambda\rangle$ are quantum numbers that correspond to eigenvalues of Hermitian operators of energy H, total angular momentum $J^2=J_x^2+J_y^2+J_z^2$, angular momentum along z-axis J_z, and helicity Λ:

$$\begin{aligned}
H\,|kjm\lambda\rangle &= \hbar ck\,|kjm\lambda\rangle \\
J^2\,|kjm\lambda\rangle &= \hbar^2 j(j+1)\,|kjm\lambda\rangle\,, \qquad j=1,2,\ldots \\
J_z\,|kjm\lambda\rangle &= \hbar m\,|kjm\lambda\rangle\,, \qquad m=-j,-j+1,\ldots,j \\
\Lambda\,|kjm\lambda\rangle &= \hbar\lambda\,|kjm\lambda\rangle\,, \qquad \lambda=\pm1.
\end{aligned}$$

In common terminology, $j=1$ states are called the dipolar fields, $j=2$ the quadrupolar fields, and so on.

A general state can be represented in the angular momentum basis by using Eqs. (4.1-4.4) in Eq. (3.30), which leads to

$$|f\rangle=\int_0^{\infty}dk\,k\sum_{\lambda=\pm1}\sum_{j=1}^{\infty}\sum_{m=-j}^{j}f_{jm\lambda}(k)\;|kjm\lambda\rangle\,, \tag{4.7}$$

and the scalar product in Eq. (3.31) can correspondingly be written in the angular momentum basis as

$$\langle g|f\rangle=\sum_{\lambda=\pm1}\int_0^{\infty}dk\,k\sum_{j=1}^{\infty}\sum_{m=-j}^{j}g^{*}_{jm\lambda}(k)f_{jm\lambda}(k). \tag{4.8}$$

The coefficients $f_{jm\lambda}(k)$ have the units of meters just as $f_\lambda(\boldsymbol{k})$.

This construction allows one to compute the representation of the angular momentum basis vector fields in $(\boldsymbol{r},t)$-space for the regular electromagnetic fields:

$$\begin{aligned}
\boldsymbol{R}_{jm\lambda}(k,\boldsymbol{r},t) &:= \sqrt{\frac{2j+1}{4\pi}}\int_0^{2\pi}d\phi\int_{-1}^{1}d(\cos\theta)\,D^{j}_{m\lambda}(\phi,\theta,0)^{*}\boldsymbol{Q}_\lambda(\boldsymbol{k},\boldsymbol{r},t) \\
&= \sqrt{\frac{c\hbar}{\epsilon_0}}\frac{k\,e^{-ikct}}{\sqrt{2}\sqrt{(2\pi)^3}}\sqrt{\frac{2j+1}{4\pi}}\int_0^{2\pi}d\phi\int_{-1}^{1}d(\cos\theta)\,D^{j}_{m\lambda}(\phi,\theta,0)^{*}\boldsymbol{e}_\lambda(\hat{\boldsymbol{k}})e^{i\boldsymbol{k}\cdot\boldsymbol{r}}.
\end{aligned} \tag{4.9}$$

Here, the integration proceeds over the polar and azimuthal angles (θ,ϕ) of the wave vector. The result of the integration is

$$\begin{aligned}
\boldsymbol{R}_{jm\lambda}(k,\boldsymbol{r},t) &= \sqrt{\frac{c\hbar}{\epsilon_0}}\frac{k\,e^{-ikct}}{\sqrt{\pi}\sqrt{2j+1}}\sum_{L=j-1}^{j+1}\sqrt{2L+1}\,i^L j_L(kr)\,C^{j\lambda}_{L0,1\lambda}\boldsymbol{Y}^{L}_{jm}(\hat{\boldsymbol{r}}) \\
&\equiv |kjm\lambda\rangle\,,
\end{aligned} \tag{4.10}$$

with Clebsch-Gordan coefficients $C^{j_3 m_3}_{j_1 m_1 j_2 m_2}$ and vector spherical harmonics as defined in [31, Sec. 7.3.1]:

$$Y^L_{jm}(\hat{\boldsymbol{r}}) = \sqrt{\frac{2L+1}{4\pi}} \sum_{\sigma=\pm1,0} \boldsymbol{e}_\sigma(\hat{\boldsymbol{z}}) D^L_{m-\sigma,0}(\phi,\theta,0)^* \, C^{jm}_{Lm-\sigma,1\sigma}. \tag{4.11}$$

The regular electromagnetic field $\boldsymbol{E}(\boldsymbol{r},t)$ can then be decomposed into the multipolar components in accordance with Eq. (4.7):

$$\boldsymbol{E}(\boldsymbol{r},t) = \int_0^\infty dk\, k \sum_{\lambda=\pm1} \sum_{j=1}^{\infty} \sum_{m=-j}^{j} f_{jm\lambda}(k) \boldsymbol{R}_{jm\lambda}(k,\boldsymbol{r},t). \tag{4.12}$$

To find the relation between constructed angular momentum basis vector fields $\boldsymbol{R}_{jm\lambda}(k,\boldsymbol{r},t)$ and the well-known usual regular electric and magnetic multipoles

$$\boldsymbol{N}_{jm}(kr,\hat{\boldsymbol{r}}) = i j_{j-1}(kr) \sqrt{\frac{j+1}{2j+1}} Y^{j-1}_{jm}(\hat{\boldsymbol{r}}) - i j_{j+1}(kr) \sqrt{\frac{j}{2j+1}} Y^{j+1}_{jm}(\hat{\boldsymbol{r}}) \tag{4.13}$$

$$\boldsymbol{M}_{jm}(kr,\hat{\boldsymbol{r}}) = j_j(kr) Y^j_{jm}(\hat{\boldsymbol{r}}) \tag{4.14}$$

one can use the expression for Clebsch-Gordan coefficients

$$C^{j\lambda}_{L0,1\lambda} = \begin{cases} \sqrt{\frac{j}{2(2j+3)}}, & \text{if } L = j+1 \\ -\frac{\lambda}{\sqrt{2}}, & \text{if } L = j \\ \sqrt{\frac{(j+1)}{2(2j-1)}}, & \text{if } L = j-1 \end{cases} \tag{4.15}$$

for $\lambda = \pm 1$. The fields $\boldsymbol{R}_{jm\lambda}(k,\boldsymbol{r},t)$ are then connected to the usual regular electric and magnetic multipoles via

$$\boxed{\begin{aligned} |kjm\lambda\rangle &\equiv \boldsymbol{R}_{jm\lambda}(k,\boldsymbol{r},t) \\ &= -\sqrt{\frac{c\hbar}{\epsilon_0}} \frac{1}{\sqrt{2\pi}} k\, i^j \Big(e^{-ikct}\, \boldsymbol{N}_{jm}(kr,\hat{\boldsymbol{r}}) + \lambda\, e^{-ikct}\, \boldsymbol{M}_{jm}(kr,\hat{\boldsymbol{r}}) \Big). \end{aligned}} \tag{4.16}$$

The corresponding inverse relations read

$$e^{-ikct}\, \boldsymbol{N}_{jm}(kr,\hat{\boldsymbol{r}}) = -\sqrt{\frac{\epsilon_0}{c\hbar}} \frac{1}{2} \Big(\boldsymbol{R}_{jm+}(k,\boldsymbol{r},t) + \boldsymbol{R}_{jm-}(k,\boldsymbol{r},t) \Big) \frac{(-i)^j \sqrt{2\pi}}{k} \tag{4.17}$$

$$e^{-ikct}\, \boldsymbol{M}_{jm}(kr,\hat{\boldsymbol{r}}) = -\sqrt{\frac{\epsilon_0}{c\hbar}} \frac{1}{2} \Big(\boldsymbol{R}_{jm+}(k,\boldsymbol{r},t) - \boldsymbol{R}_{jm-}(k,\boldsymbol{r},t) \Big) \frac{(-i)^j \sqrt{2\pi}}{k}. \tag{4.18}$$

The extra factor of k in the plane wave definition of Eq. (3.16) leads to the extra factor of k in the definition of the angular momentum basis in Eq. (4.16), contrasting with the usual definition of multipolar basis $\boldsymbol{M}$ and $\boldsymbol{N}$. This distinction guarantees that the fields $\boldsymbol{R}_{jm\lambda}(k,\boldsymbol{r},t)$ have the same transformation properties as the abstract $|kjm\lambda\rangle$ under the

action of the Poincaré group (see Sec.(4.1.3)). $\boldsymbol{R}_{jm\lambda}(k, \boldsymbol{r}, t)$ transform unitarily, in particular under Lorentz boosts, because they are unitarily connected to $\boldsymbol{Q}_\lambda(\boldsymbol{k}, \boldsymbol{r}, t)$ via Eq. (4.9), and it has already been shown that $\boldsymbol{Q}_\lambda(\boldsymbol{k}, \boldsymbol{r}, t)$ transforms unitarily under Lorentz boosts.

The next section presents the derivation of the closed-form matrix element of the Lorentz boost in the angular momentum basis. It can be used to apply Lorentz boosts directly to the regular multipolar fields, and, as it is shown later, to the irregular multipolar fields as well.

4.1.2 Matrix element of Lorentz boost

Here, the matrix element of the Lorentz boost along the z-direction in the angular momentum basis is derived. The core idea of the derivation consists in switching to the plane wave basis via Eqs. (4.1)-(4.2) and utilizing the known transformation property of the plane waves Eq. (3.20) before switching back to the angular momentum basis. The plane wave basis states $|\boldsymbol{k}\lambda\rangle$ will be referred to as $|k\theta\phi\lambda\rangle$ for convenience. First,

$$\begin{aligned} &L_z(\xi)\,|kjm\lambda\rangle = \\ &= L_z(\xi)\sqrt{\frac{2j+1}{4\pi}}\int_0^{2\pi} d\phi \int_{-1}^{1} d(\cos\theta)\, D^j_{m\lambda}(\phi,\theta,0)^*\,|k\theta\phi\lambda\rangle \\ &= \sqrt{\frac{2j+1}{4\pi}}\int_0^{2\pi} d\phi \int_{-1}^{1} d(\cos\theta)\, D^j_{m\lambda}(\phi,\theta,0)^*\,|k'\theta'\phi\lambda\rangle \end{aligned} \tag{4.19}$$

with boosted plane wave $|k'\eta'\phi\lambda\rangle$ according to Eq. (3.20). Its azimuthal angle is unchanged, the wavenumber and the polar angles are transformed according to Eqs. (2.20), (2.21):

$$\cos(\theta') = \frac{\cos(\theta)+\tanh(\xi)}{1+\cos(\theta)\tanh(\xi)} \tag{4.20}$$

$$k' = k(\cosh(\xi)+\cos(\theta)\sinh(\xi)). \tag{4.21}$$

Writing the transformed plane wave in the angular momentum basis gives

$$\begin{aligned} L_z(\xi)\,|kjm\lambda\rangle &= \sqrt{\frac{2j+1}{4\pi}}\int_0^{2\pi} d\phi \int_{-1}^{1} d(\cos\theta)\, D^j_{m\lambda}(\phi,\theta,0)^* \\ &\quad\times\sum_{j'=1}^{\infty}\sum_{m'=-j'}^{j'}\sqrt{\frac{2j'+1}{4\pi}}D^{j'}_{m\lambda}(\phi,\theta',0)\,|k'j'm\lambda\rangle \qquad (4.22) \\ &= \frac{1}{2}\int_{-1}^{1} d(\cos\theta)\sum_{j'=1}^{\infty}\sqrt{2j+1}\sqrt{2j'+1}\; d^j_{m\lambda}(\theta)d^{j'}_{m\lambda}(\theta')\,|k'j'm\lambda\rangle\,, \qquad (4.23) \end{aligned}$$

where the last step involved integration over ϕ. It is possible to write this expression in terms of the integral over wavenumber by substitution defined via Eq. (4.21):

$$L_z(\xi)\,|kjm\lambda\rangle = \frac{1}{2}\int_{ke^{-\xi}}^{ke^{\xi}}\frac{dk'}{k\sinh(\xi)}\sum_{j'=1}^{\infty}\sqrt{2j+1}\sqrt{2j'+1}\; d^j_{m\lambda}(\theta)d^{j'}_{m\lambda}(\theta')\,|k'j'm\lambda\rangle \tag{4.24}$$

$$= \frac{1}{2}\int_{ke^{-|\xi|}}^{ke^{|\xi|}}\frac{dk'}{k\sinh(|\xi|)}\sum_{j'=1}^{\infty}\sqrt{2j'+1}\sqrt{2j+1}\, d^{j'}_{m\lambda}(\theta')\, d^j_{m\lambda}(\theta)\,|k'j'm\lambda\rangle\,. \tag{4.25}$$

Both of the last equations hold for both positive and negative ξ that correspond to the movement in positive and negative z-direction. The matrix element of the Lorentz boost is defined to satisfy

$$L_z(\xi)\,|kjm\lambda\rangle = \int_0^\infty dk'\,k' \sum_{\lambda'=\pm1} \sum_{j'=1}^{\infty} \sum_{m'=-j'}^{j'} |k'j'm'\lambda'\rangle\,\langle k'j'm'\lambda'|L_z(\xi)|kjm\lambda\rangle\,. \tag{4.26}$$

Bringing Eq. (4.25) in this form leads to

$$\boxed{\langle k'j'm'\lambda'|L_z(\xi)|kjm\lambda\rangle = \delta_{\lambda'\lambda}\delta_{m'm}\Theta\big(|\xi| - |\ln(k'/k)|\big)\frac{\sqrt{2j'+1}\sqrt{2j+1}}{2k'k\sinh(|\xi|)}d^{j'}_{m\lambda}(\theta')d^{j}_{m\lambda}(\theta),} \tag{4.27}$$

with

$$\cos\theta' = \frac{k'\cosh(\xi) - k}{k'\sinh(\xi)} \tag{4.28}$$

$$\cos\theta = \frac{k' - k\cosh(\xi)}{k\sinh(\xi)}. \tag{4.29}$$

The Heaviside function

$$\Theta(x) = \begin{cases} 1, & \text{if } x \geq 0 \\ 0, & \text{if } x < 0 \end{cases} \tag{4.30}$$

accounts for the correct spectrum of boosted wave numbers $e^{-|\xi|} \leq k'/k \leq e^{|\xi|}$:

$$\int_0^\infty dk'\,\Theta\big(|\xi| - |\ln(k'/k)|\big) = \int_{ke^{-|\xi|}}^{ke^{|\xi|}} dk'. \tag{4.31}$$

Eq. (4.24) is the closed-form expression equivalent to Eq. (5.15) in [37].

Setting rapidity $\xi = 0$ in Eqs. (4.20), (4.21), (4.23) leads to

$$\begin{aligned} L_z(0)\,|kjm\lambda\rangle &= \frac{1}{2}\sqrt{2j+1}\sum_{j'=1}^{\infty}\sqrt{2j'+1}\int_{-1}^{1} d(\cos\theta)\,d^{j}_{m\lambda}(\theta)\,d^{j'}_{m\lambda}(\theta)\,|kj'm'\lambda\rangle \\ &= \sum_{j'=1}^{\infty}\delta_{j'j}\,|kj'm\lambda\rangle = |kjm\lambda\rangle\,, \end{aligned} \tag{4.32}$$

where the well-known orthogonality of small Wigner matrices is used:

$$\frac{1}{2}\sqrt{2j+1}\sqrt{2j'+1}\int_{-1}^{1} d(\cos\theta)\,d^{j}_{m\lambda}(\theta)\,d^{j'}_{m'\lambda'}(\theta) = \delta_{jj'}. \tag{4.33}$$

This validates the expected result that the zero velocity Lorentz boost acts as the identity operator.

The derived law for transformation of $|kjm\lambda\rangle$ describes the transformation properties of basis vector fields $\boldsymbol{R}_{jm\lambda}(k,\boldsymbol{r},t)$ for all space-time points $(\boldsymbol{r},t)$.

The corresponding transformation properties of the wavefunction coefficients $f_{jm\lambda}(k)$ can be derived, for example, by using Eq. (4.26)

$$L_z(\xi)\,|f\rangle = \int_0^\infty dk\,k \sum_{\lambda=\pm1}\sum_{j=1}^{\infty}\sum_{m=-j}^{j} f_{jm\lambda}(k) L_z(\xi)\,|kjm\lambda\rangle \tag{4.34}$$

$$= \int_0^\infty dk\,k \sum_{\lambda=\pm1}\sum_{j=1}^{\infty}\sum_{m=-j}^{j} f_{jm\lambda}(k) \int_0^\infty dk'\,k' \sum_{\lambda'=\pm1}\sum_{j'=1}^{\infty}\sum_{m'=-j'}^{j'} |k'j'm'\lambda'\rangle$$

$$\times\,\delta_{\lambda\lambda'}\delta_{m'm}\Theta\big(|\xi| - |\ln(k'/k)|\big)\frac{\sqrt{2j'+1}\sqrt{2j+1}}{2k'k\sinh(|\xi|)} d^{j'}_{m\lambda}(\theta')d^{j}_{m\lambda}(\theta) \tag{4.35}$$

$$= \int_0^\infty dk'\,k' \sum_{\lambda'=\pm1}\sum_{j'=1}^{\infty}\sum_{m'=-j'}^{j'} |k'j'm'\lambda'\rangle$$

$$\times \int_{k'e^{-|\xi|}}^{k'e^{|\xi|}} dk\,k \sum_{j=1}^{\infty} \frac{\sqrt{2j'+1}\sqrt{2j+1}}{2k'k\sinh(|\xi|)} d^{j'}_{m'\lambda'}(\theta')d^{j}_{m\lambda}(\theta) f_{jm'\lambda'}(k) \tag{4.36}$$

$$=: \int_0^\infty dk'\,k' \sum_{\lambda'=\pm1}\sum_{j'=1}^{\infty}\sum_{m'=-j'}^{j'} |k'j'm'\lambda'\rangle\, f'_{j'm'\lambda'}(k'), \tag{4.37}$$

with the coefficient of the transformed field $f'_{j'm'\lambda'}(k')$. After renaming primed and unprimed variables it can be written as

$$f'_{jm\lambda}(k) = \int_0^\infty dk'\,k'\,\Theta\big(|\xi| - |\ln(k/k')|\big)\frac{\sqrt{2j+1}\sqrt{2j'+1}}{2kk'\sinh(|\xi|)} d^{j}_{m\lambda}(\theta)d^{j'}_{m\lambda}(\theta') f_{\lambda'}(\boldsymbol{k}') \tag{4.38}$$

$$= \int_{ke^{-|\xi|}}^{ke^{|\xi|}} dk'\,k'\,\frac{\sqrt{2j+1}\sqrt{2j'+1}}{2kk'\sinh(|\xi|)} d^{j}_{m\lambda}(\theta)d^{j'}_{m\lambda}(\theta') f_{\lambda'}(\boldsymbol{k}'). \tag{4.39}$$

Here,

$$\cos\theta = \frac{k\cosh(\xi) - k'}{k\sinh(\xi)} \tag{4.40}$$

$$\cos\theta' = \frac{k - k'\cosh(\xi)}{k'\sinh(\xi)}. \tag{4.41}$$

Substituting k' from Eq. (4.40) gives alternative form

$$f'_\lambda(\boldsymbol{k}) = \frac{1}{2}\sqrt{2j+1}\sum_{j'=1}^{\infty}\sqrt{2j'+1}\int_{-1}^{1} d(\cos\theta)\, d^{j}_{m\lambda}(\theta)\, d^{j'}_{m\lambda}(\theta') f_{j'm\lambda}(k'), \tag{4.42}$$

with k' given by Eq. (4.40) and θ' by

$$\cos(\theta') = \frac{\cos(\theta) - \tanh(\xi)}{1 - \cos(\theta)\tanh(\xi)}. \tag{4.43}$$

Equation (4.42) can be illustrated graphically. Consider a multipolar pulse with a 50 fs Gaussian time width defined by a wavefunction $f_{jm\lambda}(k)$ with $j = 1$, $m = 1$ and $\lambda = 1$:

$$f_{111}(k) = e^{-\frac{(k-k_0)^2}{2\Delta_k}}, \tag{4.44}$$

defined on the wavenumber domain $8.72\ \mu\text{m}^{-1} \leq k \leq 9.23\ \mu\text{m}^{-1}$. The center wavelength is $\frac{2\pi}{k_0} = 700$ nm and $\frac{1}{c\Delta_k} = 50$ fs. The coefficients $f'_{j11}(k)$ of the Lorentz boosted field are computed numerically via Eq. (4.42) and depicted in Fig. (4.1). The boosted coefficients have non-zero components for all $j \in \mathbb{N}$, however, only the first 6 are plotted.

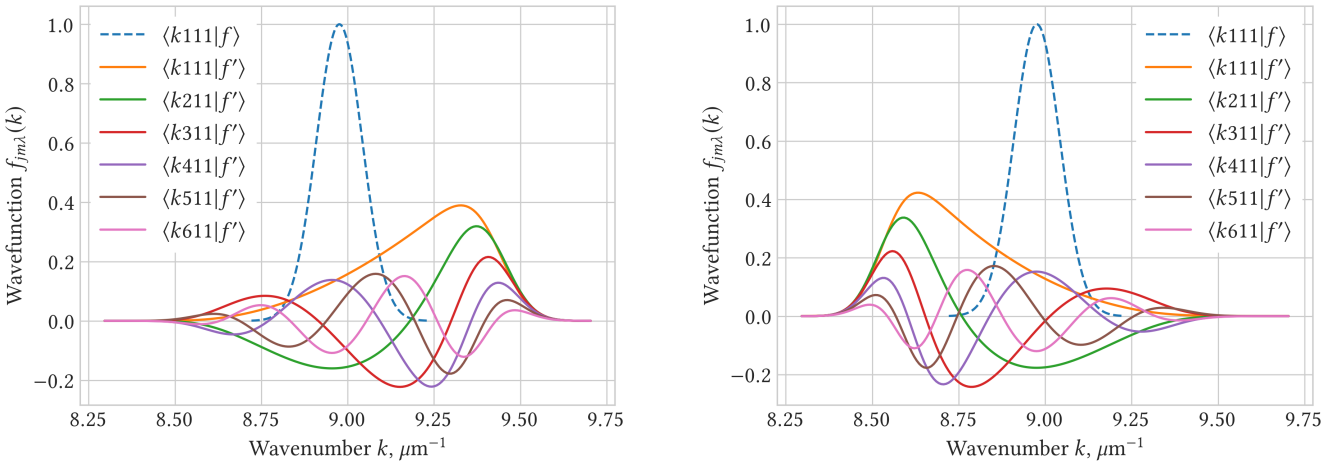

(a) (b)

Figure 4.1: Active Lorentz boost of a wave function in z-direction $|f'\rangle = L_z(\xi)\,|f\rangle$ with positive rapidity $\xi = 0.05$ (a) and negative rapidity $\xi = -0.05$ (b). The initial wave function (dashed) describes a multipolar pulse with quantum numbers $j = 1$, $m = 1$, $\lambda = 1$ and Gaussian spectral profile. The boosted coefficients $f'_{jm\lambda} = \langle jm\lambda|f'\rangle$ are shown for multipolar order up to $j = 6$. Apart from the change of the wave functions' values under the Lorentz boost one may also observe the spreading of the wave function in the wavenumber domain.

4.1.3 Complete list of transformations for $|k\,jm\lambda\rangle$ and $f_{jm\lambda}(k)$

For future reference, the complete set of transformation laws for the angular momentum basis states under the isometries of Minkowski space-time is included in this section. Apart from the Lorentz boost, these transformation properties are well-known and can be found,

for example, in [14].

$$T_t(\tau)\,|kjm\lambda\rangle = |kjm\lambda\rangle\, e^{ikc\tau} \tag{4.45}$$

$$T_z(a)\,|kjm\lambda\rangle = \sum_{j'=1}^{\infty}\sqrt{\frac{2j'+1}{2j+1}}\sum_{l=|j-j'|}^{j+j'}(2l+1)(-i)^l j_l(ak)C^{jm}_{j'm,l0}C^{j\lambda}_{j'\lambda,l0}\,|kj'm\lambda\rangle\,, \tag{4.46}$$

$$R(\alpha,\beta,\gamma)\,|kjm\lambda\rangle = \sum_{m'=-j}^{j} D^j_{m'm}(\alpha,\beta,\gamma)\,|kjm'\lambda\rangle \tag{4.47}$$

$$L_z(\xi)\,|kjm\lambda\rangle = \frac{1}{2}\sqrt{2j+1}\sum_{j'=1}^{\infty}\sqrt{2j'+1}\int_{-1}^{1} d(\cos\theta)\, d^j_{m\lambda}(\theta)\, d^{j'}_{m\lambda}(\theta')\,|k'j'm\lambda\rangle\,, \tag{4.48}$$

where θ' and k' are related to θ and k via Eqs. (4.20-4.21). $T_t(\tau)$ represents time translation by τ, $T_z(a)$ denotes translation in the positive z-direction by a, and the translation in the general direction $\hat{\boldsymbol{n}}(\alpha,\beta)$ can be described by $T_{\hat{\boldsymbol{n}}}(\xi) = R(\alpha,\beta,0)T_z(a)R^{-1}(\alpha,\beta,0)$ in the similar way as general Lorentz boosts.

The actions of parity and time reversal are given by

$$I_s\,|kjm\lambda\rangle = |kjm-\lambda\rangle\,(-1)^j \tag{4.49}$$

$$I_t\,|kjm\lambda\rangle = -\,|kj-m\lambda\rangle\,(-1)^{j+m}. \tag{4.50}$$

The corresponding rules for transformations of coefficients are

$$T_t(\tau)f_{jm\lambda}(k) = f_{jm\lambda}(k)e^{ikc\tau} \tag{4.51}$$

$$T_z(a)f_{jm\lambda}(k) = \sum_{j'=1}^{\infty}\sqrt{\frac{2j+1}{2j'+1}}\sum_{l=|j-j'|}^{j+j'}(2l+1)(-i)^l j_l(ak)C^{j'm}_{jm,l0}C^{j'\lambda}_{j\lambda,l0}\,f_{j'm\lambda}(k), \tag{4.52}$$

$$R(\alpha,\beta,\gamma)f_{jm\lambda}(k) = \sum_{m'=-j}^{j} D^j_{mm'}(\alpha,\beta,\gamma)\,f_{jm'\lambda}(k), \tag{4.53}$$

$$L_z(\xi)f_{jm\lambda}(k) = \frac{1}{2}\sqrt{2j+1}\sum_{j'=1}^{\infty}\sqrt{2j'+1}\int_{-1}^{1} d(\cos\theta)\, d^j_{m\lambda}(\theta)\, d^{j'}_{m\lambda}(\theta')f_{j'm\lambda}(k') \tag{4.54}$$

with θ' and k' given by

$$\cos(\theta') = \frac{\cos(\theta)-\tanh(\xi)}{1-\cos(\theta)\tanh(\xi)}, \tag{4.55}$$

$$k' = k\big(\cosh(\xi)-\cos(\theta)\sinh(\xi)\big). \tag{4.56}$$

The actions of parity and time reversal are

$$I_s f_{jm\lambda}(k) = f_{jm-\lambda}(k)(-1)^j \tag{4.57}$$

$$I_t f_{jm\lambda}(k) = -f^*_{j-m\lambda}(k)(-1)^{j+m}. \tag{4.58}$$

4.2 Irregular fields

The discussion has been conducted so far for regular fields, which are solutions to Maxwell's equations in the whole space without sources. It is however not sufficient to consider such fields for the complete description of electromagnetic scattering. The necessary extension contains irregular fields, which can describe electromagnetic fields that are absorbed or emitted (called incoming and outgoing). Mathematically, such fields are not defined on the whole space domain, but on a subset of it. The excluded part of the space hides singularities of functions that describe irregular fields.

4.2.1 Angular momentum basis for irregular fields $|kjm\lambda\rangle^{\text{in/out}}$

The angular momentum basis is highly convenient for the description of the incoming and outgoing fields. The extension of the regular formalism consists in considering fields similar to Eq. (4.10), with one difference in the function responsible for the radial dependence of the field. Namely, the basis for the new type of fields has spherical Hankel functions in place of the spherical Bessel functions. Here, the definition with an additional factor of $1/2$ is introduced:

$$\begin{aligned} |kjm\lambda\rangle^{\text{in/out}} &\equiv \boldsymbol{S}^{\text{in/out}}_{jm\lambda}(k,\boldsymbol{r},t) \\ &= \frac{1}{2}\sqrt{\frac{c\hbar}{\epsilon_0}}\frac{k\,e^{-ikct}}{\sqrt{\pi}\sqrt{2j+1}}\sum_{L=j-1}^{j+1}\sqrt{2L+1}\,i^L h_L^{\text{in/out}}(kr)\,C^{j\lambda}_{L0,1\lambda}\boldsymbol{Y}^L_{jm}(\hat{\boldsymbol{r}}). \end{aligned} \tag{4.59}$$

The functions $h_L^{\text{in/out}} = j_L \mp i n_L$ are spherical Hankel functions with n_L standing for spherical Neumann functions. The factor of $1/2$ in the definition of Eq. (4.59) leads to

$$\boldsymbol{S}^{\text{in}}_{jm\lambda} + \boldsymbol{S}^{\text{out}}_{jm\lambda} = \boldsymbol{R}_{jm\lambda}. \tag{4.60}$$

The convenience of defining the irregular basis field in this way will be explained in Sec. 4.2.3.

The purpose of this chapter is to prove that the basis fields in Eq. (4.59) transform under the action of the Poincaré group just as their regular counterparts do and to connect these fields to the group-theoretical formalism under the name $|kjm\lambda\rangle^{\text{in/out}} \equiv \boldsymbol{S}^{\text{in/out}}_{jm\lambda}(k,\boldsymbol{r},t)$. This will provide an important part of the theoretical foundation for polychromatic scattering.

In the monochromatic setting, the incoming/outgoing electric and magnetic multipoles are defined by substituting spherical Hankel functions of the second/first kind instead of the spherical Bessel functions in the regular multipoles in Eqs. (4.13 -4.14):

$$\boldsymbol{N}^{\text{in/out}}_{jm}(kr,\hat{\boldsymbol{r}}) = ih^{\text{in/out}}_{j-1}(kr)\sqrt{\frac{j+1}{2j+1}}\boldsymbol{Y}^{j-1}_{jm}(\hat{\boldsymbol{r}}) - ih^{\text{in/out}}_{j+1}(kr)\sqrt{\frac{j}{2j+1}}\boldsymbol{Y}^{j+1}_{jm}(\hat{\boldsymbol{r}}) \tag{4.61}$$

$$\boldsymbol{M}^{\text{in/out}}_{jm}(kr,\hat{\boldsymbol{r}}) = h^{\text{in/out}}_{j}(kr)\boldsymbol{Y}^{j}_{jm}(\hat{\boldsymbol{r}}). \tag{4.62}$$

The $|kjm\lambda\rangle^{\text{in/out}}$ can be connected to them as:

$$\boxed{\boldsymbol{S}^{\text{in/out}}_{jm\lambda}(k,\boldsymbol{r},t) = -\frac{1}{2}\sqrt{\frac{c\hbar}{\epsilon_0}}\frac{1}{\sqrt{2\pi}}\,k\,i^j\Big(e^{-ikct}\,\boldsymbol{N}^{\text{in/out}}_{jm}(kr,\hat{\boldsymbol{r}}) + \lambda\,e^{-ikct}\,\boldsymbol{M}^{\text{in/out}}_{jm}(kr,\hat{\boldsymbol{r}})\Big).} \tag{4.63}$$

The role of $\boldsymbol{M}^{\text{in/out}}$ and $\boldsymbol{N}^{\text{in/out}}$ in the context of monochromatic scattering and their connection to the theory of representations of the 3D Euclidean is discussed in [15]. One implication of this work is the fact that irregular basis states such as $\boldsymbol{S}^{\text{in/out}}_{jm\lambda}$ transform as the regular fields $\boldsymbol{R}_{jm\lambda}$ under spatial translations. It follows from the definition Eq. (4.59) that incoming and outgoing multipolar fields also transform as their regular analogs under time translation. The next section is devoted to the proof that the irregular fields $|kjm\lambda\rangle^{\text{in/out}}$ transform under Lorentz boosts as the regular $|kjm\lambda\rangle$, which will complete the picture of their transformations under all isometries of the Minkowski space-time. This result is necessary for properly connecting the T-matrix and S-matrix formalisms to the Poincaré group.

4.2.2 Lorentz boost of irregular fields

In this section, it is proved that the irregular basis vectors $\boldsymbol{S}^{\text{in/out}}_{jm\lambda}(k,\boldsymbol{r},t)$ transform under boosts in the same way as the regular basis vectors $\boldsymbol{R}_{jm\lambda}(k,\boldsymbol{r},t)$. Since the same statement holds for rotations, it is sufficient to prove the statement for Lorentz boosts in the z-direction, and the general statement will follow from the decomposition of a Lorentz boost into rotations and the Lorentz boost in the z-direction. Hence, the statement to prove is

$$\boldsymbol{S}^{\text{in/out}}_{jm\lambda}(k,\boldsymbol{r},t) \mapsto \frac{1}{2}\sqrt{2j+1}\sum_{j'=1}^{\infty}\sqrt{2j'+1}\int_{-1}^{1} d(\cos\theta)\,d^{j}_{m\lambda}(\theta)\,d^{j'}_{m\lambda}(\theta')\,\boldsymbol{S}^{\text{in/out}}_{j'm\lambda}(k',\boldsymbol{r},t), \tag{4.64}$$

which comes from Eq. (4.23) but is written in terms of irregular fields.

First, recall the definition of Lorentz boost for electromagnetic fields, which is formulated in the space-time domain and holds for electromagnetic fields of all types. Written in the form of Eq. (3.40), it implies that

$$\boldsymbol{S}^{\text{in/out}}_{jm\lambda}(k,\boldsymbol{r},t) \to \Big(\cosh(\xi)\mathbb{1} + i\lambda\sinh(\xi)\boldsymbol{e}_z\times - \frac{\sinh^2(\xi)\boldsymbol{e}_z}{\cosh(\xi)+1}\boldsymbol{e}_z\cdot\Big)\boldsymbol{S}^{\text{in/out}}_{jm\lambda}(k,\tilde{\boldsymbol{r}},\tilde{t}). \tag{4.65}$$

Lorentz boosts in the z-direction form a one-parameter Lie group, hence it is enough to prove the equality of derivatives with respect to the boost parameter ξ at zero:

$$\begin{aligned}&\partial_\xi\frac{1}{2}\sqrt{2j+1}\sum_{j'=1}^{\infty}\sqrt{2j'+1}\int_{-1}^{1} d(\cos\theta)\,d^{j}_{m\lambda}(\theta)\,d^{j'}_{m\lambda}(\theta')\,\boldsymbol{S}^{\text{in/out}}_{j'm\lambda}(k',\boldsymbol{r},t)\Big|_{\xi=0}\\ &= \partial_\xi\Big(\cosh(\xi)\mathbb{1} + i\lambda\sinh(\xi)\boldsymbol{e}_z\times - \frac{\sinh^2(\xi)\boldsymbol{e}_z}{\cosh(\xi)+1}\boldsymbol{e}_z\cdot\Big)\boldsymbol{S}^{\text{in/out}}_{jm\lambda}(k,\tilde{\boldsymbol{r}},\tilde{t})\Big|_{\xi=0}.\end{aligned} \tag{4.66}$$

The task is further simplified by the fact that regular fields already satisfy this condition. The only difference consists in the functions governing radial dependence, with spherical Hankel functions replacing spherical Bessel functions. Lengthy but straightforward calculations allow one to re-write Eq. (4.66) — as well as its counterpart for regular fields — by separating the radial and angular dependencies on both sides:

$$\begin{aligned} &rh_0^{\text{in/out}}(r)\boldsymbol{A}(\hat{\boldsymbol{r}},t) + rh_1^{\text{in/out}}(r)\boldsymbol{B}(\hat{\boldsymbol{r}},t) + \sum_{l=0}^{N} h_l^{\text{in/out}}(r)C_l(\hat{\boldsymbol{r}},t) \\ &= rh_0^{\text{in/out}}(r)\boldsymbol{A}'(\hat{\boldsymbol{r}},t) + rh_1^{\text{in/out}}(r)\boldsymbol{B}'(\hat{\boldsymbol{r}},t) + \sum_{l=0}^{N} h_l^{\text{in/out}}(r)C_l'(\hat{\boldsymbol{r}},t), \end{aligned} \tag{4.67}$$

where $\boldsymbol{A}$, $\boldsymbol{B}$, $\boldsymbol{C}$, $\boldsymbol{A}'$, $\boldsymbol{B}'$, $\boldsymbol{C}'$ are some coefficient functions, the exact form of which does not play a role in this derivation. The decomposition with primed coefficient functions corresponds to the right-hand side of Eq. (4.66) and the unprimed one to the left-hand side. N is some natural number, and for readability and without loss of generality the wavenumber k is set to 1.

Since the statement in question already holds for regular fields, the same coefficients solve the equation for spherical Bessel functions:

$$\begin{aligned} &rj_0(r)\boldsymbol{A}(\hat{\boldsymbol{r}},t) + rj_1(r)\boldsymbol{B}(\hat{\boldsymbol{r}},t) + \sum_{l=0}^{N} j_l(r)C_l(\hat{\boldsymbol{r}},t) \\ &= rj_0(r)\boldsymbol{A}'(\hat{\boldsymbol{r}},t) + rj_1(r)\boldsymbol{B}'(\hat{\boldsymbol{r}},t) + \sum_{l=0}^{N} j_l(r)C_l'(\hat{\boldsymbol{r}},t). \end{aligned} \tag{4.68}$$

Writing

$$\begin{aligned} &\sin(r)\boldsymbol{A}(\hat{\boldsymbol{r}},t) + \left(\frac{\sin(r)}{r} - \cos(r)\right)\boldsymbol{B}(\hat{\boldsymbol{r}},t) + \sum_{l=0}^{N} j_l(r)C_l(\hat{\boldsymbol{r}},t) \\ &= \sin(r)\boldsymbol{A}'(\hat{\boldsymbol{r}},t) + \left(\frac{\sin(r)}{r} - \cos(r)\right)\boldsymbol{B}'(\hat{\boldsymbol{r}},t) + \sum_{l=0}^{N} j_l(r)C_l'(\hat{\boldsymbol{r}},t) \end{aligned} \tag{4.69}$$

allows one to use the fact that the spherical Bessel functions and $\frac{\sin(r)}{r}$ vanish in the limit $r \to \infty$. Therefore, the coefficients at sin- and cos-functions must coincide: $\boldsymbol{A}(\hat{\boldsymbol{r}},t) = \boldsymbol{A}'(\hat{\boldsymbol{r}},t)$ and $\boldsymbol{B}(\hat{\boldsymbol{r}},t) = \boldsymbol{B}'(\hat{\boldsymbol{r}},t)$. Next, from

$$\sum_{l=0}^{N} j_l(r)C_l(\hat{\boldsymbol{r}},t) = \sum_{l=0}^{N} j_l(r)C_l'(\hat{\boldsymbol{r}},t) \tag{4.70}$$

and from the orthogonality of spherical Bessel functions it follows that $C_l(\hat{\boldsymbol{r}},t) = C_l'(\hat{\boldsymbol{r}},t)$ for all l. This concludes the proof that the statement in Eq. (4.67) holds for the Hankel functions as well. A similar implication also holds for any functions that satisfy the same differential equation that defines spherical Bessel functions.

4.2.3 Relation between incoming, outgoing, and regular multipolar fields

In this section the inclusion of the additional factor $1/2$ in the definition of irregular basis fields $\boldsymbol{S}^{\text{in/out}}$ is motivated, and the implications are discussed.

Consider a regular electromagnetic pulse with a Gaussian spectral profile of width Δ:

$$\boldsymbol{E}_{\text{p}}(\boldsymbol{r},t) = A\int_0^\infty dk\, k\, e^{-\frac{(k-k_0)^2}{2\Delta^2}} \boldsymbol{R}_{jm\lambda}(k,\boldsymbol{r},t), \tag{4.71}$$

with some normalization constant A. This pulse is constructed as a spectral superposition of regular basis vector fields $\boldsymbol{R}_{jm\lambda}(k,\boldsymbol{r},t)$ with some fixed j, m and λ. It can be decomposed into incoming and outgoing parts using the connection between spherical Bessel and Hankel functions $j = (h^{\text{in}} + h^{\text{out}})/2$ as

$$\boldsymbol{E}_{\text{p}}(\boldsymbol{r},t) = \boldsymbol{E}^{\text{in}}_{\text{p}}(\boldsymbol{r},t) + \boldsymbol{E}^{\text{out}}_{\text{p}}(\boldsymbol{r},t) \tag{4.72}$$

with

$$\boldsymbol{E}^{\text{in}}_{\text{p}}(\boldsymbol{r},t) = A\int_0^\infty dk\, k\, e^{-\frac{(k-k_0)^2}{2\Delta^2}} \boldsymbol{S}^{\text{in}}_{jm\lambda}(k,\boldsymbol{r},t) \tag{4.73}$$

$$\boldsymbol{E}^{\text{out}}_{\text{p}}(\boldsymbol{r},t) = A\int_0^\infty dk\, k\, e^{-\frac{(k-k_0)^2}{2\Delta^2}} \boldsymbol{S}^{\text{out}}_{jm\lambda}(k,\boldsymbol{r},t) \tag{4.74}$$

for $|\boldsymbol{r}| > 0$.

The finite length of the regular pulse $\boldsymbol{E}_p(\boldsymbol{r},t)$ allows one to define two distinct time periods: the one before the pulse initially reaches the origin at $\boldsymbol{r} = \boldsymbol{0}$ and the one after the pulse has completely traversed the origin. During the first period, the pulse is entirely composed of the incoming part:

$$\boldsymbol{E}_{\text{p}}(\boldsymbol{r},t) = \boldsymbol{E}^{\text{in}}_{\text{p}}(\boldsymbol{r},t) \tag{4.75}$$

while $\boldsymbol{E}^{\text{out}}_{\text{p}}(\boldsymbol{r},t) = 0$. On the other hand, during the second period, the pulse solely consists of the outgoing part:

$$\boldsymbol{E}_{\text{p}}(\boldsymbol{r},t) = \boldsymbol{E}^{\text{out}}_{\text{p}}(\boldsymbol{r},t) \tag{4.76}$$

while $\boldsymbol{E}^{\text{in}}_{\text{p}}(\boldsymbol{r},t) = 0$.

An illustrative example is presented in Fig. (4.2), where numerically computed values of specific Gaussian pulses are defined by Eqs. (4.71),(4.73) and (4.74) are shown. These pulses have a center wavelength of $\frac{2\pi}{k_0} = 400$ nm, Gaussian width $\Delta^{-1} = 300$ nm, total angular momentum $j = 1$, angular momentum around the z-axis $m = 1$, and helicity $\lambda = 1$. The integrals are confined to the region $5\mu\text{m}^{-1} \leq k \leq 26\ \mu\text{m}^{-1}$, covering the Gaussian profile of the wave function while excluding a negligible portion. Integration is computed using a Riemann sum with $N_k = 150$ equidistant points. The displayed space region has a radius of 6.4 μm. Points near the origin are omitted in the plots of irregular fields due to the divergence of the Hankel functions. In the scattering scenarios, the singularities will

be inside the excluded region that contains the scatterer, and the evanescent fields will be present in the near-field for the times when the object still interacts with light.

The time stamps are chosen to be within the two defined periods, where irregular pulses are either identical to the regular pulse or equal to zero. In these periods, the substitution of irregular basis fields with regular counterparts does not change the value of the total field of the pulse. This can be useful in practical applications because the spherical Bessel functions in regular fields exhibit better numerical behavior than the spherical Hankel functions [38, App. B]. The distinct separation illustrated in Fig. 4.2 does not happen for monochromatic fields. In such beams of infinite duration, the regular field at each point in time and space contains contributions from both incoming and outgoing components.

In general, the relation between regular and irregular fields that is depicted in Fig. 4.2 exists in regions of space-time when the field is known to contain only an incoming or only an outgoing part.

Now consider a general situation: given a wave function $f_{jm\lambda}(k)$ with a finite norm $\langle f|f\rangle$, then its combination with regular basis fields $\boldsymbol{R}$ represents a freely propagating physical field. When these coefficients are used in combination with outgoing basis fields $\boldsymbol{S}^{\text{out}}$, they characterize an emitted electromagnetic field that has zero values before the start of its emission and corresponds precisely with the regular field after the process responsible for emission ends. Analogously, when $f_{jm\lambda}(k)$ is combined with incoming basis fields $\boldsymbol{S}^{\text{in}}$, the resulting electromagnetic field will be the field to be absorbed in a certain time span. This field will coincide with the field generated by the same coefficients that are combined with a regular multipolar basis. After the absorption ends, the field is zero everywhere. This connection between regular and irregular fields allows one to use the scalar product Eqs. (3.31), (4.8) for emitted and absorbed fields, while initially it was defined only for regular fields. In particular, this allows computations of emitted or absorbed quantities such as energy, momentum, angular momentum, etc.

While using bra and ket notation, one should differentiate between incoming and outgoing field types sharing the same coefficients $f_{jm\lambda}(k)$ by using superscripts $|f\rangle^{\text{in}}$ or $|f\rangle^{\text{out}}$, as opposed to the regular type $|f\rangle$. Scalar product values are computed via the same formulas Eqs. (3.31), (4.8), i.e. $\langle f|g\rangle = {}^{\text{in}}\langle f|g\rangle^{\text{in}} = {}^{\text{out}}\langle f|g\rangle^{\text{out}}$ for any coefficient functions f and g. It should be emphasized that this unified formalism is universally applicable for regular, incoming, and outgoing fields due to the additional factor of $1/2$ in the proposed definition of $\boldsymbol{S}^{\text{in/out}}$. This motivates the deviation from the conventional ways of defining irregular basis fields like in [39].

4.2.4 Practical way of computing scalar product between irregular fields in finite space domain

The scalar product is defined in terms of the decomposition coefficients of electromagnetic fields, which can be obtained through experiments or numerical simulations. The step of decomposing the fields into wave functions can be bypassed by employing the formula proven in [40]:

$$\langle f|g\rangle = -\frac{i\epsilon_0}{\hbar c}\sum_{\lambda=\pm1}\int\frac{dk}{k}\int_{\partial V} d\boldsymbol{s}(\boldsymbol{r})\cdot\left[\boldsymbol{F}_\lambda(k,\boldsymbol{r})^*\times\boldsymbol{G}_\lambda(k,\boldsymbol{r})\right], \tag{4.77}$$

where it is important to note that both fields are irregular. Here, $\boldsymbol{F}_\lambda$ and $\boldsymbol{G}_\lambda$ represent the Riemann-Silberstein components of the fields, as defined in Eq. (3.12). The integration domain is the surface of a volume enclosing the sources or absorbers. The shape of this integration surface can be arbitrarily chosen, even in proximity to the radiating object, which may be particularly advantageous in simulations using software like COMSOL.

4.2.5 On the convergence regions of irregular fields

In the preceding sections, the irregular fields were generated as linear combinations of coefficient functions and irregular basis fields. Such linear combinations do not converge in the whole space. Particularly for irregular multipolar fields, the convergence region of physical fields excludes a sphere near the origin, whose radius is defined by the concrete physical situation. For example, if electromagnetic scattering is considered, then the expansion of the scattered field into the outgoing basis fields is valid outside of the sphere that encloses the scatterer [39]. Another example is the translated multipolar field of irregular type. There, the transformed field can be expanded in the irregular basis fields in the reduced region, which consists of points outside of the sphere with a radius larger by the length of the translation. One should use different expansions to describe fields inside the excluded regions. In the case of the translation of irregular fields, there is another branch of the expansion that features regular fields [41, Eq.(47ab)]. In the case of scattering, the values of the fields at points between the object and its circumscribing sphere can be evaluated with more complicated expansions [4, 5, 6, 7, 8, 9, 10]. Similarly, the Lorentz-boosted irregular electromagnetic field in Eq. (4.64) will not converge for all the $(\boldsymbol{r}, t)$ outside of the far-field branch.

Despite the occasional need for expansions with additional branches, it is crucial to note that far fields provide sufficient information to determine the field everywhere outside material objects [42, Theorems 6.9 and 6.10]. Since the wave function and the far field are bijectively connected, the knowledge of the former contains the complete information as well. It should also be noted that for a large class of physical problems, consideration of the problematic branches is not required (such as for computation of transfer of quantities between field and matter), and the far-field branch can be directly used for the solution of the problem.

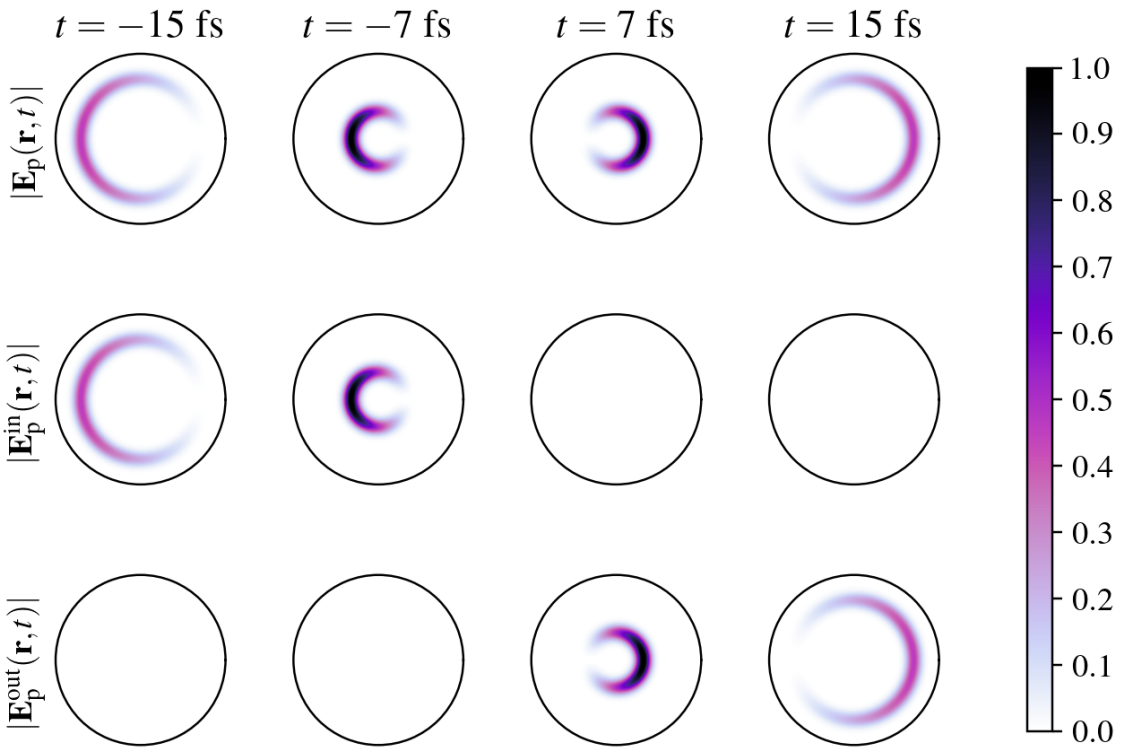

Figure 4.2: Comparison of Gaussian pulses, each with a center wavelength $\frac{2\pi}{k_0} = 400$ nm and a Gaussian width of $\Delta^{-1} = 360$ nm, constructed as spectral superpositions with the same coefficients of basis fields of different types: regular $\boldsymbol{R}_{jm\lambda}(k, \boldsymbol{r}, t)$ (top), incoming $\boldsymbol{S}^\mathrm{in}_{jm\lambda}(k, \boldsymbol{r}, t)$ (middle) and outgoing $\boldsymbol{S}^\mathrm{out}_{jm\lambda}(k, \boldsymbol{r}, t)$ (bottom), for quantum numbers $j = 1$, $m = 1$, and helicity $\lambda = 1$. The figures show the absolute values of the electric field in the zx-plane (z-axis points horizontally to the right, x-axis — vertically to the top) at different points in time. The incoming pulse is computed to be identically zero after the end of its absorption in the origin, and its values are equal to the corresponding regular field for times before the start of its absorption. Conversely, the outgoing pulse is computed to be zero before the start of its emission from the origin and is equal to the corresponding regular field for times following the end of its emission.

5 Polychromatic T-matrix and S-matrix

All the essential components are now established to define the polychromatic T-matrix. Subsequently, the polychromatic S-matrix will be introduced. Both operators contain identical information and are bijectively linked, yet they connect distinct parts of the overall electromagnetic field. The T-matrix connects the regular illumination field, referred to as the incident field, to the irregular outgoing field, referred to as the scattered field. Conversely, the S-matrix connects irregular incoming fields to irregular outgoing fields.

5.1 Polychromatic T-matrix

The usual definition of the monochromatic T-matrix [39, Sec. 5.1] is based on the fact that the total electromagnetic field outside of the sphere that encloses the scatterer can be written as a sum of the regular and outgoing multipoles. For time-harmonic fields, this is formulated as

$$\begin{aligned} \boldsymbol{E}(k,\boldsymbol{r},t) = e^{-ikct} \sum_{j=1}^{\infty} \sum_{m=-j}^{j} a_{jm}\, \boldsymbol{N}_{jm}(kr,\hat{\boldsymbol{r}}) + b_{jm}\, \boldsymbol{M}_{jm}(kr,\hat{\boldsymbol{r}}) \\ + e^{-ikct} \sum_{j=1}^{\infty} \sum_{m=-j}^{j} p_{jm}\, \boldsymbol{N}^{\mathrm{out}}_{jm}(kr,\hat{\boldsymbol{r}}) + q_{jm}\, \boldsymbol{M}^{\mathrm{out}}_{jm}(kr,\hat{\boldsymbol{r}}), \end{aligned} \tag{5.1}$$

where the convergence region for the second part of the equation consists of points outside of the smallest sphere enclosing the object. The first, regular part of Eq. (5.1) is called the incident field and the second, irregular outgoing part is called the scattered field.

In the case of a monochromatic field, the usual monochromatic T-matrix is defined as the matrix that linearly connects the coefficients of the incident and the scattered electromagnetic fields:

$$\begin{pmatrix} \vec{p} \\ \vec{q} \end{pmatrix} = T_{\mathrm{u}} \begin{pmatrix} \vec{a} \\ \vec{b} \end{pmatrix}. \tag{5.2}$$

Coefficients with arrows stand for ordered sequences $\{a_{jm}\}$, while bold letters signify vectors in 3D space. The most general linear scattering scenario, however, involves the interaction of a polychromatic field with an object. In this situation, the total field is the

spectral superposition of monochromatic fields:

$$\boldsymbol{E}(k,\boldsymbol{r},t) = \int_0^\infty dk\, e^{-ikct} \sum_{j=1}^{\infty}\sum_{m=-j}^{j} a_{jm}(k)\, \boldsymbol{N}_{jm}(kr,\hat{\boldsymbol{r}}) + b_{jm}(k)\, \boldsymbol{M}_{jm}(kr,\hat{\boldsymbol{r}}) + \int_0^\infty dk\, e^{-ikct} \sum_{j=1}^{\infty}\sum_{m=-j}^{j} p_{jm}(k)\, \boldsymbol{N}^{\text{out}}_{jm}(kr,\hat{\boldsymbol{r}}) + q_{jm}(k)\, \boldsymbol{M}^{\text{out}}_{jm}(kr,\hat{\boldsymbol{r}}). \tag{5.3}$$

The fundamental distinction from the monochromatic perspective lies in the ability of a general linear operator that connects the incident and the scattered fields to describe the coupling of different frequencies. An example of such coupling is scattering by moving scatterers: a monochromatic beam striking an object in motion will generate a scattered field with components of different frequencies. This can be seen, for example, by switching to the frame of reference of the moving object, computing the scattered field, and then boosting back to the laboratory frame using Eq. (6.37).

Continuing along the path suggested by representation theory, one can connect electric field to the wave function formulation in terms of the basis fields $\boldsymbol{R}_{jm\lambda}(k)$ and $\boldsymbol{S}^{\text{out}}_{jm\lambda}(k)$:

$$\boldsymbol{E}(\boldsymbol{r},t) = \int_0^\infty dk\, k \sum_{\lambda=\pm1}\sum_{j=1}^{\infty}\sum_{m=-j}^{j} f_{jm\lambda}(k)\, \boldsymbol{R}_{jm\lambda}(k,\boldsymbol{r},t) + \int_0^\infty dk\, k \sum_{\lambda=\pm1}\sum_{j=1}^{\infty}\sum_{m=-j}^{j} g_{jm\lambda}(k)\, \boldsymbol{S}^{\text{out}}_{jm\lambda}(k,\boldsymbol{r},t), \tag{5.4}$$

or, equivalently

$$|f\rangle + |g\rangle^{\text{out}} = \int_0^\infty dk\, k \sum_{\lambda=\pm1}\sum_{j=1}^{\infty}\sum_{m=-j}^{j} f_{jm\lambda}(k)\ |kjm\lambda\rangle \tag{5.5}$$

$$+ \int_0^\infty dk\, k \sum_{\lambda=\pm1}\sum_{j=1}^{\infty}\sum_{m=-j}^{j} g_{jm\lambda}(k)\ |kjm\lambda\rangle^{\text{out}}. \tag{5.6}$$

The coefficients f and g are connected to a and b via relations

$$f_{jm\lambda}(k) = -\sqrt{\frac{\pi\epsilon_0}{2c\hbar}}\frac{(-i)^j}{k^2}\big(a_{jm}(k) + \lambda b_{jm}(k)\big) \tag{5.7}$$

$$g_{jm\lambda}(k) = -\sqrt{\frac{2\pi\epsilon_0}{c\hbar}}\frac{(-i)^j}{k^2}\big(p_{jm}(k) + \lambda q_{jm}(k)\big), \tag{5.8}$$

which follow from Eqs. (5.4), (4.16) and (4.63). The asymmetry in relations is due to the difference in the definition of outgoing basis fields (see Sec. (4.2.1))

The crucial benefit of using f and g is the compatibility with the scalar product Eq. (4.8). In linear light-matter interactions, the coefficients of the scattered field $g_{jm\lambda}(k)$ are related

to the coefficients of the incident field $f_{jm\lambda}(k)$. The polychromatic T-matrix is defined as the linear operator mapping the regular incident field to the outgoing scattered field via

$$|g\rangle^{\text{out}} = T\,|f\rangle\,, \tag{5.9}$$

which implies for the coefficients [21]:

$$\boxed{g_{jm\lambda}(k) = \int_0^\infty dk'\,k' \sum_{\lambda'=\pm1} \sum_{j'=1}^{\infty} \sum_{m'=-j'}^{j'} T^{jm\lambda}_{j'm'\lambda'}(k,k') f_{j'm'\lambda'}(k'),} \tag{5.10}$$

where

$$T^{jm\lambda}_{j'm'\lambda'}(k,k') = {}^{\text{out}}\langle k\,jm\lambda|T|k'\,j'm'\lambda'\rangle. \tag{5.11}$$

The emergence of the factor k in the measure $\int_0^\infty dk\,k$ is dictated by the scalar product in Eq. (4.8). Also, although the integration in k is defined on the unbounded domain, this does not pose any computational limitations: physical scatterers typically only interact within specific bounded frequency ranges. Therefore, truncation of the integration domain is possible when computing the scattered field.

5.2 Monochromatic T-matrix as a special case of the polychromatic T-matrix

A significant portion of scattering processes falls into the category of frequency-preserving scattering when the frequency of the electromagnetic waves does not change throughout the light-matter interaction. Such processes can be described by polychromatic T-matrices that are diagonal in frequency. Here, it is demonstrated how T-matrices that do not mix frequencies are described as a special case of the polychromatic T-matrix. An additional focus is made on constructing the polychromatic T-matrix that is diagonal in frequency from conventional monochromatic T-matrices defined in [39].

Consider the scattering of an incident field

$$\boldsymbol{E}_{\text{inc}}(\boldsymbol{r},t) = \int_0^\infty dk\,e^{-ikct} \sum_{j=1}^{\infty} \sum_{m=-j}^{j} \boldsymbol{N}_{jm}(kr,\hat{\boldsymbol{r}})\,a_{jm}(k) + \boldsymbol{M}_{jm}(kr,\hat{\boldsymbol{r}})\,b_{jm}(k) \tag{5.12}$$

to a scattered field

$$\boldsymbol{E}_{\text{sc}}(\boldsymbol{r},t) = \int_0^\infty dk\,e^{-ikct} \sum_{j=1}^{\infty} \sum_{m=-j}^{j} \boldsymbol{N}^{\text{out}}_{jm}(kr,\hat{\boldsymbol{r}})\,p_{jm}(k) + \boldsymbol{M}^{\text{out}}_{jm}(kr,\hat{\boldsymbol{r}})\,q_{jm}(k), \tag{5.13}$$

where the incident coefficients at each frequency $\omega = kc$ are connected to the scattered coefficients of the same frequency via the usual monochromatic T-matrices

$$\begin{pmatrix}\vec{p}(k)\\ \vec{q}(k)\end{pmatrix} = T_u(k)\begin{pmatrix}\vec{a}(k)\\ \vec{b}(k)\end{pmatrix} = \begin{pmatrix}T_u^{NN}(k) & T_u^{NM}(k)\\ T_u^{MN}(k) & T_u^{MM}(k)\end{pmatrix}\begin{pmatrix}\vec{a}(k)\\ \vec{b}(k)\end{pmatrix}. \tag{5.14}$$

In accordance with Eq. (5.10), the same scattering is realized by the following polychromatic T-matrix (written in helicity basis):

$$\boxed{\begin{aligned} &T^{jm\lambda}_{j'm'\lambda'}(k,k') = \\ &\frac{1}{k'}\delta(k-k)\Big(T_u^{NN}(k')^{jm}_{j'm'} + \lambda T_u^{MN}(k')^{jm}_{j'm'} + \lambda' T_u^{NM}(k')^{jm}_{j'm'} + \lambda\lambda' T_u^{MM}(k')^{jm}_{j'm'}\Big), \end{aligned}} \tag{5.15}$$

where the Dirac delta δ is responsible for the diagonal behavior of the operator. Equation (5.15) follows from Eqs. (5.12-5.13), Eq. (5.8), and accounts for the extra factor of 2 that comes from the modified definition of the outgoing basis fields.

5.3 Polychromatic S-matrix

The S-matrix method provides a description of scattering which is equivalent to the T-matrix formalism. It is based on the decomposition of the total electromagnetic field around the scatterer into the incoming and outgoing parts [39, Eq. (5.47)]. Here, similarly to the previous section, the generalization of the usual monochromatic approach is presented. Expressing the total field as the spectral superposition of monochromatic fields

$$\begin{aligned} \boldsymbol{E}(\boldsymbol{r},t) = &\int_0^\infty dk\, e^{-ikct} \sum_{j=1}^{\infty}\sum_{m=-j}^{j} a_{jm}(k)\, \boldsymbol{N}^{\mathrm{in}}_{jm}(kr,\hat{\boldsymbol{r}}) + b_{jm}(k)\, \boldsymbol{M}^{\mathrm{in}}_{jm}(kr,\hat{\boldsymbol{r}}) \\ &+ \int_0^\infty dk\, e^{-ikct} \sum_{j=1}^{\infty}\sum_{m=-j}^{j} p_{jm}(k)\, \boldsymbol{N}^{\mathrm{out}}_{jm}(kr,\hat{\boldsymbol{r}}) + q_{jm}(k)\, \boldsymbol{M}^{\mathrm{out}}_{jm}(kr,\hat{\boldsymbol{r}}), \end{aligned} \tag{5.16}$$

one can proceed by writing the total field Eq. (5.16) in terms of $\boldsymbol{S}^{\mathrm{in/out}}_{jm\lambda}$:

$$\begin{aligned} \boldsymbol{E}(\boldsymbol{r},t) = &\int_0^\infty dk\, k \sum_{\lambda=\pm1}\sum_{j=1}^{\infty}\sum_{m=-j}^{j} f_{jm\lambda}(k)\, \boldsymbol{S}^{\mathrm{in}}_{jm\lambda}(k,\boldsymbol{r},t) \\ &+ \int_0^\infty dk\, k \sum_{\lambda=\pm1}\sum_{j=1}^{\infty}\sum_{m=-j}^{j} h_{jm\lambda}(k)\, \boldsymbol{S}^{\mathrm{out}}_{jm\lambda}(k,\boldsymbol{r},t), \end{aligned} \tag{5.17}$$

or equivalently

$$|f\rangle^{\mathrm{in}} + |h\rangle^{\mathrm{out}} = \int_0^\infty dk\, k \sum_{\lambda=\pm1}\sum_{j=1}^{\infty}\sum_{m=-j}^{j} f_{jm\lambda}(k)\ |kjm\lambda\rangle^{\mathrm{in}} \tag{5.18}$$

$$+ \int_0^\infty dk\, k \sum_{\lambda=\pm1}\sum_{j=1}^{\infty}\sum_{m=-j}^{j} h_{jm\lambda}(k)\ |kjm\lambda\rangle^{\mathrm{out}}. \tag{5.19}$$

The relation between coefficients follows from Eq. (5.16) and Eq. (4.63)

$$\boxed{\begin{aligned} f_{jm\lambda}(k) &= -\sqrt{\frac{2\pi\epsilon_0}{c\hbar}}\frac{(-i)^j}{k^2}\big(a_{jm}(k)+\lambda b_{jm}(k)\big) && (5.20)\\ h_{jm\lambda}(k) &= -\sqrt{\frac{2\pi\epsilon_0}{c\hbar}}\frac{(-i)^j}{k^2}\big(p_{jm}(k)+\lambda q_{jm}(k)\big). && (5.21)\\ & && (5.22)\end{aligned}}$$

The coefficients f and h are the wavefunctions compatible with the scalar product in Eq. (4.8).

In linear light-matter interactions, the outgoing field is linearly related to the incoming field. The polychromatic S-matrix is defined as a linear operator mapping the coefficients of the incoming field to the coefficients of the outgoing field via

$$|h\rangle^{\text{out}} = S\,|f\rangle^{\text{in}}, \tag{5.23}$$

which implies

$$\boxed{h_{jm\lambda}(k) = \int_0^\infty dk'\,k' \sum_{\lambda'=\pm1}\sum_{j'=1}^{\infty}\sum_{m'=-j'}^{j'} S^{jm\lambda}_{j'm'\lambda'}(k,k') f_{j'm'\lambda'}(k')} \tag{5.24}$$

with

$$S^{jm\lambda}_{j'm'\lambda'}(k,k') = {}^{\text{out}}\langle kjm\lambda|S|k'j'm'\lambda'\rangle^{\text{in}}. \tag{5.25}$$

The relation between the polychromatic T-matrix and S-matrix formalisms follows from decompositions of the total field Eq. (5.4) and Eq. (5.17). The T-matrix decomposition of the total field into the incident and the scattered parts can be divided into the incoming and outgoing parts as

$$|f\rangle + |g\rangle^{\text{out}} = |f\rangle^{\text{in}} + |f\rangle^{\text{out}} + |g\rangle^{\text{out}}. \tag{5.26}$$

This allows one to use the definition of the S-matrix:

$$S\,|f\rangle^{\text{in}} = |f\rangle^{\text{out}} + |g\rangle^{\text{out}} =: |h\rangle^{\text{out}}, \tag{5.27}$$

while the T-matrix maps the fields as

$$T\,|f\rangle = |g\rangle^{\text{out}}. \tag{5.28}$$

In the new convention, the wave functions of the incident and of the incoming fields are equal, namely $f_{jm\lambda}(k)$, and the wave function of the outgoing field is related to the wave functions of the incident and of the scattered fields via

$$h_{jm\lambda}(k) = f_{jm\lambda}(k) + g_{jm\lambda}(k). \tag{5.29}$$

Eqs. (5.27-5.28) determine the relation between the T-matrix and the S-matrix to be

$$\boxed{S\,|f\rangle^{\text{in}} = |f\rangle^{\text{out}} + T\,|f\rangle} \tag{5.30}$$

for arbitrary coefficients $f_{jm\lambda}(k)$. Numerically, when the elements of the T-matrix are known, the elements of the S-matrix may be computed straightforwardly using the simple relation

$$S = \mathbb{1} + T, \tag{5.31}$$

as the distinction between incident, incoming, and outgoing fields becomes relevant only when combining coefficients with corresponding basis elements to build the physical field $\boldsymbol{E}(\boldsymbol{r}, t)$.

Eq. (5.31) also allows to straightforwardly obtain results identical to Sec. 5.2 for the S-matrix which is diagonal in frequency.

Note that Eq. (5.31) deviates from a more common formula

$$S_{\text{u}} = \mathbb{1} + 2T_{\text{u}}, \tag{5.32}$$

where the subscript 'u' denotes the usual way of defining basis states. The distinction arises from the new definition of outgoing basis fields $\boldsymbol{S}^{\text{out}}_{jm\lambda}$ with additional division by 2 compared to the regular basis fields $\boldsymbol{R}_{jm\lambda}$.

6 Transfer of fundamental quantities between light and matter

6.1 Transfer of momentum and energy between a light pulse and an object

The first application example of the proposed theory concerns the interaction of electromagnetic pulses and matter at rest. In particular, the amount of energy and linear momentum transferred between a light pulse and a silicon sphere. The latter is represented with a frequency-diagonal polychromatic T-matrix defined by Eq. (5.15).

The quantities will be computed with the help of a scalar product defined by Eq. (3.31) and Eq. (4.8). The amount of fundamental physical quantities carried by the field $|f\rangle$ can be written as

$$\langle \Gamma \rangle = \langle f|\Gamma|f\rangle \,. \tag{6.1}$$

Here Γ is the Hermitian operator that corresponds to the physical quantity: generator of time translations $cP^0 = H$ for energy, generators for spatial translations P_α ($\alpha = x, y, z$) for linear momentum, and generators of rotations J_α ($\alpha = x, y, z$) for angular momentum. The core idea lies in computing the difference between the quantities contained in incoming and outgoing fields. This difference is equal to the amount of the quantity received or extracted from the object, due to the corresponding conservation law. Using the S-matrix formalism, this difference can be written as follows.

For the incoming field $|f\rangle^{\text{in}}$ and the outgoing field $|h\rangle^{\text{out}} = S\,|f\rangle^{\text{in}}$, the transferred amount $\langle \Delta\Gamma \rangle$ is [19, Eq. (3)]:

$$\langle \Delta\Gamma \rangle = {}^{\text{in}}\langle f|\Gamma|f\rangle^{\text{in}} - {}^{\text{out}}\langle h|\Gamma|h\rangle^{\text{out}} \tag{6.2}$$

$$= {}^{\text{in}}\langle f|\Gamma - S^\dagger \Gamma S|f\rangle^{\text{in}}. \tag{6.3}$$

Alternatively, in terms of the T-matrix, from Eq. (5.30):

$$\langle \Delta\Gamma \rangle = -{}^{\text{out}}\langle f|\Gamma T|f\rangle - \langle f|T^\dagger \Gamma|f\rangle^{\text{out}} - \langle f|T^\dagger \Gamma T|f\rangle. \tag{6.4}$$

The superscripts describe the correct types of the fields, however, as explained in Sec. (4.2.3), the values of the scalar products are independent of field types.

To illustrate the transfer of quantities one illuminates the sphere with a left-handed ($\lambda = +1$) circularly polarized pulse that has a Gaussian spectral profile. It is described by the wave function at positive $\cos\theta$ as

$$f_+(\boldsymbol{k}) = A\, e^{i\phi} \cos\theta(1 + \cos\theta)\, e^{-(k-k_0)^2\Delta_t^2 c^2/2}\, e^{-k^2(1-\cos^2\theta)\Delta_\rho^2/2}, \tag{6.5}$$

$$f_-(\boldsymbol{k}) = 0, \tag{6.6}$$

while set $f_\lambda(\boldsymbol{k}) = 0$ for $\cos\theta < 0$. The angles θ, ϕ are the polar and azimuthal angles of $\boldsymbol{k}$. The time width of the pulse is chosen to be $\Delta_t = 15$ fs, spacial parameter $\Delta_\rho = 1$ µm, and the central wavelength is $\frac{2\pi}{k_0} = 400$ nm. The constructed pulse is focused along the z-direction, such that the values of the coefficients that correspond to polar angles with $\cos\theta < 0.975$ are vanishingly small. This will be used for more efficient discretization of the integrals in the plane wave basis.

The normalization constant $A = 1.77 \times 10^{11}$ nm is set to fix the energy of the pulse to 5 mJ via Eq. (6.1):

$$\langle f|H|f\rangle = \sum_{\lambda=\pm1} \int \frac{d^3\boldsymbol{k}}{k} |f_\lambda(\boldsymbol{k})|^2 c\hbar k = 5.00 \times 10^{-3}\ \mathrm{J}, \tag{6.7}$$

Here and in the following, the integration over k is truncated outside of the region $14.9\ \mu\mathrm{m}^{-1} \leq k \leq 16.6\ \mu\mathrm{m}^{-1}$. At points excluded from this region, the values of the pulse are negligible (see green part of Fig. (6.2a)). The integration over wavenumber k is conducted via a Riemann sum with $N_k = 150$ points placed equidistantly. The integration over angles of the wave function is truncated to the region $\int_0^{2\pi} d\phi \int_{0.975}^{1} d(\cos\theta)$ with discretization parameters $N_\phi = 200$ and $N_{\cos\theta} = 300$. The maximal multipolar order of the sum over j is set to $j_{\max} = 2$, above which the T-matrix elements are negligible in the relevant wave number band, see Fig. (6.1).

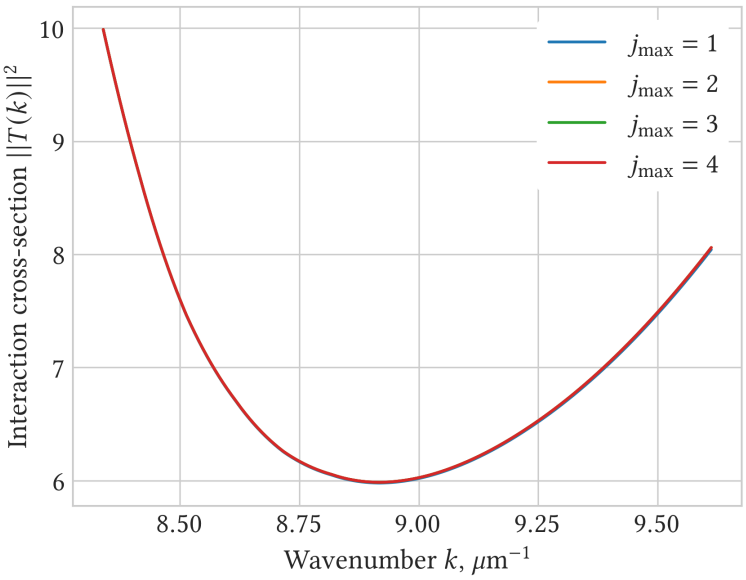

Figure 6.1: Interaction cross-section of a silicon sphere with a radius 100 nm at different wave numbers. The interaction cross-section is computed as the Frobenius norm of the monochromatic T-matrix at different truncation orders $j_{\max}$. The multipole orders higher than $j_{\max} = 2$ do not contribute to the precision significantly.

Similarly, the momentum in z-direction that is carried by the field is

$$\langle f|P_z|f\rangle = \sum_{\lambda=\pm1} \int \frac{d^3\boldsymbol{k}}{k} |f_\lambda(\boldsymbol{k})|^2 \hbar k \cos\theta = 1.66 \times 10^{-11}\ \mathrm{kg\,m\,s^{-1}}. \tag{6.8}$$

Now consider a silicon sphere of radius 100 nm that is put in the origin of the reference frame. The optical parameters of silicon [43] are depicted in Fig. (6.2a), together with the photon density per frequency $\omega = kc$ of the illumination pulse:

$$N(\omega) := \frac{\omega}{c^2} \sum_{\lambda=\pm1} \int_0^{2\pi} d\phi \int_{-1}^{1} d(\cos\theta) |f_\lambda(\boldsymbol{k})|^2. \tag{6.9}$$

To compute the transfer of the energy and of the momentum in the $|kjm\lambda\rangle$-basis, one requires the generators of the transformation laws Eqs. (4.45-4.46), which read

$$Hf_{jm\lambda}(k) = \hbar c k f_{jm\lambda}(k) \tag{6.10}$$

$$P_z f_{jm\lambda}(k) = \hbar k \sqrt{2j+1}(-1)^{m-\lambda} \sum_{j'=j-1}^{j+1} \sqrt{2j'+1} \begin{pmatrix} j & j' & 1 \\ -m & m & 0 \end{pmatrix} \begin{pmatrix} j & j' & 1 \\ -\lambda & \lambda & 0 \end{pmatrix} f_{j'm\lambda}(k). \tag{6.11}$$

Here $\begin{pmatrix} j_1 & j_2 & j_3 \\ m_1 & m_2 & m_3 \end{pmatrix}$ are the Wigner 3-j symbols. The monochromatic T-matrices of the sphere are generated for different wavenumbers for $j_{\max} = 8$ with the `treams` python package [44, 45], which is publicly available at `https://github.com/tfp-photonics/treams`, and use Eq. (6.4). The transfer of energy and momentum to the object is computed to be:

$$\langle \Delta H \rangle = 4.98 \times 10^{-5}\ \mathrm{J} \tag{6.12}$$

$$\langle \Delta P_z \rangle = 3.39 \times 10^{-13}\ \mathrm{kg\,m\,s^{-1}}. \tag{6.13}$$

A more detailed view on the transfer is provided in Fig (6.2b). The density with respect to the frequency is plotted for both energy $\langle \Delta H \rangle(\omega)$ and momentum $\langle \Delta P_z \rangle(\omega)$ transfer. The total transfer transfer is written in terms of these densities as

$$\langle \Delta H \rangle = \int_0^\infty d\omega\ \langle \Delta H \rangle(\omega) \tag{6.14}$$

$$\langle \Delta P_z \rangle = \int_0^\infty d\omega\ \langle \Delta P_z \rangle(\omega). \tag{6.15}$$

The presented method allows one to efficiently achieve accurate results by benefiting from the group-theoretical principles. In particular, from the scalar product for the wave functions Eq. (4.8), which is very easy to implement numerically using any linear algebra package. This approach differs from the alternatives that make use of Maxwell's stress tensor [46, 47]. The approach used in [47] extends the Lorenz–Mie theory to the polychromatic setting and is only applicable to spherical objects.

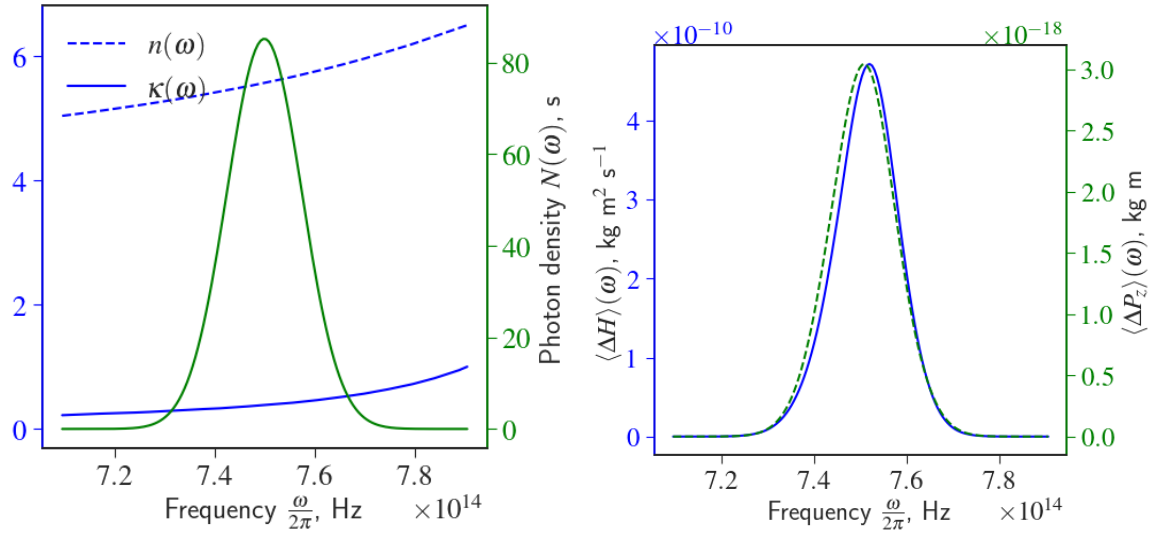

(a) (b)

Figure 6.2: (a) Photon density with respect to the frequency of the incident field (green), together with refractive index $n(\omega)$ and extinction coefficient $\kappa(\omega)$ of silicon as a function of frequency (blue). (b) Transfer of energy between the pulse and the object per frequency (blue), together with the transfer of linear momentum in z-direction from the pulse to the object per frequency (green). The total transferred quantities are the integrals of the corresponding functions.

The presented results may be straightforwardly validated by directly using the definitions of quantities that are contained in a localized field at a fixed time. For example, the energy E_{em}:

$$E_{\mathrm{em}} = \frac{\epsilon_0}{2} \int d^3\boldsymbol{r}\, |\boldsymbol{\mathcal{E}}(\boldsymbol{r},t)|^2 + |c\boldsymbol{\mathcal{B}}(\boldsymbol{r},t)|^2, \tag{6.16}$$

which can be alternatively written in terms of helicity components of the field using Eq. (3.14) and Eq. (3.4):

$$E_{\mathrm{em}} = \epsilon_0 \int d^3\boldsymbol{r}\, |\boldsymbol{F}_+(\boldsymbol{r},t) + \boldsymbol{F}_-^*(\boldsymbol{r},t)|^2. \tag{6.17}$$

Given the wave functions of the incident $f_{jm\lambda}(k)$ and the scattered field $g_{jm\lambda}(k)$, the equivalent incoming and outgoing coefficients read (see Sec. 5.3):

$$f^{\mathrm{in}}_{jm\lambda}(k) = f_{jm\lambda}(k) \tag{6.18}$$

$$f^{\mathrm{out}}_{jm\lambda}(k) = f_{jm\lambda}(k) + g_{jm\lambda}(k). \tag{6.19}$$

To get the required $\boldsymbol{F}_+(\boldsymbol{r},t)$, one combines them with the incoming and outgoing basis fields in Eq. (4.59), and using Eq. (3.14) arrives at:

$$\boldsymbol{F}^{\mathrm{in/out}}_{\lambda}(\boldsymbol{r},t) = \sqrt{2} \int_0^\infty dk\, k \sum_{j=1}^{\infty} \sum_{m=-j}^{j} \sum_{\lambda=\pm1} f^{\mathrm{in/out}}_{jm\lambda}(k) \boldsymbol{S}^{\mathrm{in/out}}_{jm\lambda}(k,\boldsymbol{r},t). \tag{6.20}$$

Again, the integrals are truncated to the region $14.9\ \mu\text{m}^{-1} \leq k \leq 16.6\ \mu\text{m}^{-1}$. Since the scatterer does not interact with the parts of the field with $j > j_{\max} = 4$, a higher multipolar component of the outgoing field will be the same as the corresponding components of the incoming field. Hence, the difference of their carried energy will be zero, and they do not contribute to the energy transfer. This allows one to focus on the transfer of energy due to $j \leq j_{\max} = 4$ components of the field.

The energy density of the $j \leq 4$ components of the incoming and the outgoing fields at specific times is depicted in Fig. (6.3).

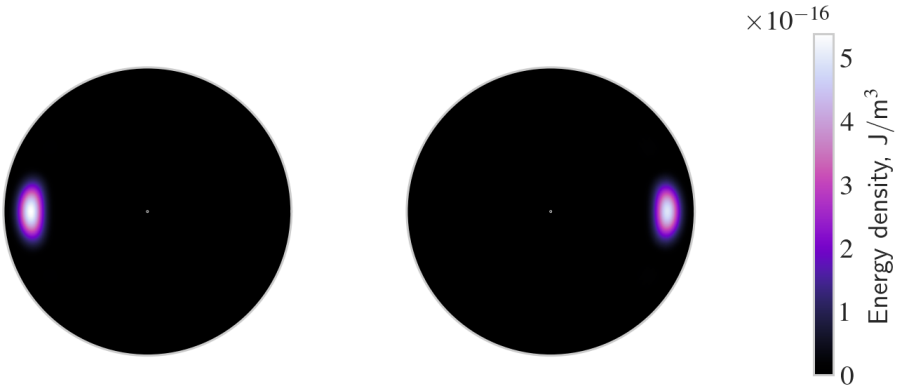

Figure 6.3: Energy density of the incoming (left) and the outgoing (right) parts of the total field for multipole order up to $j_{\max} = 8$, plotted in the zx-plane with horizontal z-axis and vertical x-axis. The radial dimension of the plot is 55 microns, the incoming field is plotted at time −150 fs and the outgoing field at time 150 fs. The white circle in the middle represents the silicon sphere of radius 100 nm.

Numerical integration of Eq. (6.17) is conducted in spherical coordinates as a Riemann sum in $r \in [0, 55]\mu\text{m}$, $\theta \in [0, \pi]$, and $\phi \in [0, 2\pi]$, for $N_r = 250$, $N_\theta = 500$ and $N_\phi = 201$ equidistant points, preceded by the integration of Eq. (6.20) over $N_k = 150$ equidistant points. The incoming field is considered at time $t = -150$ fs and the outgoing at $t = 150$ fs. The resulting energy difference is

$$E_{\text{em}}^{\text{in}} - E_{\text{em}}^{\text{out}} = 1.36061 \times 10^{-3}\text{J} - 1.31058 \times 10^{-4}\text{J} = 5.00277 \times 10^{-5}\text{J}, \tag{6.21}$$

which is in very good agreement with the value given by the scalar product approach 4.9833×10^{-5}J. The small difference can be further reduced by using finer discretization.

6.2 Interaction of a light pulse and a relativistically moving object

The foundation of the polychromatic T-matrix formalism is tightly connected to the symmetry group of the Minkowski space-time, the Poincaré group. This group includes Lorentz boosts, transformations that are responsible for changing to the frame of reference moving with constant speed. Similarly, they may be used to describe moving objects. In

this section the focus is set on the interaction between light and a moving silicon sphere, in particular on the difference of energy and momentum contained in light before and after the interaction with the object. First, the interaction is computed in the reference frame of the scatterer (the co-moving frame), and second, in the laboratory frame.

6.2.1 Co-moving frame of reference

Consider an incident field $|f\rangle$ present in the laboratory frame, defined by the wave function in plane wave basis similarly to the previous section as

$$f_+(\boldsymbol{k}) = A\, e^{i\phi} \cos\theta(1+\cos\theta)\, e^{-(k-k_0)^2\Delta_t^2 c^2/2}\, e^{-k^2(1-\cos^2\theta)\Delta_\rho^2/2}, \tag{6.22}$$

$$f_-(\boldsymbol{k}) = 0. \tag{6.23}$$

The angles θ, ϕ are the polar and azimuthal angles of $\boldsymbol{k}$. The time width of the pulse is now chosen to be $\Delta_t = 20$ fs, spacial parameter $\Delta_\rho = 1$ µm, and the central wavelength $\frac{2\pi}{k_0} = 700$ nm.

Setting the normalization constant $A = 2.095 \times 10^{11}$ nm fixes the energy of the pulse to 5 mJ via

$$\langle f|H|f\rangle = \sum_{\lambda=\pm1} \int \frac{d^3\boldsymbol{k}}{k} |f_\lambda(\boldsymbol{k})|^2 c\hbar k = 5.00 \times 10^{-3}\ \text{J}. \tag{6.24}$$

Consider the interaction of the pulse with a silicon sphere that moves along the z-axis at some constant speed $v = c\tanh\xi$ away or towards the pulse. In the co-moving frame, the object is stationary and is described by the frequency-diagonal T-matrix. Note that the scatterer perceives the incident field to be Lorentz boosted in the opposite direction $L_z(-\xi)\,|f\rangle$.

The numerical computations are conducted for the span of velocities $-0.8 \le v/c \le 0.8$ with $0.8 \approx \tanh(1.1)$, corresponding to the rapidity range between $\xi_{\text{max/min}} = \pm 1.1$. Positive v corresponds to the sphere moving in the positive z-direction, and negative v to the movement in the negative direction. Since for each velocity, the transformed field has significant components in different parts of the frequency spectrum, the maximal multipole order of the T-matrix that is required for the precise scattering simulation may change as well. This is the case when the scatterer moves toward the pulse and perceives smaller wavelengths. If the pulse in the laboratory frame is completely described on the wave number domain $k_{\min} \le k \le k_{\max}$, then the optical properties of the object should be known at least in the wave number region $e^{-\xi}k_{\min} \le k \le e^{\xi}k_{\max}$. Fig. (6.4a) depicts the optical properties of the silicon sphere on the total wave number band required for computation in the chosen range of velocities. Fig. (6.4b) illustrates the interaction cross-section of the T-matrix at different maximal multipole orders on the same domain, justifying the truncation order to be $j_{\max} = 6$.

The transfer of energy and momentum in the z-direction between the field and the object are computed in the same manner as in the stationary case in the previous section but with fields boosted in the direction opposite to the movement of the object $L_z(-\xi)\,|f\rangle$. It is important, that the wave function $|f\rangle$ is defined analytically in the plane wave basis

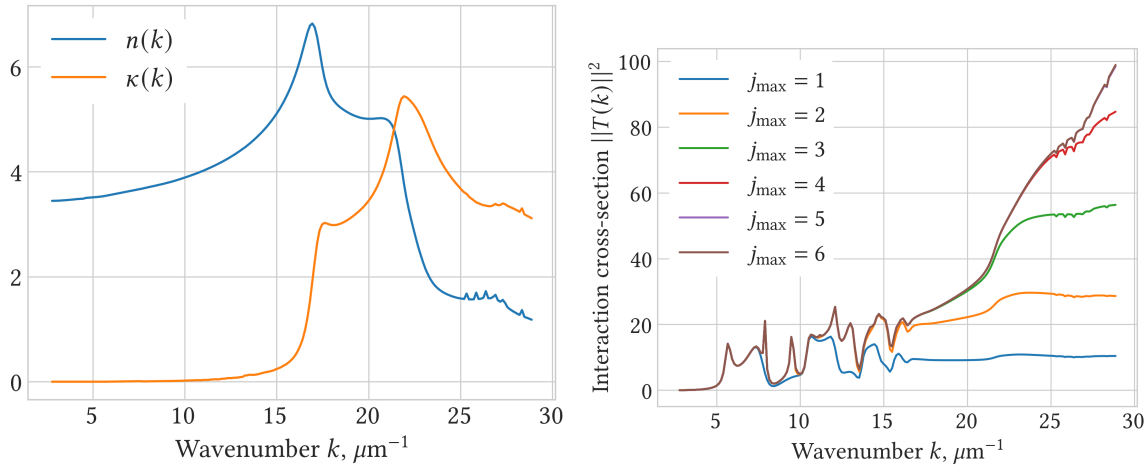

(a) (b)

Figure 6.4: (a) Refractive index $n(k)$ and extinction coefficient $\kappa(k)$ of silicon as functions of wavenumber on the whole domain required for the computation. (b) Interaction cross-section of a silicon sphere with radius of 150 nm as a function of wavenumber, computed via the Frobenius norm of the monochromatic T-matrix at different maximal multipolar orders $j_{\max}$. The brown line corresponding to $j_{\max} = 6$ completely covers the purple line of $j_{\max} = 6$, bringing no additional precision.

and has the number of significant angular momentum components which is larger than the chosen $j_{\max}$. This means that the Lorentz boost should be applied before the truncation of the maximal multipolar order in the wave function. Otherwise, significant angular momentum components of the boosted pulse will not be accounted in the scattering. Practically, using [14, Eq. (10.4-24)] one may boost fields in plane wave basis via

$$L_z(\xi) f_\lambda(\boldsymbol{k}) = f_\lambda(\boldsymbol{k}') \tag{6.25}$$

with $\boldsymbol{k}' = L_z^{-1}(\xi)\boldsymbol{k}$, which loses no information about the wave function. Only after this transformation the relevant (up to $j_{\max}$) angular momentum components $f_{jm\lambda}(k) = \langle k jm\lambda | L_\xi(z) | f \rangle$ should be extracted and considered for the interaction with the scatterer. In our convention $S = \mathbb{1} + T$, so the coefficients of the incoming field are equal to the coefficients of the incident field, and the outgoing part of the field is computed as

$$h_{jm\lambda}(k) = f_{jm\lambda}(k) + (Tf)_{jm\lambda}(k) \tag{6.26}$$

$$= f_{jm\lambda}(k) + \sum_{\lambda'=\pm1} \sum_{j'=1}^{j_{\max}} \sum_{m'=-j'}^{j'} T^{jm\lambda}_{j'm'\lambda'}(k) f_{j'm'\lambda'}(k). \tag{6.27}$$

Transfer of energy and momentum to the scatterer is computed as the difference between the quantities contained in the incoming and the outgoing parts of the field:

$$\langle \Delta H \rangle = \langle f | H | f \rangle - \langle h | H | h \rangle \tag{6.28}$$

$$\langle \Delta P_z \rangle = \langle f | P_z | f \rangle - \langle h | P_z | h \rangle \,. \tag{6.29}$$

The final results for the transfer of energy and momentum are depicted in Fig. (6.5a) and Fig. (6.5b).

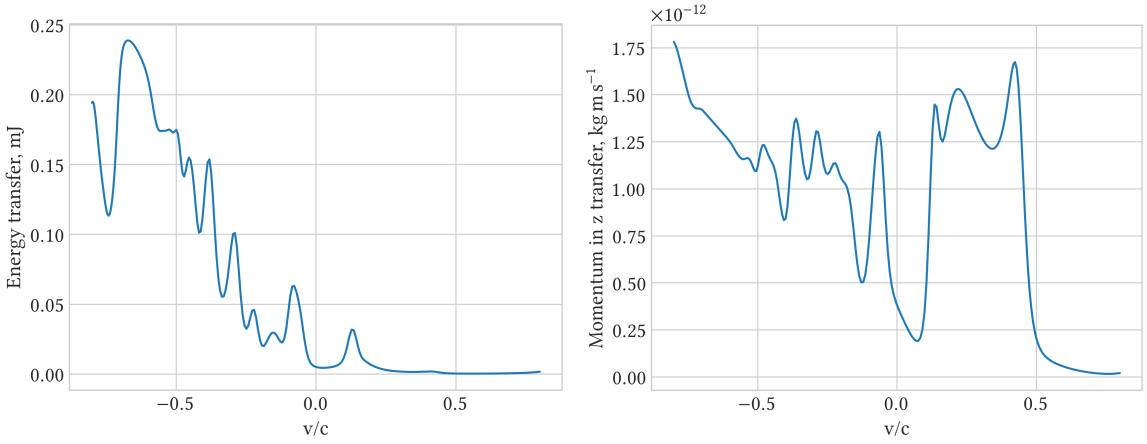

(a) (b)

Figure 6.5: Transfer of (a) energy and (b) momentum in the z-direction from the electromagnetic pulse $|f\rangle$ to the silicon sphere that moves at different velocities along the z-axis. Computed in the reference frame of the sphere. The positive sign of v/c corresponds to the movement of the sphere in the positive z-direction, when observed in the laboratory frame.

The number of equidistant discretization points for the wave function in the plane wave basis $f_\lambda(\boldsymbol{k})$ is chosen to be $N_k = 400$, $N_\phi = 100$, $N_\theta = 400$. After the transformation $L_z(\xi) f_\lambda(\boldsymbol{k})$ via Eq. (6.25), the domain stops being equidistant in k and θ. After extracting the required angular momentum components of the boosted wave function, one must make sure that the correct T-matrix is used, i.e. it corresponds to the transformed wave number domain. This allows the computation of outgoing coefficients via Eq. (6.26). The final result is evaluated for rapidities between $\xi_{\min} = -1.1$ and $\xi_{\max} = 1.1$ in equidistant steps for $N_\xi = 300$ points using

$$\langle f|H|f\rangle = \sum_{\lambda=\pm1} \int \frac{d^3\boldsymbol{k}}{k} |f_\lambda(\boldsymbol{k})|^2 c\hbar k \tag{6.30}$$

$$\langle f|P_z|f\rangle = \sum_{\lambda=\pm1} \int \frac{d^3\boldsymbol{k}}{k} |f_\lambda(\boldsymbol{k})|^2 \hbar k \cos\theta. \tag{6.31}$$

The shape of the transfer profiles in Fig. (6.5) can be explained with the help of the interaction cross-section of the silicon sphere at rest. For each Lorentz boost parameter, the center wavelength of the pulse k_0 is shifted, making the position of the new center wavelength depend on the rapidity (or, equivalently, on speed):

$$\begin{aligned} k_p &\approx k_0(\cosh(\xi) - \cos(0)\sinh(\xi)) \\ &= k_0 e^{-\xi} = k_0 e^{-\operatorname{arctanh} v/c}, \end{aligned} \tag{6.32}$$

where the approximation holds only because the incident pulse is focused along the positive z-axis. The pulse interacts with the sphere in the wave number domain around the new center wavelength, which makes the interaction stronger or weaker depending on the velocity. The interaction cross-section of the silicon sphere at each wavelength that corresponds to the boosting velocity is shown in Fig. (6.6), the resonances of which are clearly reflected in Fig. (6.5).

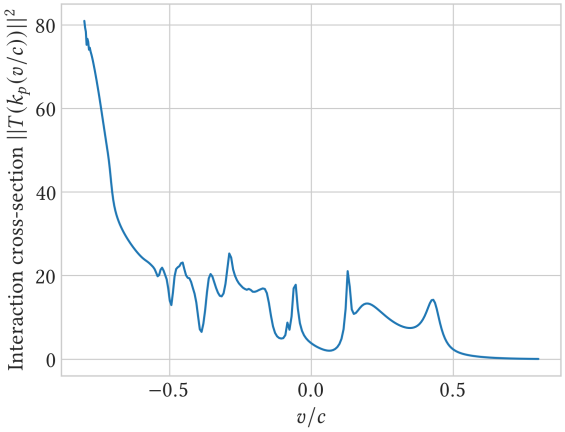

Figure 6.6: Interaction cross-section of the silicon sphere as a function of the Doppler shifted wavenumber of the pulse's peak. One may observe correspondence of some local maxima of its profile to that of the transfer profiles.

6.2.2 Laboratory frame of reference

Now the transfer of quantities is computed in the laboratory frame of reference. One may use the transformation properties of generators responsible for the corresponding quantities: $H = cP^0$ for energy and $P_z = P^3$ for momentum in the z-direction. From [14, Eq. (10.2-5)] follows

$$L_z(\xi) H L_z^{-1}(\xi) = \cosh(\xi) H - c \sinh(\xi) P_z \tag{6.33}$$

$$L_z(\xi) P_z L_z^{-1}(\xi) = -\frac{1}{c} \sinh(\xi) H + \cosh(\xi) P_z, \tag{6.34}$$

which implies the connection between the scalar product values in two frames to be

$$\langle \Delta H \rangle^{\text{lab}} = \cosh(\xi) \langle \Delta H \rangle^{\text{obj}} - c \sinh(\xi) \langle \Delta P_z \rangle^{\text{obj}} \tag{6.35}$$

$$\langle \Delta P_z \rangle^{\text{lab}} = -\frac{1}{c} \sinh(\xi) \langle \Delta H \rangle^{\text{obj}} + \cosh(\xi) \langle \Delta P_z \rangle^{\text{obj}} . \tag{6.36}$$

The values for the interaction in the laboratory frame are shown in Fig. (6.7).

An interesting effect is observed at negative v, where in the reference frame of the object the electromagnetic pulse gains energy. Together with the absorption of the energy by the object, this is accounted by the loss of the kinetic energy of the scatterer.

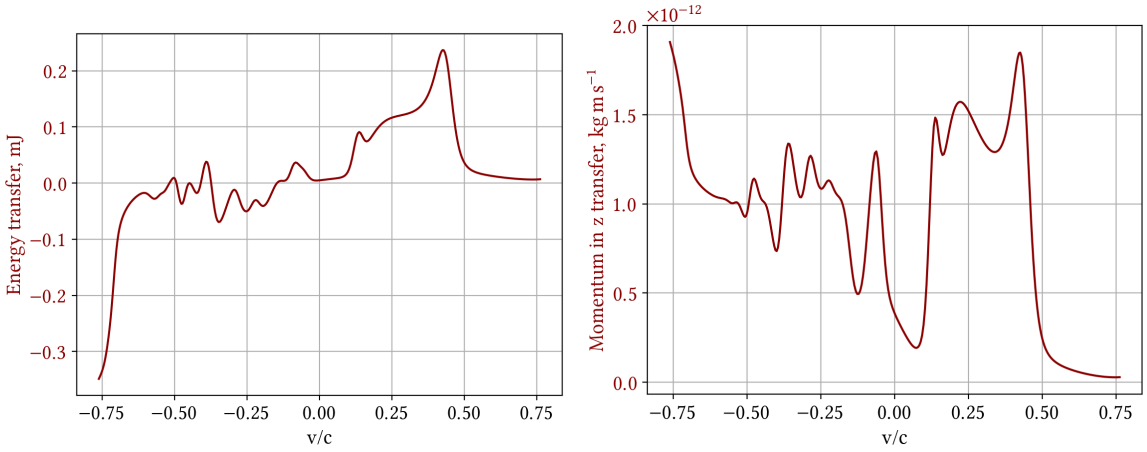

(a) (b)

Figure 6.7: Loss of (a) energy and (b) momentum in the z-direction from the electromagnetic pulse $|f\rangle$ caused by scattering on a silicon sphere that moves at different velocities along the z-axis. Computed in the reference frame of the sphere. A positive sign of v/c corresponds to the movement of the sphere in the positive z-direction.

6.2.3 Lorentz boost of a frequency-diagonal T-matrix

The scattering in the laboratory frame of reference can also be described via the boosted T-matrix, which acts on the unchanged incident field $|f\rangle$. In this section, the Lorentz boosted T-matrix of the silicon sphere is numerically computed and used to evaluate the change of momentum and energy of the pulse, as seen in the laboratory frame.

The matrix element of the Lorentz boost in the angular momentum basis, as derived in Eq. (6.37), is

$$\begin{aligned}\langle k' j' m' \lambda' | L_z(\xi) | k j m \lambda \rangle &= \\ &= \delta_{\lambda'\lambda}\delta_{m'm}\Theta\big(|\xi| - |\ln(k'/k)|\big)\frac{\sqrt{2j'+1}\sqrt{2j+1}}{2k'k\sinh(|\xi|)} d^{j'}_{m\lambda}(\theta') d^{j}_{m\lambda}(\theta),\end{aligned} \tag{6.37}$$

can be used to transform a T-matrix via $\widetilde{T} = L_z(\xi)\, T\, L_z^{-1}(\xi)$:

$$\widetilde{T}^{j_1 m_1 \lambda_1}_{j_2 m_2 \lambda_2}(k_1, k_2) = \langle k_1 j_1 m_1 \lambda_1 | L_z(\xi)\, T\, L_z^{-1}(\xi) | k_2 j_2 m_2 \lambda_2 \rangle \tag{6.38}$$

$$= \int_0^\infty dk_1'\, k_1' \int_0^\infty dk_2'\, k_2' \sum_{j_1'=1}^{\infty}\sum_{j_2'=1}^{\infty} T^{j_1' m_1 \lambda_1}_{j_2' m_2 \lambda_2}(k_1', k_2') \times \tag{6.39}$$

$$\times \frac{1}{2}\sqrt{2j_1+1}\sqrt{2j_1'+1}\,\frac{\Theta\big(|\xi| - |\ln(k_1/k_1')|\big)}{k_1 k_1' |\sinh\xi|}\, d^{j_1}_{m_1\lambda_1}(\theta_1)\, d^{j_1'}_{m_1\lambda_1}(\theta_1') \tag{6.40}$$

$$\times \frac{1}{2}\sqrt{2j_2'+1}\sqrt{2j_2+1}\,\frac{\Theta\big(|\xi| - |\ln(k_2'/k_2)|\big)}{k_2' k_2 |\sinh\xi|}\, d^{j_2'}_{m_2\lambda_2}(\theta_2')\, d^{j_2}_{m_2\lambda_2}(\theta_2). \tag{6.41}$$

Here $\theta_{1,2}$, $\theta'_{1,2}$ are defined via

$$\cos\theta_1 = \frac{k_1\cosh\xi - k'_1}{k_1\sinh\xi}, \qquad \cos\theta'_1 = \frac{k_1 - k'_1\cosh\xi}{k'_1\sinh\xi}, \tag{6.42}$$

$$\cos\theta'_2 = -\frac{k'_2\cosh\xi - k_2}{k'_2\sinh\xi}, \qquad \cos\theta_2 = -\frac{k'_2 - k_2\cosh\xi}{k_2\sinh\xi}. \tag{6.43}$$

Since the T-matrix of the sphere is diagonal in frequency, this general expression can be simplified. Using

$$T^{j_1 m_1 \lambda_1}_{j_2 m_2 \lambda_2}(k_1, k_2) = T^{j_1 m_1 \lambda_1}_{j_2 m_2 \lambda_2}(k_2)\,\frac{1}{k_2}\,\delta(k_1 - k_2), \tag{6.44}$$

the transformed T-matrix is written as

$$\begin{aligned}
&\widetilde{T}^{j_1 m_1 \lambda_1}_{j_2 m_2 \lambda_2}(k_1, k_2) = \qquad (6.45)\\
&= \int_0^\infty dk'_1\,k'_1 \int_0^\infty dk'_2\,k'_2 \sum_{j'_1=1}^{\infty}\sum_{j'_2=1}^{\infty} T^{j'_1 m_1 \lambda_1}_{j'_2 m_2 \lambda_2}(k'_2)\,\frac{1}{k'_2}\,\delta(k'_1 - k'_2)\times\\
&\times \frac{1}{2}\sqrt{2j_1+1}\sqrt{2j'_1+1}\,\frac{\Theta\big(|\xi| - |\ln(k_1/k'_1)|\big)}{k_1 k'_1|\sinh\xi|}\,d^{j_1}_{m_1\lambda_1}(\theta_1)\,d^{j'_1}_{m_1\lambda_1}(\theta'_1)\\
&\times \frac{1}{2}\sqrt{2j'_2+1}\sqrt{2j_2+1}\,\frac{\Theta\big(|\xi| - |\ln(k'_2/k_2)|\big)}{k'_2 k_2|\sinh\xi|}\,d^{j'_2}_{m_2\lambda_2}(\theta'_2)\,d^{j_2}_{m_2\lambda_2}(\theta_2). \qquad (6.46)
\end{aligned}$$

Integration over the wave number eliminates k_1, and one of the Heaviside functions truncates the integral in k_2:

$$\begin{aligned}
&\widetilde{T}^{j_1 m_1 \lambda_1}_{j_2 m_2 \lambda_2}(k_1, k_2) = \int_0^\infty dk'_2\,k'_2 \sum_{j'_1=1}^{\infty}\sum_{j'_2=1}^{\infty} T^{j'_1 m_1 \lambda_1}_{j'_2 m_2 \lambda_2}(k'_2)\times\\
&\times \frac{1}{2}\sqrt{2j_1+1}\sqrt{2j'_1+1}\,\frac{\Theta\big(|\xi| - |\ln(k_1/k'_2)|\big)}{k_1 k'_1|\sinh\xi|}\,d^{j_1}_{m_1\lambda_1}(\theta)\,d^{j'_1}_{m_1\lambda_1}(\theta')\\
&\times \frac{1}{2}\sqrt{2j'_2+1}\sqrt{2j_2+1}\,\frac{\Theta\big(|\xi| - |\ln(k'_2/k_2)|\big)}{k'_2 k_2|\sinh\xi|}\,d^{j'_2}_{m_2\lambda_2}(\theta'_2)\,d^{j_2}_{m_2\lambda_2}(\theta_2) \qquad (6.47)\\
&= \int_{k_1 e^{-|\xi|}}^{k_1 e^{|\xi|}} dk'_2\,k'_2 \sum_{j'_1=1}^{\infty}\sum_{j'_2=1}^{\infty} T^{j'_1 m_1 \lambda_1}_{j'_2 m_2 \lambda_2}(k'_2)\times\\
&\times \frac{1}{2}\sqrt{2j_1+1}\sqrt{2j'_1+1}\,\frac{1}{k_1 k'_1|\sinh\xi|}\,d^{j_1}_{m_1\lambda_1}(\theta)\,d^{j'_1}_{m_1\lambda_1}(\theta')\\
&\times \frac{1}{2}\sqrt{2j'_2+1}\sqrt{2j_2+1}\,\frac{\Theta\big(|\xi| - |\ln(k'_2/k_2)|\big)}{k'_2 k_2|\sinh\xi|}\,d^{j_2}_{m_2\lambda_2}(\theta_2)\,d^{j'_2}_{m_2\lambda_2}(\theta'_2), \qquad (6.48)
\end{aligned}$$

with

$$\cos\theta = \frac{k_1\cosh\xi - k_2'}{k_1\sinh\xi}, \qquad \cos\theta' = \frac{k_1 - k_2'\cosh\xi}{k_2'\sinh\xi},$$
$$\cos\theta_2 = -\frac{k_2' - k_2\cosh\xi}{k_2\sinh\xi}, \qquad \cos\theta_2' = -\frac{k_2'\cosh\xi - k_2}{k_2'\sinh\xi} \tag{6.49}$$

One may see that the Lorentz boost of the frequency-diagonal T-matrix of the silicon sphere makes it non-diagonal in frequency, as expected for moving objects. The element of the boosted T-matrix with $j_{1,2} = 1$, $m_{1,2} = 1$, $\lambda_{1,2} = 1$, as a function of incident wave number k_1 and scattered wave number k_2, is illustrated in Fig. (6.8). The values are computed for rapidity $\xi = 0.005$ and 0.015.

The difference of momentum between the outgoing and incoming fields is found similarly to the stationary case:

$$\langle \Delta P_z \rangle = \langle f|P_z|f\rangle - \langle h|P_z|h\rangle\,, \tag{6.50}$$

but now the computation of the outgoing field involves integration over the incident wave number:

$$h_{jm\lambda}(k) = f_{jm\lambda}(k) + \int_0^\infty dk'\,k' \sum_{\lambda'=\pm1}\sum_{j'=1}^{j_{\max}}\sum_{m'=-j'}^{j} \widetilde{T}^{jm\lambda}_{j'm'\lambda'}(k,k') f_{j'm'\lambda'}(k'). \tag{6.51}$$

The integral in k' can be truncated to the region of the significant part of the Gaussian wave number profile of f.

Finally, the transfer of momentum is computed for a number of rapidities $\xi = 0.0001$, 0.005, 0.01, 0.015, and the results are depicted in Fig. (6.9), next to the reference computed in the last section.

It should be noted that the T-matrix of the moving object has significant elements for all values of the total angular momentum $j \in \mathbb{N}$, because the interaction may happen arbitrarily far from the origin of the reference frame. Therefore, the range of the multipolar order can not be truncated without loss of the information about the scatterer as it is often done for the T-matrix of a stationary object. Practically, this means that the value of $j_{\max}$ in Eq. (6.51) is dictated by the character of the incident field. In particular, $j_{\max}$ should encompass a region around the origin large enough to completely account for the spacial domain of the interaction between the field and the scatterer. For example, consider an interaction of a localized pulse hitting a moving object when they both are near the origin of the reference frame. A smaller $j_{\max}$ is required in this case compared to the interaction of the same moving object with a pulse designed to hit the object further from the origin. Similarly, it is impossible to find a $j_{\max}$ to completely describe the interaction of a plane wave with a moving object, since there will be points in space where the interaction is happening and that are arbitrarily far from the origin.

One must note that the computation of the boosted T-matrix Eq. (6.48) is highly expensive from the computational point of view. The reason is that for each incident wavenumber k_2 and for each scattered wavenumber k_1 one must compute one integral in k, the domain of which changes with k_2 (or, alternatively, with k_1). Also, given the monochromatic

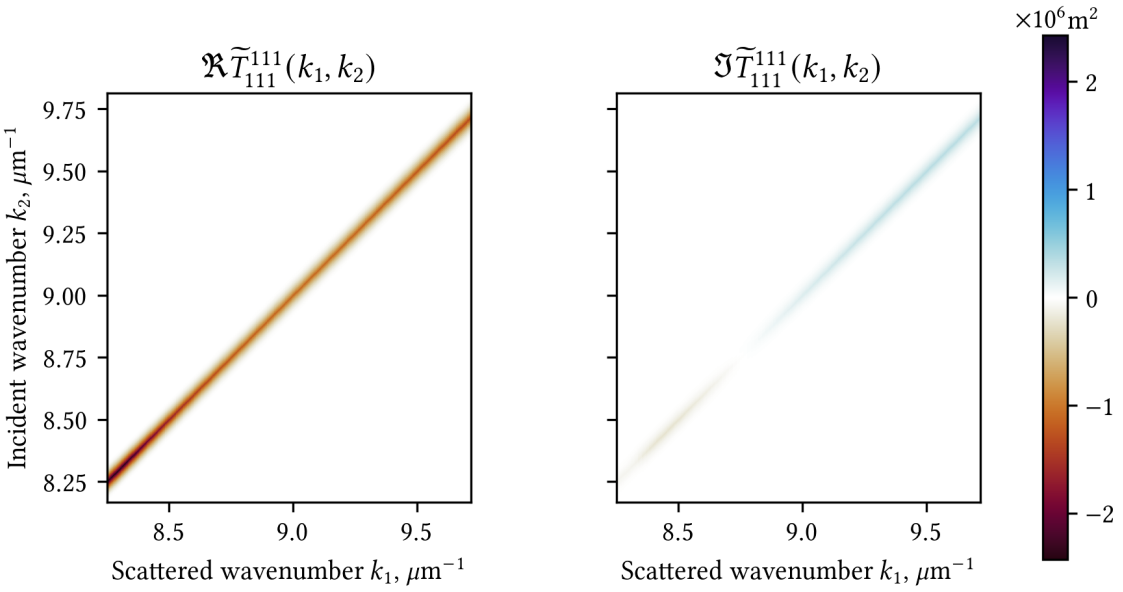

(a) $\xi = 0.005$

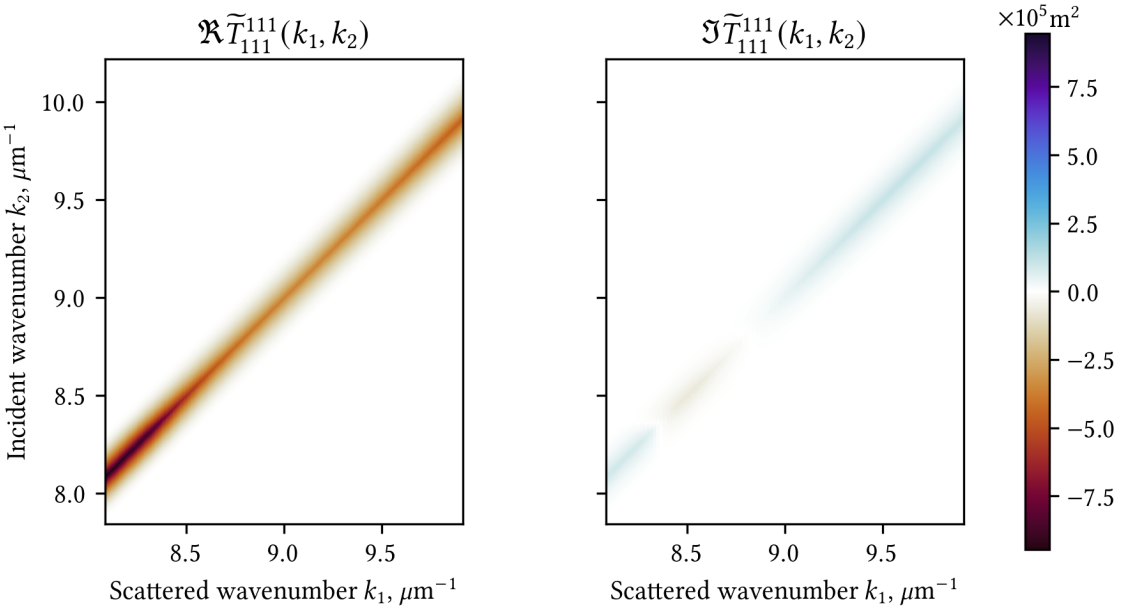

(b) $\xi = 0.015$

Figure 6.8: Real and imaginary parts of $T^{111}_{111}(k_1, k_2)$ element of the polychromatic T-matrix for the silicon sphere, boosted with (a) $\xi = 0.005$ and (b) $\xi = 0.015$. The higher the velocity, the wider the spreading of the scattered wave number for a fixed incident wave number.

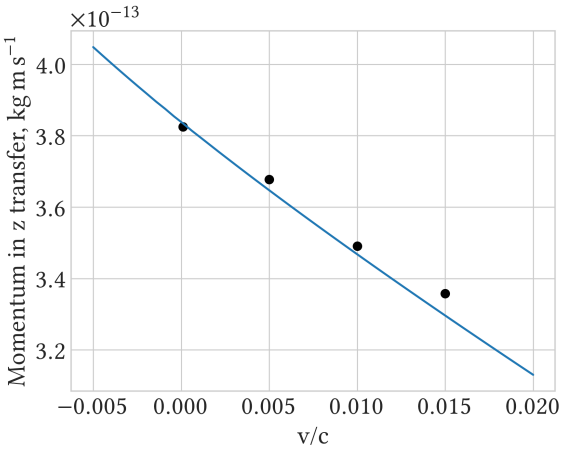

Figure 6.9: Transfer of momentum P_z between the electromagnetic pulse $|f\rangle$ and the moving silicon sphere in the laboratory frame, computed via the polychromatic T-matrix (black) and via transformed quantities from the co-moving frame (blue) as reference.

T-matrix on an initially discretized wavenumber domain, each of the mentioned integrals demands new computation or interpolation of the T-matrix on the new set of wavenumbers. Moreover, the higher the velocity of the object, the higher the multipolar order $j_{\max}$ is required to encompass the region around the origin where the interaction with the pulse takes place, which further complicates the calculations. Since computations in the co-moving frame lack the mentioned disadvantages, the object's frame should be preferred over the laboratory frame for the computation of light-matter interactions.

7 Analysis of chiral objects

The phenomenon of chirality manifests itself in a diverse array of physical phenomena, from the left-right asymmetry of weak interactions in particle physics to the chiral magnetic fields of the early universe. In practice, the ability to differentiate and select specific molecular enantiomers is crucial in fields such as pharmacology: often, chemical reactions yield both enantiomers of a chiral molecule, yet typically only one of these isomers possesses the desired medical properties. The ability to influence such reactions is another practical question.

There are also a number of theoretical questions related to chirality, one of which is the quantification of chirality. If an object is chiral, how chiral is it? And how can one quantitatively distinguish between two versions of the chiral object?

Since the T-matrix contains the complete information about the object that is relevant for its interaction with the electromagnetic field, it is convenient to formalize chirality measures as functions on the set of T-matrices. The question of how chiral is a chiral object on a scale from 0 to 1 was answered in such a manner in [26]. In the current chapter, a further development [48] is presented, which aims to answer the question: given the T-matrices of two enantiomers, how can one distinguish one from another? A label called chirality signature is proposed, and its invariance under the largest group of symmetry of Maxwell's equations is investigated.

7.1 Electromagnetic chirality

First, it is necessary to briefly explain the method introduced in [26]. The notion of chirality is re-formulated in the context of light-matter interactions with the help of a T-matrix. Its parts that are responsible for mapping between fields of definite helicity

$$T = \begin{pmatrix} T^{++} & T^{+-} \\ T^{-+} & T^{--} \end{pmatrix} \tag{7.1}$$

are considered as operators on their own, $T^{\lambda\lambda'}$. A scatterer is then said to be electromagnetically achiral if

$$\begin{aligned} T^{++} &= U_1 T^{--} V_1^\dagger \\ T^{-+} &= U_2 T^{+-} V_2^\dagger \end{aligned} \tag{7.2}$$

for some unitary $U_{1,2}$ and $V_{1,2}$. This definition may be applied to both versions of the T-matrix, the mono- and polychromatic ones.

This definition of electromagnetic chirality (em-chirality) contains the common geometric definition, which can be seen from the following considerations. A most general mirror

transformation can be decomposed into parity, rotation, and possibly translation. Parity transformation changes the eigenvalue of helicity to the opposite Eq. (4.50), while rotations and translations do not change helicity. They all, however, are represented unitarily on the domain of $T^{\lambda\lambda'}$. Hence the mirror reflection of a T-matrix can be written as

$$T = \begin{pmatrix} T^{++} & T^{+-} \\ T^{-+} & T^{--} \end{pmatrix} \mapsto T_{\text{mirr}} = \begin{pmatrix} UT^{--}U^\dagger & UT^{-+}V^\dagger \\ VT^{+-}U^\dagger & VT^{++}V^\dagger \end{pmatrix} \tag{7.3}$$

with some unitary U and V, different because the action of the transformation depends on helicity. The object defined by T is geometrically achiral if there are rotations and translations that can transform T into T_{mirr}, which can be written as

$$\begin{pmatrix} \widetilde{U}T^{++}\widetilde{U}^\dagger & \widetilde{U}T^{+-}\widetilde{V}^\dagger \\ \widetilde{V}T^{-+}\widetilde{U}^\dagger & \widetilde{V}T^{--}\widetilde{V}^\dagger \end{pmatrix} = \begin{pmatrix} UT^{--}U^\dagger & UT^{-+}V^\dagger \\ VT^{+-}U^\dagger & VT^{++}V^\dagger \end{pmatrix}, \tag{7.4}$$

where $\widetilde{U}$ and $\widetilde{V}$ are compositions of the new rotation and translation in the helicity subspaces. One may see that if Eq. (7.4) is satisfied, then Eqs. (7.2) are satisfied automatically, which means that geometrically achiral objects are electromagnetically achiral.

Since the set of all unitary transformations is larger than the set of rotations and translations, there exist electromagnetically achiral objects that are not geometrically chiral. For example, in case of polychromatic T matrix, those that fulfill Eqs. (7.2) with Lorentz transformations and not with rotations or translations.

The scalar measure of em-chirality χ was introduced in [26] to answer the question: to which degree a given scatterer is electromagnetically chiral? It is defined as

$$\chi(T) = \sqrt{\sum_k \left(\sigma_k(T^{++}) - \sigma_k(T^{--})\right)^2 + \sum_k \left(\sigma_k(T^{+-}) - \sigma_k(T^{-+})\right)^2} \tag{7.5}$$

$$=: \sqrt{|\vec{\sigma}(T^{++}) - \vec{\sigma}(T^{--})|^2 + |\vec{\sigma}(T^{+-}) - \vec{\sigma}(T^{-+})|^2}. \tag{7.6}$$

Here $\vec{\sigma}(T^{\lambda\lambda'})$ denotes the sequence of singular values of $T^{\lambda\lambda'}$. The singular value decomposition (SVD) of a compact operator is defined as

$$T^{\lambda\lambda'} = \sum_{n=1}^{\infty} \sigma_n(T^{\lambda\lambda'}) \left|\psi_n\right\rangle \left\langle\phi_n\right|,$$

with a unique sequence of non-increasing singular values $\sigma_k(T^{\lambda\lambda'})$ and two non-unique families of orthonormal vectors $|\psi_n\rangle$ and $|\phi_n\rangle$.

It is assumed that the operators in Eq. (7.6) have finite Hilbert-Schmidt norm

$$\left\|T^{\lambda\lambda'}\right\|_{\text{HS}}^2 := \int dk\, k \int dk'\, k' \sum_{jm} \sum_{j'm'} \left|T^{jm\lambda}_{j'm'\lambda'}\right|^2 < \infty, \tag{7.7}$$

for a polychromatic T-matrix, or

$$\left\|T^{\lambda\lambda'}\right\|_{\text{HS}}^2 := \sum_{jm} \sum_{j'm'} \left|T^{jm\lambda}_{j'm'\lambda'}(k,k')\right|^2 < \infty, \tag{7.8}$$

for a monochromatic one. This ensures the existence of singular value decomposition, and the following equation holds:

$$\left\|T^{\lambda\lambda'}\right\|_{\mathrm{HS}}^2 = \vec{\sigma}(T^{\lambda\lambda'}) \cdot \vec{\sigma}(T^{\lambda\lambda'}) \coloneqq \sum_{n=1}^{\infty} \sigma_n(T^{\lambda\lambda'})\sigma_n(T^{\lambda\lambda'}). \tag{7.9}$$

One may normalize the definition of scalar em-chirality $\xi(T)$ to assume values between 0 and 1 by dividing the right-hand side of Eq. (7.6) by the square root of the total interaction cross-section

$$C_{\mathrm{int}} = \sum_{\lambda,\lambda'} \left\|T^{\lambda\lambda'}\right\|_{\mathrm{HS}}^2 \tag{7.10}$$

so

$$\hat{\chi}(T) \coloneqq \frac{\chi(T)}{\sqrt{C_{\mathrm{int}}}} \in [0,1]. \tag{7.11}$$

In [48], a new interpretation of Eq. (7.6) is given, as an exemplar from the class of Procrustes problems [49]. Namely, that the scalar measure of em-chirality solves

$$\boxed{\chi(T) = \sqrt{\min_{U_1V_1}\|T^{++} - U_1T^{--}V_1^{\dagger}\|_{\mathrm{HS}}^2 + \min_{U_2V_2}\|T^{-+} - U_2T^{+-}V_2^{\dagger}\|_{\mathrm{HS}}^2},} \tag{7.12}$$

where the minimization is performed with respect to all unitary $U_{1,2}$ and $V_{1,2}$.

The proof uses von Neumann trace inequality for Hilbert-Schmidt operators [50] and proceeds as follows. First, it is shown that for any two Hilbert-Schmidt operators A and B the equation holds

$$\min_{U,V}\|A - UBV^{\dagger}\|_{\mathrm{HS}}^2 = |\vec{\sigma}(A) - \vec{\sigma}(B)|^2, \tag{7.13}$$

where U and V are unitary operators, $\vec{\sigma}(A)$ and $\vec{\sigma}(B)$ being non-increasing sequences of singular values, and $|\vec{\sigma}(A) - \vec{\sigma}(B)|^2 \coloneqq (\vec{\sigma}(A) - \vec{\sigma}(B)) \cdot (\vec{\sigma}(A) - \vec{\sigma}(B))$.

Using the Hilbert-Schmidt scalar product one re-writes the left-hand side as

$$\begin{aligned}
&\min_{U,V}\|A - UBV^{\dagger}\|_{\mathrm{HS}}^2 = && (7.14)\\
&\qquad = \min_{U,V} \langle A - UBV^{\dagger},\ A - UBV^{\dagger}\rangle && (7.15)\\
&\qquad = \min_{U,V} \left\{ \langle A, A\rangle + \langle UBV^{\dagger}, UBV^{\dagger}\rangle - \langle A, UBV^{\dagger}\rangle - \langle UBV^{\dagger}, A\rangle \right\} && (7.16)\\
&\qquad = \|A\|_{\mathrm{HS}}^2 + \|UBV^{\dagger}\|_{\mathrm{HS}}^2 - \max_{U,V} \left\{ \langle UBV^{\dagger}, A\rangle + \langle A, UBV^{\dagger}\rangle \right\} && (7.17)\\
&\qquad = \|A\|_{\mathrm{HS}}^2 + \|B\|_{\mathrm{HS}}^2 - 2\max_{U,V} \left\{\mathrm{Re}\,\langle A, UBV^{\dagger}\rangle \right\}, && (7.18)
\end{aligned}$$

and the problem reduces to maximizing $\mathrm{Re}\,\langle A, UBV^{\dagger}\rangle$. The von Neumann trace inequality for Hilbert-Schmidt operators states [50] that any two Hilbert-Schmidt operators X, Y fulfill the condition

$$\mathrm{Re}\,\langle X, Y\rangle \leq \sum_{n=1}^{\infty} \sigma_n(X)\sigma_n(Y) \tag{7.19}$$

with equality holding if and only if X and Y share singular vectors. It is always possible to find such unitary U and V that transform the singular vectors of B onto those of A by the following construction. Consider singular value decompositions of A and B:

$$A = U_a \Sigma_a V_a^\dagger \tag{7.20}$$

$$B = U_b \Sigma_b V_b^\dagger. \tag{7.21}$$

Then for

$$U \coloneqq U_a U_b^\dagger \tag{7.22}$$

$$V \coloneqq V_a V_b^\dagger \tag{7.23}$$

one gets

$$UBV^\dagger = U_a U_b^\dagger U_b \Sigma_b V_b^\dagger (V_a V_b^\dagger)^\dagger = U_a \Sigma_b V_a^\dagger, \tag{7.24}$$

which according to the von Neumann trace inequality realizes the maximal value

$$\max_{U,V} \left\{ \mathrm{Re}\, \langle A, UBV \rangle \right\} = \sum_{n=1}^{\infty} \sigma_n(A)\sigma_n(B) = \vec{\sigma}(A) \cdot \vec{\sigma}(B). \tag{7.25}$$

Now, using $\|A\|_{\mathrm{HS}}^2 = \vec{\sigma}(A) \cdot \vec{\sigma}(A) =: \vec{\sigma}^2(A)$, and, similarly $\|B\|_{\mathrm{HS}}^2 = \vec{\sigma}^2(B)$, one finally writes Eq. (7.18) as

$$\min_{U,V} \|A - UBV^\dagger\|_{\mathrm{HS}}^2 = \vec{\sigma}^2(A) + \vec{\sigma}^2(B) - 2\,\vec{\sigma}(A) \cdot \vec{\sigma}(B) \tag{7.26}$$

$$= |\vec{\sigma}(A) - \vec{\sigma}(B)|^2. \tag{7.27}$$

Application of this formula to the definition of the scalar em-chirality (7.6) results in

$$\chi^2(T) = |\vec{\sigma}(T^{++}) - \vec{\sigma}(T^{--})|^2 + |\vec{\sigma}(T^{+-}) - \vec{\sigma}(T^{-+})|^2 \tag{7.28}$$

$$= \min_{U_1 V_1} \|T^{++} - U_1 T^{--} V_1\|_{\mathrm{HS}}^2 + \min_{U_2 V_2} \|T^{-+} - U_2 T^{+-} V_2\|_{\mathrm{HS}}^2. \tag{7.29}$$

This property of em-chirality in Eq. (7.29) allows straightforward formulations of T-matrix-based scalar measures of geometrical chirality. It suffices to restrict the U_i/V_i to compositions of rotations and translations. Such an approach was studied in [51].

7.2 Chiral connectedness

Now the attention is turned towards differentiating between enantiomers. Remarkably, one can not (in general) continuously apply labels 'left-handed' and 'right-handed' to all chiral entities in a given space of objects [27, 28]. The reason is the phenomenon of chiral connectedness: if the objects under consideration are more complicated than tetrahedrons, then any chiral object can morph into its mirror image via a continuous transformation, staying chiral throughout the process [52, 53]. This means that any attempt to define a

continuous separation rule for all chiral objects, say into objects with chirality -1 (left) and +1 (right), will fail due to the intermediate value theorem [29]. There will be a point in the transformation process, where the object is chiral and the handedness will suffer a discontinuous jump.

As an example of how such an attempt can fail, consider a modification of the scalar em-chirality, where it is multiplied by a complex factor:

$$\boxed{\chi_c(T) = \hat{\chi}(T)\exp(i\phi(T)),} \tag{7.30}$$

with

$$\phi(T) := -\frac{\pi}{2}\left(\frac{\|T^{++}\|^2 + \|T^{-+}\|^2 - \|T^{+-}\|^2 - \|T^{--}\|^2}{\|T\|^2} - 1\right) \tag{7.31}$$

$$= \pi\frac{\|T^{+-}\|^2 + \|T^{--}\|^2}{\|T\|^2} \in [0,\pi]. \tag{7.32}$$

Here and in the following, the Hilbert-Schmidt norm is implied.

The absolute value of the complex em-chirality is the normalized scalar em-chirality $|\chi_c(T)| = \hat{\chi}(T)$ and the real part $\mathfrak{R}(\chi_c)$ will be referred to as the handedness measure of the scatterer.

The defining property of the phase factor consists in its behavior under arbitrary mirror transformations. The T-matrix is transformed as

$$\begin{pmatrix} T^{++} & T^{+-} \\ T^{-+} & T^{--} \end{pmatrix} \to \begin{pmatrix} \widetilde{T}^{--} & \widetilde{T}^{-+} \\ \widetilde{T}^{+-} & \widetilde{T}^{++} \end{pmatrix}, \tag{7.33}$$

where the tilde indicates a reflection of a T-suboperator, which is a unitary transformation. The permutation of suboperators is due to the change of the helicity under mirror transformations.

The phase of the complex em-chirality ϕ changes under mirror transformations according to

$$\phi(T) = \pi\frac{\|T^{+-}\|^2 + \|T^{--}\|^2}{\|T\|^2} \to \pi\frac{\|T^{-+}\|^2 + \|T^{++}\|^2}{\|T\|^2} \tag{7.34}$$

$$= \pi\frac{\|T\|^2 - \|T^{+-}\|^2 - \|T^{--}\|^2}{\|T\|^2} \tag{7.35}$$

$$= \pi - \phi(T), \tag{7.36}$$

so the mirror transformation reflects the complex em-chirality with respect to the imaginary axis

$$\hat{\chi}(T)\exp(i\phi(T)) \to \hat{\chi}(T)\exp(i(\pi - \phi(T))), \tag{7.37}$$

which changes the sign of handedness.

To illustrate the idea of chiral connectedness on a concrete example, consider a chiral constellation of 7 dielectric spheres as depicted in Fig. (7.1a). The spheres have radii

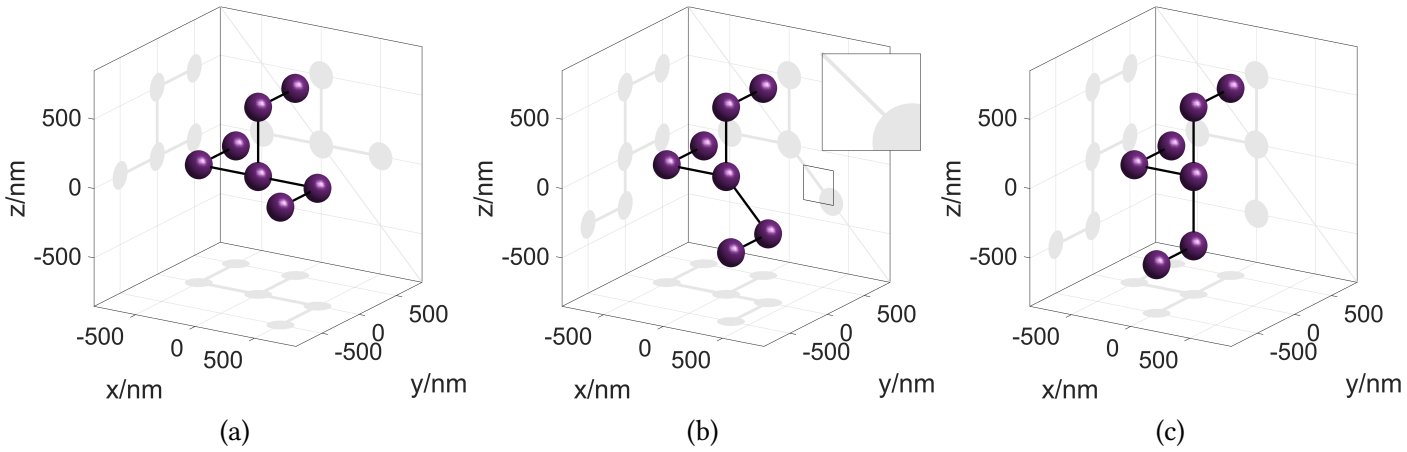

Figure 7.1: Continuous transformation of a chiral configuration of seven spheres (a) to its enantiomer (c) passing an achiral configuration (b): two spheres of the right leg are rotated by $\pi/2$ about the y-axis. The configuration (b) is achiral since it is mirror symmetric with respect to the plane $z+x=0$. The configuration (c) is the mirror antipode of the configuration (a): the mirror reflection of the initial configuration (a) with respect to the xy-plane followed by a rotation about the y-axis by $\pi/2$ results in the final configuration (c).

$r = 100$ nm, relative permittivity $\epsilon_r^s = 4$ and centered at points $(-a, a, 0)$, $(-a, 0, 0)$, $(0, 0, 0)$, $(0, 0, a)$, $(0, a, a)$, $(a, 0, 0)$ and $(a, -a, 0)$, with $a = 500$ nm.

Two transformations will be compared. In the first one, as depicted in Figs. (7.1a-7.1c), the right leg of the configuration is continuously rotated around the y-axis in the positive direction by $\pi/2$. The final state in Fig. (7.1c) is the enantiomer of the initial one in Fig. (7.1a). This can be seen by reflecting the starting configuration with respect to the xy-plane and then rotating the resulting object about the y-axis by $\pi/2$. The middle point of the transformation Fig. (7.1a) is an achiral state since the system has a mirror symmetry.

The second transformation, shown in Fig. (7.2), is designed to avoid achiral arrangements by breaking the mirror symmetry of Fig. (7.1b) while having the same starting and ending configurations as the first transformation.

Application of complex em-chirality χ_c to the T-matrix of the system at all points of the first transformation is depicted in Fig. (7.3a). The starting configuration is right-handed $\mathfrak{R}(\chi_c) < 0$ and the final configuration is left-handed $\mathfrak{R}(\chi_c) > 0$. The zero value of complex em-chirality corresponds to the arrangement of Fig. (7.1b), which is geometrically achiral because of its obvious mirror symmetry. As mentioned previously, geometrically achiral objects are electromagnetically achiral, which is the reason for vanishing χ_c.

The trajectory of complex em-chirality χ_c for the second transformation process is depicted in Fig. (7.3b). It is seen that at no point of this transformation the configuration becomes electromagnetically achiral. The existence of such transformations is guaranteed by the chiral connectedness property. If one tries to apply the introduced definition of handedness to the states of this process, the so-called "false chiral zero" arises. The point at the intersection of the trajectory with the imaginary line describes a chiral state, however the handedness can not be assigned to it since the real part of χ_c is zero. In other words, a

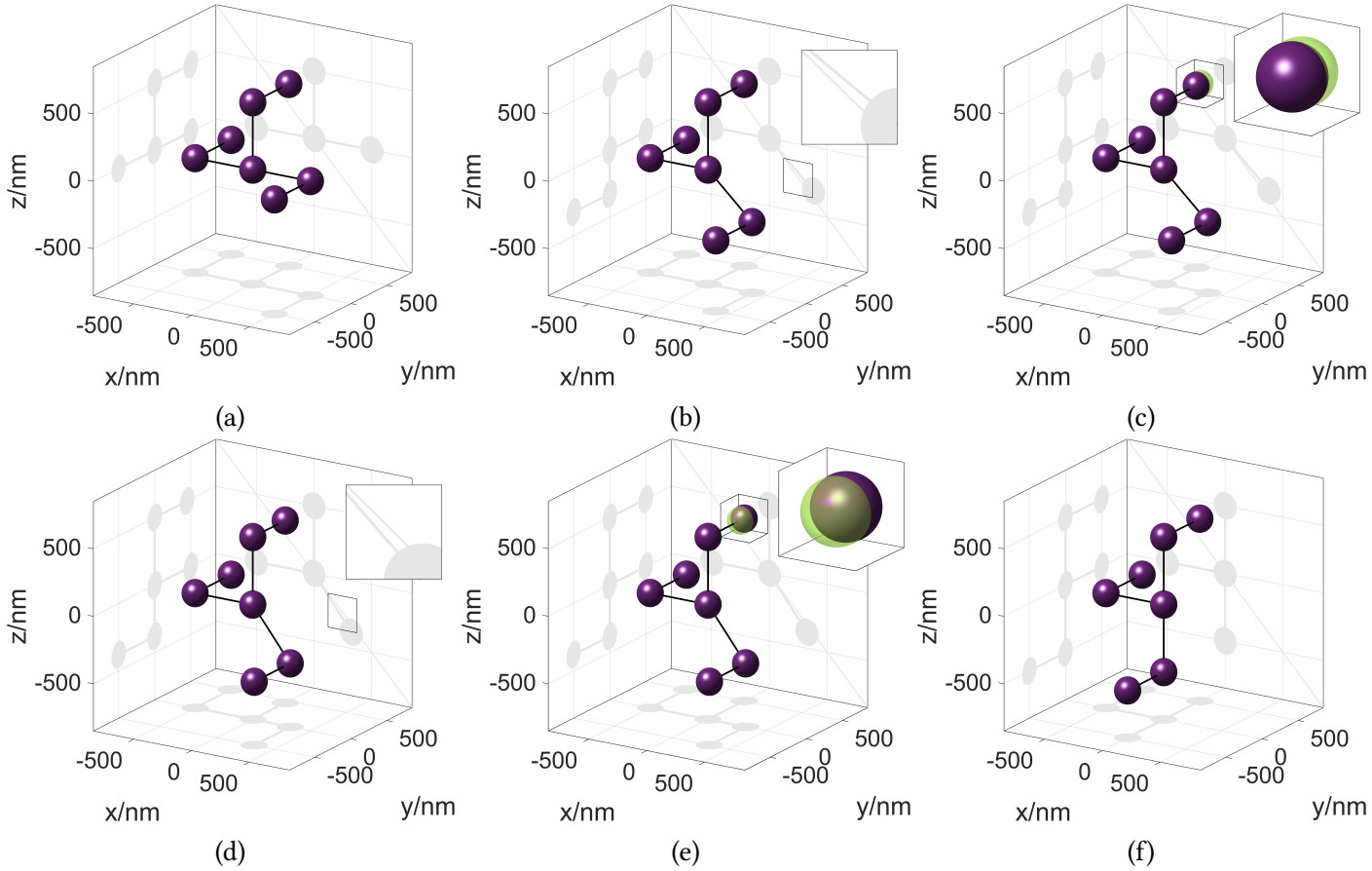

Figure 7.2: Continuous transformation of the initial chiral configuration (a) to its enantiomer (f) avoiding any intermediate achiral configurations. The transformation is similar to that of Fig. (7.1), but the achiral state Fig. (7.1b) is avoided as follows. First, the right leg is rotated about the y-axis by $9\pi/40$ (b). Then, the furthest top sphere is shifted by 50nm along the negative direction of the y-axis (c) – the transparent blue sphere depicts the position of the sphere before the shift (also enlarged in the top right corner). Then the right leg is rotated by an extra $2\pi/40$ (d). Afterwards, the shifted top sphere is brought back to its initial position (e) and finally, the right leg is rotated by the remaining $9\pi/40$ onto the final configuration. Configurations (b) and (e) are chiral, contrary to the configuration in Fig. (7.1b). This can be clearly seen in the corresponding insets containing zoomed-in versions of the shadows of the right leg on the y-z plane. In (b) and (e) here, such shadow does not coincide with the reference diagonal, breaking the mirror symmetry that can be seen in Fig. (7.1b).

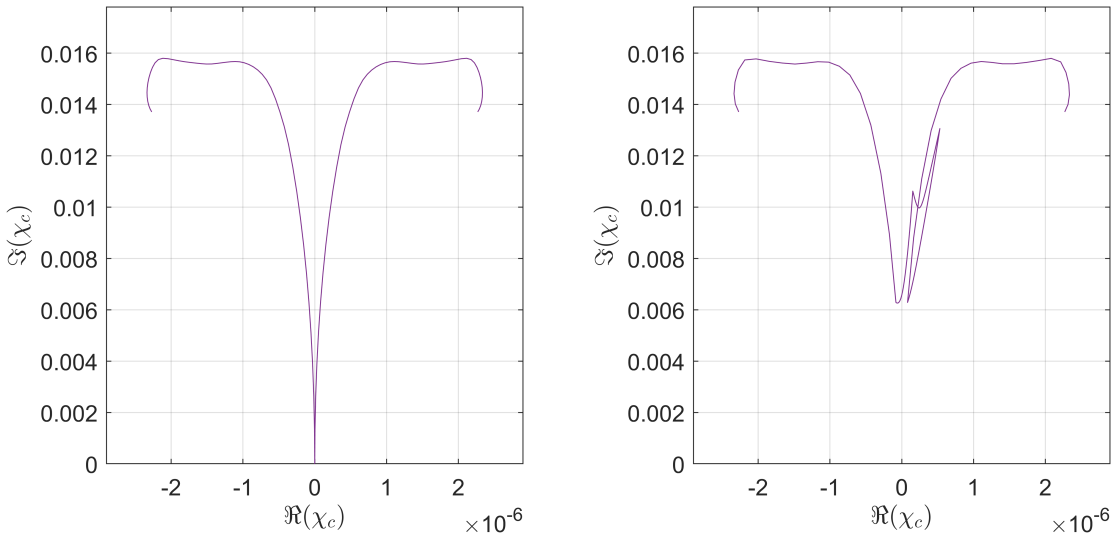

(a) (b)

Figure 7.3: Trajectories of complex em-chirality for (a) the continuous transformation that passes the achiral configuration (corresponds to Fig. (7.1)) and (b) the continuous transformation that avoids the achiral configuration (corresponds to Fig. (7.2)). The trajectories start in the left-handed region $\mathfrak{R}(\chi_c) < 0$ and end in the right-handed region $\mathfrak{R}(\chi_c) > 0$. The absolute value of χ_c equals the scalar em-chirality and the real part is the pseudoscalar handedness measure.

mirror enantiomer to the object at this point exists, which would have the same value of χ_c. It means that there are pairs of enantiomers that can not be distinguished by complex em-chirality.

In the next section, the solution to the problem of the complete description of em-chirality is provided, which will allow one to distinguish *any* pair of enantiomers by classifying objects with respect to their chirality signature.

7.3 Chirality signature

The fact that chiral unhanded states $\chi_c \neq 0$, $\mathfrak{R}(\chi_c) = 0$ exist reveals that complex em-chirality does not contain the full information about the chiral properties of an object. The complete picture would be described by a function $\chi_s(T)$ that, for an object T and its mirror antipode $\widetilde{T}$, fulfills

$$\chi_s(T) = -\chi_s(\widetilde{T}), \tag{7.38}$$

$$T \text{ is em-achiral} \Rightarrow \chi_s(T) = 0, \tag{7.39}$$

$$\chi_s(T) = 0 \Rightarrow T \text{ is em-achiral.} \tag{7.40}$$

Violation of Eq. (7.40) by the handedness part of the complex em-chirality $\mathfrak{R}(\chi_c)$ is the reason why unhanded states appeared.

Now a quantity is introduced that fulfills the properties (7.38) - (7.40). Consider the difference of the sequences of singular values

$$\vec{\chi}_1(T) \coloneqq \vec{\sigma}(T^{++}) - \vec{\sigma}(T^{--}) \tag{7.41}$$
$$\vec{\chi}_2(T) \coloneqq \vec{\sigma}(T^{+-}) - \vec{\sigma}(T^{-+}). \tag{7.42}$$

According to Eq. (7.33) and the corresponding discussion, a mirror transformation changes the sign of each element of the sequences (7.41)-(7.42):

$$\vec{\chi}_1(\widetilde{T}) = \vec{\sigma}(T^{--}) - \vec{\sigma}(T^{++}) = -\vec{\chi}_1(T) \tag{7.43}$$
$$\vec{\chi}_2(\widetilde{T}) = \vec{\sigma}(T^{-+}) - \vec{\sigma}(T^{+-}) = -\vec{\chi}_2(T). \tag{7.44}$$

Additionally, the achirality condition (7.2) is equivalent to $\vec{\chi}_1(T) = \vec{\chi}_2(T) = \vec{0}$. It follows that the properties (7.38)-(7.40) are fulfilled by the tuple

$$\boxed{\vec{\chi}_s(T) \coloneqq (\vec{\chi}_1(T), \vec{\chi}_2(T)),} \tag{7.45}$$

which is the definition of the *chirality signature*.

The scalar em-chirality (Eq. (7.6)) can be written as a function of $\vec{\chi}_s(T)$ in the following way:

$$\chi(T) = \sqrt{\vec{\chi}_1(T) \cdot \vec{\chi}_1(T) + \vec{\chi}_2(T) \cdot \vec{\chi}_2(T)}. \tag{7.46}$$

One can show that reciprocal scatterers [54, Eq. 2.22]

$$\langle \boldsymbol{k}\lambda|T|\boldsymbol{k}'\lambda'\rangle = \langle -\boldsymbol{k}'\lambda'|T|-\boldsymbol{k}\lambda\rangle\,, \tag{7.47}$$

fulfill $\vec{\sigma}(T^{+-}) - \vec{\sigma}(T^{-+}) = \vec{0}$, so the second part of the tuple is zero:

$$\vec{\chi}_2(T) = \vec{0}. \tag{7.48}$$

For this large class of objects, the chirality signature may be identified only with the sequence $\vec{\chi}_1$:

$$\boxed{\vec{\chi}_s(T) \coloneqq \vec{\sigma}(T^{--}) - \vec{\sigma}(T^{++}).} \tag{7.49}$$

Now an illustration of this definition applied to a reciprocal system is given. Consider a system from the previous section. The values of $\vec{\chi}_s(T_a)$, $\vec{\chi}_s(T_b)$ and $\vec{\chi}_s(T_c)$ are shown in Fig. (7.4), where the T-matrices correspond to the configurations described in Figs. (7.1a), (7.1b), and (7.1c).

Fig. (7.4) shows that the components of the chirality signature of enantiomeric configurations have opposite signs

$$\vec{\chi}_s(T_a) = -\vec{\chi}_s(T_c), \tag{7.50}$$

and the chirality signature of the achiral configuration has only zero components

$$\vec{\chi}_s(T_b) = \vec{0}, \tag{7.51}$$

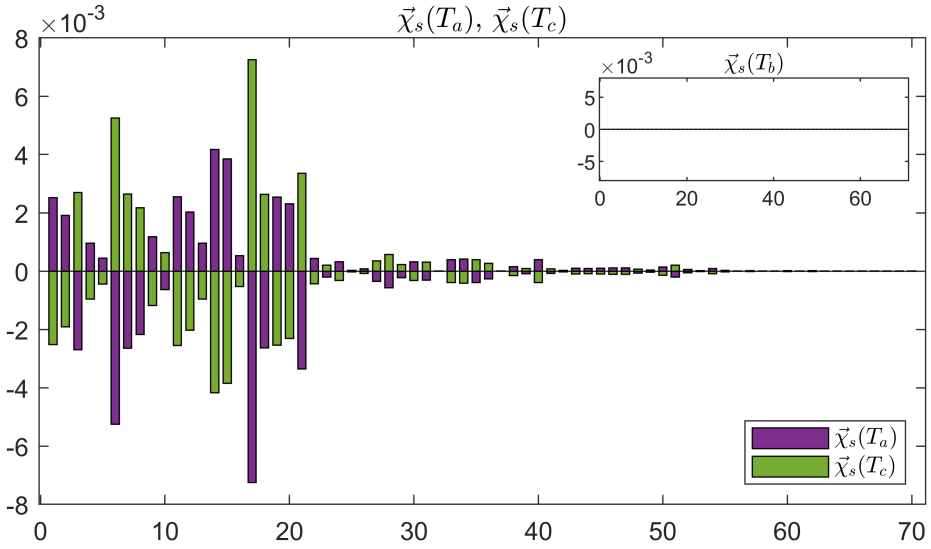

Figure 7.4: First 70 components of the chirality signature for the initial T_a, achiral T_b, and final T_c configurations from Fig. (7.1). The mirror antipodes have components of opposite signs $\vec{\chi}_s(T_a) = -\vec{\chi}_s(T_c)$, and the achiral configuration has all components equal to zero $\vec{\chi}_s(T_b) = \vec{0}$. The square root of the sum of the squares of the components equals the scalar em-chirality $\hat{\chi} = 0.014$.

as expected.

An important property of the chirality signature concerns the possibility of representing it numerically. Although there is an infinite number of components for a general T-matrix, the series of singular values can be truncated. It is well-known that for large enough values of multipolar order, the response of spatially localized scatterers vanishes. Hence, the matrices $T^{\lambda\lambda'}$ represent compact operators with singular values that converge to zero. This allows the truncation of chirality signature at some point after which the contributions to the scalar em-chirality are negligible.

Every component of $\vec{\chi}_s$ acts as an independent pseudoscalar handedness measure, which changes its sign to the opposite after a mirror transformation and is zero if the object is achiral. A single component of $\vec{\chi}_s$ may occasionally equal zero for a chiral state, producing a false chiral zero. However, only when *all* the elements of $\vec{\chi}_s$ are zero, the object is em-achiral. This provides, for the first time, a quantitative description of the infinite-dimensional nature of chirality.

It should be emphasized that the method of chirality signature fundamentally differs from the conventional approach, where enantiomers are distinguished by a single pseudoscalar such as optical rotation or circular dichroism. The values of such characteristics are typically very small and can be zero for chiral objects. An example of such characteristics was incorporated in the phase of complex em-chirality. As it is seen from Fig. (7.3), the handedness part of complex em-chirality (the real part of χ_c) is at least 3 orders of magnitude smaller than the corresponding scalar em-chirality (the absolute value of χ_c). This implies that the contribution of the selected pseudoscalar property to the chirality of the object may have very low significance for this concrete system. In fact, the handedness part of the computed χ_c is smaller than the 70'th component of the chirality signature $\vec{\chi}_s$.

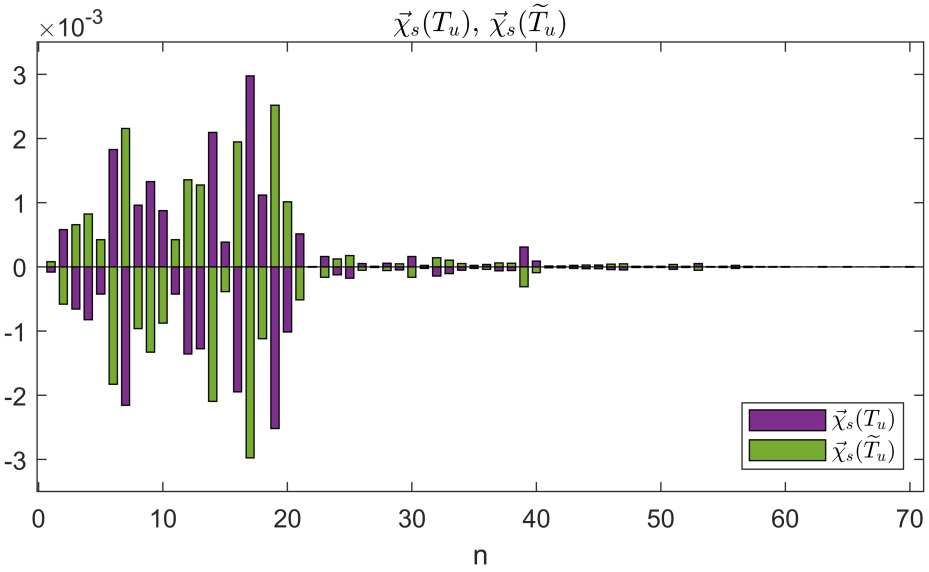

Figure 7.5: First 70 components of the chirality signature for the chiral unhanded configuration T_u, corresponding to the point with $\mathfrak{R}(\chi_c) = 0$ in Fig. (7.3b). The chirality signature of its enantiomer $\widetilde{T}_u$ has components negative to the ones of T_u. The chirality signature is able to distinguish both enantiomers, while the complex em-chirality has the same value for them both.

The proposed chirality signature, on the other hand, provides the complete description, as defined by Eqs. (7.38)-(7.40), and decomposes the scalar em-chirality into its pseudoscalar components. Since the norm of chirality signature equals the scalar em-chirality, $\vec{\chi}_s$ provides access to the most significant pseudoscalar components. These are of the same order of magnitude as the scalar em-chirality itself, as can be seen in Fig. (7.4). Hence, differentiation of enantiomers using this description may be much more stable with respect to perturbations of the geometry of the object or to uncertainties in the entries of the T-matrix.

It should be emphasized that the chirality signature allows one to continuously distinguish *any* pair of chiral enantiomers. While the conventional approach fails for the "unhanded" state T_u — the one that corresponds to the chiral unhanded state $\mathfrak{R}(\chi_c) = 0$ in Fig. (7.3b), — chirality signature provides a satisfactory description. Since the configuration of T_u is chiral, there exists its geometric enantiomer $\widetilde{T}_u$, which is a different object. But both T_u and $\widetilde{T}_u$ acquire the same value of complex em-chirality

$$\chi_c(T_u) = \chi_c(\widetilde{T}_u), \tag{7.52}$$

which means that the complex em-chirality is unable to differentiate these two enantiomers from each other. The chirality signature, on the other hand, describes both T_u and $\widetilde{T}_u$ with two different pseudovectors, as depicted in Fig. (7.5).

7.4 Conformal invariance

The conformal group of transformations is the largest symmetry group that preserves the form of Maxwell's equations [55]. It includes the ten-parameter Poincaré group (encompassing four space-time translations, three rotations, and three Lorentz boosts), along with a dilation and four special conformal transformations. In this section, it is proven that the introduced em-chirality measures, when applied to the polychromatic T-matrix, are invariant under the whole conformal group.

The first step is to prove their Poincaré invariance. When a general Poincaré transformation (denoted as X) is applied to a plane wave, the helicity λ stays unchanged [14, p. 198]:

$$X\,|\boldsymbol{k}\,\lambda\rangle = |X\boldsymbol{k}\,\lambda\rangle\, e^{-i\alpha(\boldsymbol{k},\lambda,X)}, \tag{7.53}$$

and the transformed plane wave acquires a complex phase with angle depending on the initial momentum, helicity, and parameters of the transformation. Each of the four operators $T^{\lambda\lambda'}$ also transforms independently and without changing their singular values:

$$T^{\lambda\lambda'} = \sum_k \sigma_k\, |\psi_k\rangle\, \langle\phi_k| \to \sum_k \sigma_k X\, |\psi_k\rangle\, \langle\phi_k|\, X^\dagger = \sum_k \sigma_k\, |\psi'_k\rangle\, \langle\phi'_k|\,. \tag{7.54}$$

Here, $|\psi'_k\rangle = X\,|\psi_k\rangle$ and $|\phi'_k\rangle = X\,|\phi_k\rangle$ constitute new orthonormal vector families, which follow from the unitarity of X. Since the scalar em-chirality (7.6), the complex em-chirality (7.30), and the chirality signature (7.45) are defined in terms of singular values, they are all invariant under the Poincaré transformations.

To prove the conformal invariance, one may use a statement proven in [56]. There, it is shown that the conformal group, when acting in the massless unitary irreducible representation of the Poincaré group, is represented unitarily as well. Moreover, the generators of dilation and special conformal transformations can be written in terms of generators of the Poincaré group (the equations are reproduced from the article without any changes):

$$D = \frac{1}{2}[P_0 P_k/P^2, J_{0k}]_+ \tag{7.55}$$

$$K_0 = \frac{1}{2}[P_0/P^2, J_{0k}J_{0k} + \Lambda^2 - 1/2]_+ \tag{7.56}$$

$$K_i = \frac{1}{2}[P_0/P^2, [J_{0k}, J_{ik}]_+]_+ - \frac{1}{2}[P_i/P^2, J_{0k}J_{0k} + \Lambda^2 - 1/2]_+, \tag{7.57}$$

where the summation over $k = 1, 2, 3$ is implied, P_μ and $J_{\mu\nu}$ are generators of the Poincaré group, Λ is the helicity operator, and $[\cdot,\cdot]_+$ denotes the anti-commutator.

The helicity operator Λ commutes with all elements of the Poincaré group, and so, based on Eqs. (7.55)-(7.57), it also commutes with all the conformal generators. This implies that helicity remains unchanged by conformal transformations. Since the singular values of $T^{\lambda\lambda'}$ are unchanged by the unitary conformal transformations, one concludes that all the defined em-chirality measures are conformally invariant.

For any object and its T-matrix, the values of $\chi(T)$, $\chi_c(T)$, and $\vec{\chi}_s(T)$ remain the same, no matter how the object is transformed conformally. Essentially, each $\vec{\chi}_s(T)$ corresponds to a class of objects related through conformal transformations.

Interestingly, a combination of this discussion with the group-theoretical representation of electromagnetic fields suggests that electromagnetic waves maintain their polarization handedness under conformal transformations. This insight, to the best of the author's knowledge, hasn't been discussed previously in the literature.

The fact that the measures of em-chirality are conformally invariant is quite unique. Most physical properties, such as energy, momentum, and mass (except when it's zero), change under conformal transformations. In contrast, the em-chirality measures are invariant under the actions of the whole conformal group. This high level of invariance suggests a special kind of description, that focuses only on information that is inherent to the scatterer.

8 A new description of scattering

Here a novel approach is presented, that describes scattering via a complex-valued function and that is equivalent to the approaches that use operators, like T- and S-matrices.

Consider a monochromatic T-matrix $T^{j_1 m_1 \lambda_1}_{j_2 m_2 \lambda_2}$. Its values are the matrix elements of the operator $T(k)$:

$$T(k) = \sum_{\lambda_1=\pm1} \sum_{j_1=1}^{\infty} \sum_{m_1=-j_1}^{j_1} \sum_{\lambda_2=\pm1} \sum_{j_2=1}^{\infty} \sum_{m_2=-j_2}^{j_2} T^{j_1 m_1 \lambda_1}_{j_2 m_2 \lambda_2}(k) \, |k j_1 m_1 \lambda_1\rangle \langle k j_2 m_2 \lambda_2| \,. \tag{8.1}$$

This operator acts in the spaces of irreducible representations of the 3D Euclidean group [15], with representations labeled with helicity $\lambda = \pm 1$ and a wave number k. Since the Poincaré group contains the 3D Euclidean group, most of the properties of the representations coincide. One difference between kets $|kjm\lambda\rangle$ (written the same for both groups) is that in the Poincaré group k labels basis vectors inside a representation, while in the Euclidean group k labels whole representation spaces. This implies the normalization for the Poincaré group to be

$$\langle kjm\lambda | k' j' m' \lambda \rangle = \frac{1}{k} \delta(k - k') \delta_{jj'} \delta_{mm'}, \tag{8.2}$$

while the normalization of kets in the Euclidean group is

$$\langle kjm\lambda | kj' m' \lambda \rangle = \delta_{jj'} \delta_{mm'}. \tag{8.3}$$

Setting $k = k'$ in Eq. (8.2) produces infinity $\delta(0)$ which is not present in Eq. (8.3). Normalization from Eq. (8.3) is used throughout this chapter. The rules for translation, rotation, parity, as well as for change between angular momentum and plane wave basis are the same in spaces of irreducible representations for both groups.

The idea of the presented method is to decompose T into the actions of the suitable symmetry group. For the monochromatic T-matrix, this is the 3D Euclidean group extended with parity, and for the polychromatic T-matrix, this would be the Poincaré group extended with parity. Here, the monochromatic case is investigated. The decomposition inside each irreducible representation is to be found in the following form:

$$\boxed{T = \int dg \, f(g) \, U(g),} \tag{8.4}$$

where $U(g)$ is the action of the group element and $f(g)$ is the coefficient of the decomposition and dg is the invariant measure on the group manifold. In the current case, the group is

the 3D Euclidean group extended with parity. The decomposition of the monochromatic T-matrix is searched in the form

$$T(k) = \sum_{\lambda=\pm1} \int d\boldsymbol{a} \int d\Omega\, f_0^{k\lambda}(\boldsymbol{a},\Omega)\bar{T}(\boldsymbol{a})R(\Omega) + \sum_{\lambda=\pm1} \int d\boldsymbol{a} \int d\Omega\, f_1^{k\lambda}(\boldsymbol{a},\Omega)\bar{T}(\boldsymbol{a})R(\Omega)I_s, \tag{8.5}$$

with translation operator $\bar{T}(\boldsymbol{a})$, where bar is used to avoid confusion with the T-matrix T and $\boldsymbol{a}$ is the vector of translation. $R(\Omega) = R(\alpha,\beta,\gamma)$ is the rotation operator and I_s is the parity operator. For notational brevity, three Euler angles are parametrized with $\Omega = (\alpha,\beta,\gamma)$, and

$$\int d^3\Omega \coloneqq \int_0^{2\pi} d\alpha \int_{-1}^{1} d(\cos\theta) \int_0^{2\pi} d\gamma. \tag{8.6}$$

The parity operator in the decomposition Eq. (8.5) is required to account for the ability of the scatterer to change the polarization handedness of the incident field since no rotation or translation can change it. This decomposition will be connected to the operator, written in the form

$$T(k) = \sum_{\lambda=\pm1} \sum_{j_1=1}^{\infty} \sum_{m_1=-j_1}^{j_1} \sum_{j_2=1}^{\infty} \sum_{m_2=-j_2}^{j_2} T^{j_1m_1\lambda}_{j_2m_2\lambda}(k)\, |kj_1m_1\lambda\rangle \langle kj_2m_2\lambda| \tag{8.7}$$

$$+ \sum_{\lambda=\pm1} \sum_{j_1=1}^{\infty} \sum_{m_1=-j_1}^{j_1} \sum_{j_2=1}^{\infty} \sum_{m_2=-j_2}^{j_2} T^{j_1m_1\lambda}_{j_2m_2-\lambda}(k)\, |kj_1m_1\lambda\rangle \langle kj_2m_2-\lambda|, \tag{8.8}$$

which separates it into a part that preserves the helicity of the incident field and a part that changes it.

The decomposition coefficients $f_0^{k\lambda}(\boldsymbol{a},\Omega)$, $f_0^{k\lambda}(\boldsymbol{a},\Omega)$ in Eq. (8.5) are called scattering functions and it will be shown that they are bijectively connected to the matrix elements $T^{j_1m_1\lambda}_{j_2m_2\lambda}(k)$ and $T^{j_1m_1\lambda}_{j_2m_2-\lambda}(k)$, correspondingly. This follows from a generalization of the Peter-Weyl theorem to the 3D Euclidean group, which is proven in the next section. It consists of the orthogonality and completeness of irreducible functions

$$\langle kj_1m_1\lambda|\bar{T}(\boldsymbol{a})R(\Omega)|kj_2m_2\lambda\rangle \equiv [\bar{T}(\boldsymbol{a})R(\Omega)]^{kj_1m_1\lambda}_{kj_2m_2\lambda}. \tag{8.9}$$

Here k and λ hold a special place since they are labels of the irreducible representations and not of the basis vectors like j and m. The latter can be changed by the actions of the Euclidean group, while k and λ can not.

The orthogonality property will be proven to be

$$\frac{1}{(2\pi)^4} \int d^3\boldsymbol{a} \int d^3\Omega\, [\bar{T}(\boldsymbol{a})R(\Omega)]^{kj_1m_1\lambda}_{kj_2m_2\lambda}\, [\bar{T}(\boldsymbol{a})R(\Omega)]^{k'j_1'm_1'\lambda'*}_{k'j_2'm_2'\lambda'} = \frac{1}{k^2}\delta(k-k')\delta_{\lambda\lambda'}\delta_{j_1j_1'}\delta_{m_1m_1'}\delta_{j_2j_2'}\delta_{m_2m_2'} \tag{8.10}$$

while the completeness statement is

$$\boxed{\int_0^\infty dk\, k^2 \sum_{\lambda=-\infty}^{\infty} \sum_{j_1=|\lambda|}^{\infty} \sum_{m_1=-j_1}^{j_1} \sum_{j_2=|\lambda|}^{\infty} \sum_{m_2=-j_2}^{j_2} [\bar{T}(\boldsymbol{a})R(\Omega)]^{kj_1m_1\lambda}_{kj_2m_2\lambda} [\bar{T}(\boldsymbol{a}')R(\Omega')]^{kj_1m_1\lambda *}_{kj_2m_2\lambda} = (2\pi)^4 \delta^{(3)}(\boldsymbol{a}-\boldsymbol{a}')\delta^{(3)}(\Omega-\Omega').} \tag{8.11}$$

The statements follow from the action of the group in the irreducible representation spaces [14]:

$$\langle kj_1m_1\lambda|R(\Omega)|kj_2m_2\lambda\rangle = \delta_{j_1j_2} D^{j_2}_{m_1m_2}(\Omega) \tag{8.12}$$

$$\langle kj_1m_1\lambda|\bar{T}_z(a)|kj_2m_2\lambda\rangle = \delta_{m_1m_2}\sqrt{\frac{2j_1+1}{2j_2+1}} \sum_{l=|j_2-j_1|}^{j_2+j_1} (2l+1)(-i)^l j_l(ak) C^{j_2m_2}_{j_1m_2,l0} C^{j_2\lambda}_{j_1\lambda,l0}, \tag{8.13}$$

with $\bar{T}(\boldsymbol{a}) = R(\hat{\boldsymbol{a}})\bar{T}_z(a)R^\dagger(\hat{\boldsymbol{a}})$.

8.1 Orthogonality in E_3

The proof of orthogonality starts with integration over the Euler angles Ω:

$$\begin{aligned}
&\frac{1}{(2\pi)^4}\int d^3\boldsymbol{a}\int d^3\Omega\, [\bar{T}(\boldsymbol{a})R(\Omega)]^{kj_1m_1\lambda}_{kj_2m_2\lambda} [\bar{T}(\boldsymbol{a})R(\Omega)]^{k'j_1'm_1'\lambda'*}_{k'j_2'm_2'\lambda'} \\
&= \frac{1}{(2\pi)^4}\sum_{jj'mm'}\int d^3\boldsymbol{a}\int d^3\Omega\, \bar{T}(\boldsymbol{a})^{kj_1m_1\lambda}_{kjm\lambda} R(\Omega)^{kjm\lambda}_{kj_2m_2\lambda} \bar{T}(\boldsymbol{a})^{k'j_1'm_1'\lambda'*}_{k'j'm'\lambda'} R(\Omega)^{k'j'm'\lambda'*}_{k'j_2'm_2'\lambda'} \\
&= \frac{1}{(2\pi)^4}\sum_{jj'mm'}\int d^3\boldsymbol{a}\int d^3\Omega\, \bar{T}(\boldsymbol{a})^{kj_1m_1\lambda}_{kjm\lambda} \bar{T}(\boldsymbol{a})^{k'j_1'm_1'\lambda'*}_{k'j'm'\lambda'} \delta_{j_2j}\delta_{j_2'j'} D^{j_2}_{mm_2}(\Omega) D^{j_2'}_{m'm_2'}(\Omega)^* \\
&= \frac{1}{(2\pi)^4}\sum_{mm'}\int d^3\boldsymbol{a}\, \bar{T}(\boldsymbol{a})^{kj_1m_1\lambda}_{kj_2m\lambda} \bar{T}(\boldsymbol{a})^{k'j_1'm_1'\lambda'*}_{k'j_2'm'\lambda'} \frac{8\pi^2}{2j_2+1}\delta_{j_2j_2'}\delta_{mm'}\delta_{m_2m_2'} \\
&= \frac{\delta_{j_2j_2'}\delta_{m_2m_2'}}{2\pi^2(2j_2+1)}\sum_m \int d^3\boldsymbol{a}\, \bar{T}(\boldsymbol{a})^{kj_1m_1\lambda}_{kj_2m\lambda} \bar{T}(\boldsymbol{a})^{k'j_1'm_1'\lambda'*}_{k'j_2m\lambda'}.
\end{aligned} \tag{8.14}$$

Here, the orthogonality of Wigner D-matrices was used when integrating over Ω. To evaluate the remaining integral, it is most convenient to switch to the plane wave basis for the translation operator using the connection

$$|kjm\lambda\rangle = \sqrt{\frac{2j+1}{4\pi}}\int_0^{2\pi} d\phi \int_{-1}^{1} d(\cos\theta)\, D^j_{m\lambda}(\phi,\theta,0)^*\, |\boldsymbol{k}\lambda\rangle\,. \tag{8.15}$$

The action of the translation on a plane wave is a multiplication by a complex exponent:

$$\begin{aligned}
&\langle k j_1 m_1 \lambda | \bar{T}(\boldsymbol{a}) | k j_2 m_2 \lambda \rangle = \\
&= \sqrt{\frac{2j_1+1}{4\pi}} \sqrt{\frac{2j_2+1}{4\pi}} \int d^2\hat{\boldsymbol{k}}_1 \int d^2\hat{\boldsymbol{k}}_2 \, D^{j_1}_{m_1\lambda}(\hat{\boldsymbol{k}}_1) D^{j_2}_{m_2\lambda}(\hat{\boldsymbol{k}}_2)^* \, \langle \boldsymbol{k}_1 \lambda | \bar{T}(\boldsymbol{a}) | \boldsymbol{k}_2 \lambda \rangle \\
&= \sqrt{\frac{2j_1+1}{4\pi}} \sqrt{\frac{2j_2+1}{4\pi}} \int d^2\hat{\boldsymbol{k}}_1 \int d^2\hat{\boldsymbol{k}}_2 \, D^{j_1}_{m_1\lambda}(\hat{\boldsymbol{k}}_1) D^{j_2}_{m_2\lambda}(\hat{\boldsymbol{k}}_2)^* e^{-i\boldsymbol{a}\cdot\boldsymbol{k}_1} \delta^{(2)}(\hat{\boldsymbol{k}}_1 - \hat{\boldsymbol{k}}_2) \\
&= \sqrt{\frac{2j_1+1}{4\pi}} \sqrt{\frac{2j_2+1}{4\pi}} \int d^2\hat{\boldsymbol{k}} \, D^{j_1}_{m_1\lambda}(\hat{\boldsymbol{k}}) D^{j_2}_{m_2\lambda}(\hat{\boldsymbol{k}})^* e^{-i\boldsymbol{a}\cdot\boldsymbol{k}}.
\end{aligned} \tag{8.16}$$

The integral from Eq. (8.14) becomes, using orthogonality of complex exponentials:

$$\begin{aligned}
&\int d^3\boldsymbol{a} \, \bar{T}(\boldsymbol{a})^{k j_1 m_1 \lambda}_{k j_2 m \lambda} \, \bar{T}(\boldsymbol{a})^{k' j_1' m_1' \lambda' *}_{k' j_2 m \lambda'} = \sqrt{\frac{2j_1+1}{4\pi}} \sqrt{\frac{2j_2+1}{4\pi}} \sqrt{\frac{2j_1'+1}{4\pi}} \sqrt{\frac{2j_2+1}{4\pi}} \\
&\quad \times \int d^3\boldsymbol{a} \int d^2\hat{\boldsymbol{k}} \, D^{j_1}_{m_1\lambda}(\hat{\boldsymbol{k}}) D^{j_2}_{m\lambda}(\hat{\boldsymbol{k}})^* e^{-i\boldsymbol{a}\cdot\boldsymbol{k}} \int d^2\hat{\boldsymbol{k}}' \, D^{j_1'}_{m_1'\lambda'}(\hat{\boldsymbol{k}}')^* D^{j_2}_{m\lambda'}(\hat{\boldsymbol{k}}') e^{i\boldsymbol{a}\cdot\boldsymbol{k}'} \\
&= \frac{2j_2+1}{4\pi} \sqrt{\frac{2j_1+1}{4\pi}} \sqrt{\frac{2j_1'+1}{4\pi}} \int d^2\hat{\boldsymbol{k}} \, D^{j_1}_{m_1\lambda}(\hat{\boldsymbol{k}}) D^{j_2}_{m\lambda}(\hat{\boldsymbol{k}})^* \\
&\quad \times \int d^2\hat{\boldsymbol{k}}' \, D^{j_1'}_{m_1'\lambda'}(\hat{\boldsymbol{k}}')^* D^{j_2}_{m\lambda'}(\hat{\boldsymbol{k}}') (2\pi)^3 \delta^{(3)}(\boldsymbol{k} - \boldsymbol{k}') \\
&= \frac{\pi}{2k^2} \delta(k - k') (2j_2+1) \sqrt{2j_1+1} \sqrt{2j_1'+1} \int d^2\hat{\boldsymbol{k}} \, D^{j_1}_{m_1\lambda}(\hat{\boldsymbol{k}}) D^{j_2}_{m\lambda}(\hat{\boldsymbol{k}})^* \, D^{j_1'}_{m_1'\lambda'}(\hat{\boldsymbol{k}})^* D^{j_2}_{m\lambda'}(\hat{\boldsymbol{k}}).
\end{aligned} \tag{8.17}$$

The remaining integral of four Wigner D-functions can be computed via reduction to the integral over three Wigner D-functions. In general,

$$\begin{aligned}
&\int d^3\Omega \, D^{j_1}_{m_1 n_1}(\Omega) D^{j_2}_{m_2 n_2}(\Omega) D^{j_3}_{m_3 n_3}(\Omega) D^{j_4}_{m_4 n_4}(\Omega) = \\
&= \sum_J (2J+1)(-1)^{-m_1-m_2-n_1-n_2} \begin{pmatrix} j_1 & j_2 & J \\ m_1 & m_2 & -m_1-m_2 \end{pmatrix} \begin{pmatrix} j_1 & j_2 & J \\ n_1 & n_2 & -n_1-n_2 \end{pmatrix} \\
&\quad \times \int d^3\Omega \, D^{J}_{m_1+m_2, n_1+n_2}(\Omega) D^{j_3}_{m_3 n_3}(\Omega) D^{j_4}_{m_4 n_4}(\Omega) \\
&= 8\pi^2 \sum_J (2J+1)(-1)^{-m_1-m_2-n_1-n_2} \begin{pmatrix} j_1 & j_2 & J \\ m_1 & m_2 & -m_1-m_2 \end{pmatrix} \begin{pmatrix} j_1 & j_2 & J \\ n_1 & n_2 & -n_1-n_2 \end{pmatrix} \\
&\quad \times \begin{pmatrix} j_3 & j_4 & J \\ m_3 & m_4 & -m_3-m_4 \end{pmatrix} \begin{pmatrix} j_3 & j_4 & J \\ n_3 & n_4 & -n_3-n_4 \end{pmatrix}.
\end{aligned} \tag{8.18}$$

Applying this idea to the integral in Eq. (8.17) gives

$$\begin{aligned}
&\int d^2\hat{\boldsymbol{k}}\, D^{j_2}_{m\lambda'}(\hat{\boldsymbol{k}}) D^{j_2}_{m\lambda}(\hat{\boldsymbol{k}})^*\, D^{j_1}_{m_1\lambda}(\hat{\boldsymbol{k}})\, D^{j_1'}_{m_1'\lambda'}(\hat{\boldsymbol{k}})^* = \\
&= (-1)^{m-\lambda}(-1)^{m_1'-\lambda'} \int d^2\hat{\boldsymbol{k}}\, D^{j_2}_{m\lambda'}(\hat{\boldsymbol{k}}) D^{j_2}_{-m-\lambda}(\hat{\boldsymbol{k}}) D^{j_1}_{m_1\lambda}(\hat{\boldsymbol{k}}) D^{j_1'}_{-m_1'-\lambda'}(\hat{\boldsymbol{k}}) \qquad (8.19)\\
&= (-1)^{m-\lambda}(-1)^{m_1'-\lambda'} 4\pi \sum_J (2J+1)(-1)^{-\lambda'+\lambda} \begin{pmatrix} j_2 & j_2 & J \\ m & -m & 0 \end{pmatrix} \begin{pmatrix} j_2 & j_2 & J \\ \lambda' & -\lambda & -\lambda'+\lambda \end{pmatrix} \\
&\quad \times \begin{pmatrix} j_1 & j_1' & J \\ m_1 & -m_1' & -m_1+m_1' \end{pmatrix} \begin{pmatrix} j_1 & j_1' & J \\ \lambda & -\lambda' & -\lambda+\lambda' \end{pmatrix}. \qquad (8.20)
\end{aligned}$$

Here, the fact that the sum of all second lower indices in Eq. (8.19) vanishes, $\lambda-\lambda+\lambda'-\lambda' = 0$, allows one to apply the formula analogous to Eq. (8.18) (this can be seen by writing it in terms of small Wigner D-matrices). Ultimately, the sum of Eq. (8.20) over m is of interest (see Eq. (8.14)). Using

$$\sum_m (-1)^m \begin{pmatrix} j_2 & j_2 & J \\ m & -m & 0 \end{pmatrix} = (-1)^{j_2}\sqrt{2j_2+1}\,\delta_{J0} \qquad (8.21)$$

one proceeds, taking into account selection rules for the Wigner 3j-symbols:

$$\begin{aligned}
&\sum_m \int d^2\hat{\boldsymbol{k}}\, D^{j_2}_{m\lambda'}(\hat{\boldsymbol{k}}) D^{j_2}_{m\lambda}(\hat{\boldsymbol{k}})^*\, D^{j_1}_{m_1\lambda}(\hat{\boldsymbol{k}})\, D^{j_1'}_{m_1'\lambda'}(\hat{\boldsymbol{k}})^* = \\
&= 4\pi\,\delta_{\lambda\lambda'}\delta_{j_1j_1'}\delta_{m_1m_1'}(-1)^{m_1}(-1)^{j_2}\sqrt{2j_2+1} \begin{pmatrix} j_2 & j_2 & 0 \\ \lambda & -\lambda & 0 \end{pmatrix} \begin{pmatrix} j_1 & j_1 & 0 \\ m_1 & -m_1 & 0 \end{pmatrix} \begin{pmatrix} j_1 & j_1 & 0 \\ \lambda & -\lambda & 0 \end{pmatrix} \\
&= 4\pi\,\delta_{\lambda\lambda'}\delta_{j_1j_1'}\delta_{m_1m_1'}(-1)^{m_1}(-1)^{j_2}\sqrt{2j_2+1}\frac{(-1)^{j_2-\lambda}}{\sqrt{2j_2+1}}\frac{(-1)^{j_1-m_1}}{\sqrt{2j_1+1}}\frac{(-1)^{j_1-\lambda}}{\sqrt{2j_1+1}} \\
&= \delta_{\lambda\lambda'}\delta_{j_1j_1'}\delta_{m_1m_1'}\frac{4\pi}{2j_1+1}, \qquad (8.22)
\end{aligned}$$

where in the second step the identity

$$\begin{pmatrix} j & j & 0 \\ m & -m & 0 \end{pmatrix} = \frac{(-1)^{j-m}}{\sqrt{2j+1}} \qquad (8.23)$$

was used.

Finally, the substitution of Eq. (8.22) into Eq. (8.17) and into Eq. (8.14) gives

$$\begin{aligned}
&\frac{1}{(2\pi)^4}\int d^3\boldsymbol{a} \int d^3\Omega\, [\bar{T}(\boldsymbol{a})R(\Omega)]^{kj_1m_1\lambda}_{kj_2m_2\lambda}\, [\bar{T}(\boldsymbol{a})R(\Omega)]^{k'j_1'm_1'\lambda'*}_{k'j_2'm_2'\lambda'} \\
&= \frac{\delta_{j_2j_2'}\delta_{m_2m_2'}}{2\pi^2(2j_2+1)}\frac{\pi}{2k^2}\delta(k-k')(2j_2+1)\sqrt{2j_1+1}\sqrt{2j_1'+1}\delta_{\lambda\lambda'}\delta_{j_1j_1'}\delta_{m_1m_1'}\frac{4\pi}{2j_1+1} \\
&= \frac{1}{k^2}\delta(k-k')\delta_{\lambda\lambda'}\delta_{j_1j_1'}\delta_{j_2j_2'}\delta_{m_1m_1'}\delta_{m_2m_2'} \qquad (8.24)
\end{aligned}$$

8.2 Completeness in E_3

This section is devoted to the proof of the formula

$$\sum_{\lambda=-\infty}^{\infty}\int_0^\infty dk\,k^2\sum_{j_1=|\lambda|}^{\infty}\sum_{m_1=-j_1}^{j_1}\sum_{j_2=|\lambda|}^{\infty}\sum_{m_2=-j_2}^{j_2}[\bar{T}(\boldsymbol{a})R(\Omega)]^{kj_1m_1\lambda}_{kj_2m_2\lambda}\,[\bar{T}(\boldsymbol{a}')R(\Omega')]^{kj_1m_1\lambda *}_{kj_2m_2\lambda}$$
$$=(2\pi)^4\delta^{(3)}(\boldsymbol{a}-\boldsymbol{a}')\delta^{(3)}(\Omega-\Omega'). \quad (8.25)$$

As in the previous section, it is convenient to use the plane wave basis

$$|kjm\lambda\rangle=\sqrt{\frac{2j+1}{4\pi}}\int_0^{2\pi}d\phi\int_{-1}^{1}d(\cos\theta)\,D^j_{m\lambda}(\phi,\theta,0)^*\,|\boldsymbol{k}\lambda\rangle\,, \quad (8.26)$$

since the action of the translation on a plane wave is just a multiplication by an exponent:

$$\begin{aligned}\langle kj_1m_1\lambda|\bar{T}(\boldsymbol{a})R(\Omega)|kj_2m_2\lambda\rangle&=\sqrt{\frac{2j_1+1}{4\pi}}\int d^2\hat{\boldsymbol{k}}_1\,D^{j_1}_{m_1\lambda_1}(\hat{\boldsymbol{k}}_1)\,\langle\boldsymbol{k}_1\lambda|\bar{T}(\boldsymbol{a})R(\Omega)|kj_2m_2\lambda\rangle\\&=\sqrt{\frac{2j_1+1}{4\pi}}\int d^2\hat{\boldsymbol{k}}_1\,D^{j_1}_{m_1\lambda_1}(\hat{\boldsymbol{k}}_1)\,e^{i\boldsymbol{a}\cdot\boldsymbol{k}_1}\,\langle\boldsymbol{k}_1\lambda|R(\Omega)|kj_2m_2\lambda\rangle\,,\end{aligned} \quad (8.27)$$

with $|\boldsymbol{k}_1|=k$. The left hand side of Eq. (8.25) then becomes

$$\begin{aligned}&\sum_\lambda\int_0^\infty dk\,k^2\sum_{j_1m_1}\sum_{j_2m_2}[\bar{T}(\boldsymbol{a})R(\Omega)]^{kj_1m_1\lambda}_{kj_2m_2\lambda}\,[\bar{T}(\boldsymbol{a}')R(\Omega')]^{kj_1m_1\lambda *}_{kj_2m_2\lambda}=\\&=\sum_\lambda\int_0^\infty dk\,k^2\sum_{j_1m_1}\sum_{j_2m_2}\frac{2j_1+1}{4\pi}\int d^2\hat{\boldsymbol{k}}_1\,D^{j_1}_{m_1\lambda_1}(\hat{\boldsymbol{k}}_1)e^{i\boldsymbol{a}\cdot\boldsymbol{k}_1}\,\langle\boldsymbol{k}_1\lambda|R(\Omega)|kj_2m_2\lambda\rangle\\&\quad\times\int d^2\hat{\boldsymbol{k}}'_1\,D^{j_1}_{m_1\lambda_1}(\hat{\boldsymbol{k}}'_1)^*e^{-i\boldsymbol{a}'\cdot\boldsymbol{k}'_1}\,\langle\boldsymbol{k}'_1\lambda|R(\Omega')|kj_2m_2\lambda\rangle^*\\&=\sum_\lambda\int_0^\infty dk\,k^2\sum_{j_2m_2}\int d^2\hat{\boldsymbol{k}}_1\,e^{i\boldsymbol{a}\cdot\boldsymbol{k}_1}\,\langle\boldsymbol{k}_1\lambda|R(\Omega)|kj_2m_2\lambda\rangle\,e^{-i\boldsymbol{a}'\cdot\boldsymbol{k}_1}\,\langle\boldsymbol{k}_1\lambda|R(\Omega')|kj_2m_2\lambda\rangle^*\\&=\int d^3\boldsymbol{k}_1\,e^{i(\boldsymbol{a}-\boldsymbol{a}')\cdot\boldsymbol{k}_1}\sum_\lambda\sum_{j_2m_2}\langle\boldsymbol{k}_1\lambda|R(\Omega)|kj_2m_2\lambda\rangle\,\langle\boldsymbol{k}_1\lambda|R(\Omega')|kj_2m_2\lambda\rangle^*\,,\end{aligned} \quad (8.28)$$

where the completeness of Wigner D-matrices was used to eliminate the integration over $\hat{\boldsymbol{k}}_2$. Now, the summation part is written completely in the angular momentum basis, and

the completeness of Wigner D-matrices is applied once again:

$$\begin{aligned}
&\sum_{\lambda}\sum_{j_2 m_2} \langle \boldsymbol{k}_1\lambda|R(\Omega)|kj_2m_2\lambda\rangle \, \langle \boldsymbol{k}_1\lambda|R(\Omega')|kj_2m_2\lambda\rangle^* = \\
&= \sum_{\lambda}\sum_{j_2 m_2}\sum_{jm}\sum_{j'm'} \frac{2j+1}{4\pi} D^{j}_{m\lambda}(\hat{\boldsymbol{k}}_1)^* D^{j'}_{m'\lambda}(\hat{\boldsymbol{k}}_1) \, \langle kjm\lambda|R(\Omega)|kj_2m_2\lambda\rangle \, \langle kj'm'\lambda|R(\Omega')|kj_2m_2\lambda\rangle^* \\
&= \sum_{\lambda}\sum_{j_2 m_2}\sum_{mm'} \frac{2j+1}{4\pi} D^{j_2}_{m\lambda}(\hat{\boldsymbol{k}}_1)^* D^{j_2}_{m'\lambda}(\hat{\boldsymbol{k}}_1) D^{j_2}_{mm_2}(\Omega) D^{j_2}_{m'm_2}(\Omega')^* \\
&= \sum_{\lambda}\sum_{j_2 m_2} \frac{2j+1}{4\pi} [R^{-1}(\hat{\boldsymbol{k}}_1)R(\Omega')]^{j_2}_{\lambda m_2} [R^{-1}(\hat{\boldsymbol{k}}_1)R(\Omega')]^{j_2 *}_{\lambda m_2} \\
&= \sum_{\lambda}\sum_{j_2 m_2} \frac{2j+1}{4\pi} D^{j_2}_{\lambda m_2}(\boldsymbol{\Gamma}) D^{j_2 *}_{\lambda m_2}(\boldsymbol{\Gamma}') = 2\pi\, \delta^{(3)}(\boldsymbol{\Gamma}-\boldsymbol{\Gamma}').
\end{aligned} \tag{8.29}$$

Here, the fact was used that the composition of two rotations is another rotation:

$$R(\boldsymbol{\Gamma}) \coloneqq R^{-1}(\hat{\boldsymbol{k}}_1)R(\Omega) \tag{8.30}$$

$$R(\boldsymbol{\Gamma}') \coloneqq R^{-1}(\hat{\boldsymbol{k}}_1)R(\Omega'), \tag{8.31}$$

Since the Dirac delta $\delta^{(3)}(\boldsymbol{\Gamma}-\boldsymbol{\Gamma}')$ is defined with respect to the measure that is invariant under rotations, Eq. (8.31) allows to write it as

$$\delta^{(3)}(\boldsymbol{\Gamma}-\boldsymbol{\Gamma}') = \delta^{(3)}(\Omega-\Omega') \tag{8.32}$$

Returning to Eq. (8.28) gives the final result:

$$\begin{aligned}
&\sum_{\lambda=-\infty}^{\infty} \int_0^{\infty} dk\, k^2 \sum_{j_1=|\lambda|}^{\infty} \sum_{m_1=-j_1}^{j_1} \sum_{j_2=|\lambda|}^{\infty} \sum_{m_2=-j_2}^{j_2} [\bar{T}(\boldsymbol{a})R(\Omega)]^{kj_1m_1\lambda}_{kj_2m_2\lambda} [\bar{T}(\boldsymbol{a}')R(\Omega')]^{kj_1m_1\lambda *}_{kj_2m_2\lambda} = \\
&= \int d^3\boldsymbol{k}_1\, e^{i(\boldsymbol{a}-\boldsymbol{a}')\cdot\boldsymbol{k}_1}\, 2\pi\, \delta^{(3)}(\Omega-\Omega') \\
&= (2\pi)^4 \delta^{(3)}(\boldsymbol{a}-\boldsymbol{a}')\delta^{(3)}(\Omega-\Omega').
\end{aligned} \tag{8.33}$$

8.3 Scattering function

Now, one is ready to decompose the T-matrix into the actions of the group. The proven orthogonality and completeness relations allow to introduce the projector formula

$$|kj_1m_1\lambda\rangle \, \langle kj_2m_2\lambda| = \frac{1}{(2\pi)^4} \int d^3\boldsymbol{a} \int d^3\Omega \, [\bar{T}(\boldsymbol{a})R(\Omega)]^{kj_1m_1\lambda *}_{kj_2m_2\lambda} \, \bar{T}(\boldsymbol{a})R(\Omega), \tag{8.34}$$

which is then used to re-write the T-operator as

$$\begin{aligned}
&\sum_{\lambda=\pm1}\sum_{j_1=1}^{\infty}\sum_{m_1=-j_1}^{j_1}\sum_{j_2=1}^{\infty}\sum_{m_2=-j_2}^{j_2} T^{j_1m_1\lambda}_{j_2m_2\lambda}(k)\,|kj_1m_1\lambda\rangle\,\langle kj_2m_2\lambda| \\
&= \sum_{\lambda=\pm1}\sum_{j_1=1}^{\infty}\sum_{m_1=-j_1}^{j_1}\sum_{j_2=1}^{\infty}\sum_{m_2=-j_2}^{j_2} T^{j_1m_1\lambda}_{j_2m_2\lambda}(k)\frac{1}{(2\pi)^4}\int d^3\boldsymbol{a}\int d^3\Omega\,[\bar{T}(\boldsymbol{a})R(\Omega)]^{kj_1m_1\lambda*}_{kj_2m_2\lambda}\,\bar{T}(\boldsymbol{a})R(\Omega) \\
&= \frac{1}{(2\pi)^4}\int d^3\boldsymbol{a}\int d^3\Omega\sum_{\lambda=\pm1}\sum_{j_1=1}^{\infty}\sum_{m_1=-j_1}^{j_1}\sum_{j_2=1}^{\infty}\sum_{m_2=-j_2}^{j_2} T^{j_1m_1\lambda}_{j_2m_2\lambda}(k)[\bar{T}(\boldsymbol{a})R(\Omega)]^{kj_1m_1\lambda*}_{kj_2m_2\lambda}\,\bar{T}(\boldsymbol{a})R(\Omega) \\
&= \sum_{\lambda=\pm1}\int d^3\boldsymbol{a}\int d^3\Omega\, f_0^{\lambda k}(\boldsymbol{a},\Omega)\,R(\Omega)\bar{T}(\boldsymbol{a}),
\end{aligned} \tag{8.35}$$

with

$$\begin{aligned}
f_0^{\lambda k}(\boldsymbol{a},\Omega) &= \frac{1}{(2\pi)^4}\sum_{j_1=1}^{\infty}\sum_{m_1=-j_1}^{j_1}\sum_{j_2=1}^{\infty}\sum_{m_2=-j_2}^{j_2} T^{j_1m_1\lambda}_{j_2m_2\lambda}(k)[\bar{T}(\boldsymbol{a})R(\Omega)]^{kj_1m_1\lambda*}_{kj_2m_2\lambda} \\
&= \frac{1}{(2\pi)^4}\mathrm{Tr}\big[T^{\lambda\lambda}(k)R^{\dagger}(\Omega)\bar{T}^{\dagger}(\boldsymbol{a})\big],
\end{aligned} \tag{8.36}$$

where Tr stands for the trace of the matrix. Analogically, the part of the T-matrix that changes helicity of the incident field may be decomposed as:

$$\begin{aligned}
&\sum_{\lambda=\pm1}\sum_{j_1=1}^{\infty}\sum_{m_1=-j_1}^{j_1}\sum_{j_2=1}^{\infty}\sum_{m_2=-j_2}^{j_2} T^{j_1m_1\lambda}_{j_2m_2-\lambda}(k)\,|kj_1m_1\lambda\rangle\,\langle kj_2m_2-\lambda| \\
&= \sum_{\lambda=\pm1}\sum_{j_1=1}^{\infty}\sum_{m_1=-j_1}^{j_1}\sum_{j_2=1}^{\infty}\sum_{m_2=-j_2}^{j_2} T^{j_1m_1\lambda}_{j_2m_2-\lambda}(k)(-1)^{j_2}\,|kj_1m_1\lambda\rangle\,\langle kj_2m_2\lambda|\,I_s \\
&= \frac{1}{(2\pi)^4}\int d^3\boldsymbol{a}\int d^3\Omega\sum_{\lambda=\pm1}\sum_{j_1=1}^{\infty}\sum_{m_1=-j_1}^{j_1}\sum_{j_2=1}^{\infty}\sum_{m_2=-j_2}^{j_2} T^{j_1m_1\lambda}_{j_2m_2-\lambda}(k)(-1)^{j_2} \\
&\quad\times[\bar{T}(\boldsymbol{a})R(\Omega)]^{kj_1m_1\lambda*}_{kj_2m_2\lambda}\,\bar{T}(\boldsymbol{a})R(\Omega)I_s \\
&= \sum_{\lambda=\pm1}\int d^3\boldsymbol{a}\int d^3\Omega\, f_1^{\lambda k}(\boldsymbol{a},\Omega)\,R(\Omega)\bar{T}(\boldsymbol{a})I_s,
\end{aligned} \tag{8.37}$$

with

$$\begin{aligned}
f_1^{\lambda k}(\boldsymbol{a},\Omega) &= \frac{1}{(2\pi)^4}\sum_{j_1=1}^{\infty}\sum_{m_1=-j_1}^{j_1}\sum_{j_2=1}^{\infty}\sum_{m_2=-j_2}^{j_2} T^{j_1m_1\lambda}_{j_2m_2-\lambda}(k)(-1)^{j_2}[\bar{T}(\boldsymbol{a})R(\Omega)]^{kj_1m_1\lambda*}_{kj_2m_2\lambda} \\
&= \frac{1}{(2\pi)^4}\mathrm{Tr}\big[T^{\lambda,-\lambda}(k)\,I_s\,R^{\dagger}(\Omega)\bar{T}^{\dagger}(\boldsymbol{a})\big].
\end{aligned} \tag{8.38}$$

Completeness and orthogonality relations ensure that the T-matrix $T^{j_1 m_1 \lambda_1}_{j_2 m_2 \lambda_2}(k)$ is bijectively connected to the scattering function $f_s^{\lambda k}(\Omega, \boldsymbol{a})$. Since the T-matrix contains the complete information that can be extracted from the object through light-matter interactions, the scattering function contains this information as well. The fact that its domain consists of geometrical parameters such as distances $\boldsymbol{a}$ and angles Ω may suggest an easier access to the geometrical properties and symmetries of the object, compared to the description via the T-matrix.

It should be noted that the scattering function of the S-matrix is almost identical to the one computed from the T-matrix. Since both operators are connected via $S = \mathbb{1} + T$, it is enough to know the representation of the identity operator $\mathbb{1}$ in terms of the group actions. This is a trivial question, since by definition the identity is represented via a single point on the group manifold: the origin with $\boldsymbol{a} = \boldsymbol{0}$ and $\Omega = (0, 0, 0)$. This means that both versions of the scattering function, of the T- and of the S-operators, only differ in this single point.

It is convenient to discuss the physical meaning of the scattering function within the S-matrix formalism. In particular, Eqs. (8.35) and (8.37) suggest the following intuitive understanding. Consider an incoming and an outgoing field in one scattering process. If both the incoming and the outgoing fields were regular fields (with the same wave functions), then the sums in Eqs. (8.35) and (8.37) would decompose the regularized outgoing field as a sum of many transformed (rotated, translated and reflected) versions of the regularized incoming field. Remarkable is, that the set of such transformations depends only on the object and is the same for all pairs or incoming and outgoing fields. There are enough transformations in this set to combine many transformed versions of the incoming field, producing the correct outgoing field. Of course, this is possible due to the fact that there are infinite ways of transforming one regular field into another one.

An illustration of the scattering function for a concrete object is given in Fig. (8.1). The scatterer consists of three silicon spheres with radius 50 nm placed at points $[0, 0, a]$, $[0, -a, 0]$ and $[0, 0, -a]$, with $a = 500$ nm. The scattering function f_0^{+k} is computed via Eq. (8.36) from the corresponding T-matrix at wavelength 500 nm and $j_{\max} = 9$.

One may observe that the slice of the scattering function $f_0^{+k}(0, y, z, \pi, \pi, 0)$ with $k = \frac{2\pi}{500 \text{ nm}}$ reflects the geometry of the cluster in the zy-plane, up to the scaling by 2. Here, the choice of the slice at $\alpha = \pi$, $\beta = \pi$, $\gamma = 0$ is necessary to regain the geometric information in the zy-plane, which follows from the transformation properties of the scattering function.

To discuss the transformation properties of the scattering function, consider the transformation of both sides of Eq. (8.4) with some group element $\tilde{g}$:

$$
\begin{aligned}
U(\tilde{g}) T U^{-1}(\tilde{g}) &= U(\tilde{g}) \int dg\, f(g)\, U(g) U^{-1}(\tilde{g}) \\
&= \int dg\, f(g)\, U(\tilde{g}) U(g) U^{-1}(\tilde{g}) && (8.39) \\
&= \int dg\, f(g)\, U(\tilde{g} g \tilde{g}^{-1}) && (8.40) \\
&= \int dg\, f(\tilde{g}^{-1} g\, \tilde{g})\, U(g) && (8.41)
\end{aligned}
$$

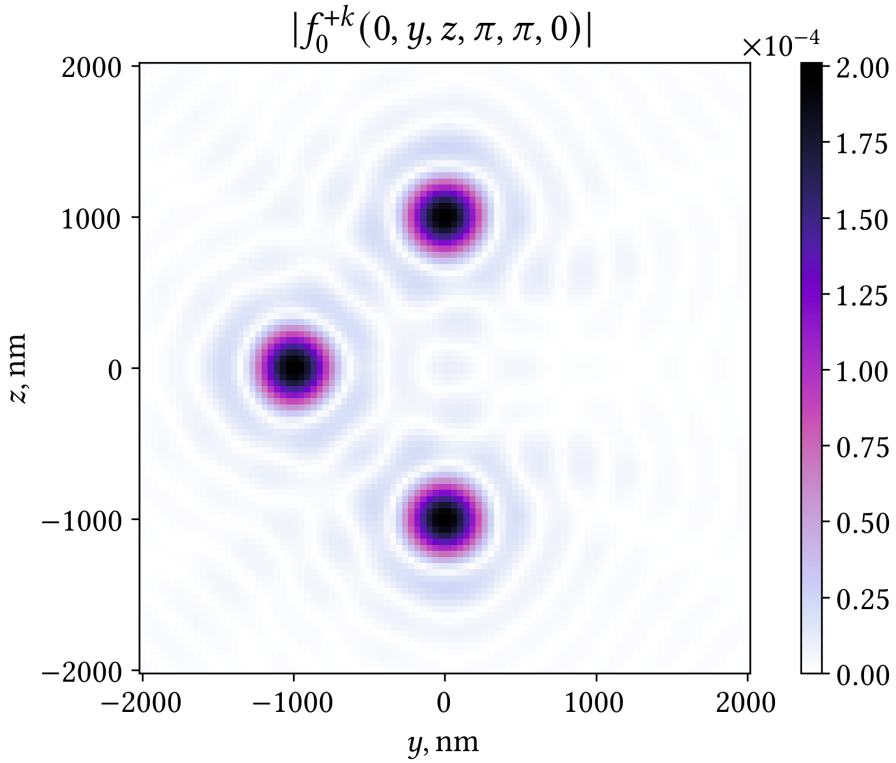

Figure 8.1: Scattering function of three silicon spheres with radii $r = 50$ nm. The slice of the scattering function at specific parameters $x = 0$, $\alpha = \pi$, $\beta = \pi$, $\gamma = 0$ allows to restore the geometric position of the spheres in the given plane, up to the scaling by 2.

where we first used the definition of U as a representation of the group, and the fact that dg is the invariant measure of the group manifold — when substituting $\tilde{g}^{-1}g\tilde{g}$. This leads to the following transformation law of the scattering function under the action of the group element $\tilde{g}$:

$$\boxed{\tilde{f}(g) = f(\tilde{g}^{-1}g\,\tilde{g})} \tag{8.42}$$

To apply this general formula to monochromatic scattering, the defining product rule of the 3D Euclidean group is required. The product of two elements, $g_1 = (\boldsymbol{a}, \Omega)$ and $g_2 = (\boldsymbol{b}, \Gamma)$ follows from [14, p.167]:

$$\begin{aligned}
\bar{T}(\boldsymbol{a})R(\Omega)\bar{T}(\boldsymbol{b})R(\Gamma) &= \bar{T}(\boldsymbol{a})R(\Omega)\bar{T}(\boldsymbol{b})R(\Gamma) && (8.43)\\
&= \bar{T}(\boldsymbol{a})R(\Omega)\bar{T}(\boldsymbol{b})R^{-1}(\Omega)R(\Omega)R(\Gamma) && (8.44)\\
&= \bar{T}(\boldsymbol{a})\bar{T}(R(\Omega)\boldsymbol{b})R(\Omega)R(\Gamma) && (8.45)\\
&= \bar{T}(\boldsymbol{a} + R(\Omega)\boldsymbol{b})R(\Phi), && (8.46)
\end{aligned}$$

where $R(\Omega)\boldsymbol{b}$ stands for the rotated vector $\boldsymbol{b}$ in 3D space, via the well-known rotation rule in 3D. The angles Φ solve $R(\Phi) = R(\Omega)R(\Gamma)$.

Now consider the product in Eq. (8.42), with pure translation of the scattering function by $\boldsymbol{x}$, with $\tilde{g} = (\boldsymbol{b}, \boldsymbol{0})$, while the argument of the scattering function is general $g = (\boldsymbol{a}, \Omega)$. One can show using Eq. (8.46) that

$$f(\tilde{g}^{-1}g\,\tilde{g}) = f(\boldsymbol{a} + R(\Omega)\boldsymbol{b} - \boldsymbol{b}, \Omega). \tag{8.47}$$

This translation formula has a particular property: if angular arguments of the scattering function Ω are such that $R(\Omega)\boldsymbol{b} - \boldsymbol{b} = -2\boldsymbol{b}$, then the translation of the object will be reflected in the translation of the object's scattering function, scaled by 2:

$$\tilde{f}(\boldsymbol{a}, \Omega) = f(\boldsymbol{a} - 2\boldsymbol{b}, \Omega) \tag{8.48}$$

In the zy-plane, the property $R(\Omega)\boldsymbol{b} - \boldsymbol{b} = -2\boldsymbol{b}$ is fulfilled by angles $\Omega = (\pi, \pi, 0)$.

One way to understand why this specific slice of the scattering function restores the particle's positions is as follows: if spheres inside a cluster are sufficiently from each other, their global T-matrix can be roughly approximated as the sum of their separate T-matrices, disregarding their mutual interactions. Given the additivity of the scattering function in the domain of operators, the scattering function for such a cluster can be approximated by summing the scattering functions of individual spheres, each translated from the origin by the corresponding displacement. Eq. (8.48) then provides the observed geometric pattern.

While this argument is relevant for clusters of distant objects, the fact that the scattering function contains complete information about an object's properties in light-matter interactions suggests new potential for extracting such information from general objects as well. At this point, two promising avenues for further explorations emerge. The first is the application of the scattering function in imaging and inverse design. The second concerns progress toward a deeper understanding of the Rayleigh hypothesis: the scattering function has successfully predicted the shape of a cluster within the encompassing sphere of the cluster, an area inaccessible to T- and S-matrix formalisms.

9 Conclusion and outlook

Here, the main contributions are discussed, together with potential directions for further scientific advancements that they enable.

9.1 Polychromatic T-matrix

Chapter 4 introduced a new definition for multipolar basis fields, achieved by focusing on the unitarity behavior of their transformations under the symmetry group of 4D space-time. This led to the unification of incoming, outgoing, and regular fields, allowing to use the same scalar product across all three types of fields. Additionally, it was demonstrated that incoming, outgoing, and regular fields undergo identical transformations under Lorentz boosts. The matrix element of the Lorentz boost in the multipolar basis was derived. These theoretical developments allowed to introduce the polychromatic T-matrix formalism in Chapter 5. Such formalism provides a substantial extension of the well-established monochromatic T-matrix method, now enabling the account of interactions between electromagnetic pulses and matter, as well as the description of linear scattering scenarios involving coupling of frequencies.

In Chapter 6, the polychromatic T-matrix method was applied to numerical simulations of light-matter interactions involving an electromagnetic pulse and an object. The transfer of energy and momentum between the pulse and the object was computed, considering scenarios where the object is both at rest and in constant uniform relativistic motion. The latter calculations were performed in both the laboratory frame and the co-moving frame of reference, demonstrating the generality the method.

9.2 Chirality signature

In Chapter 7, a longstanding problem of chirality analysis was solved within the context of light-matter interactions: how to continuously differentiate between any pair of enantiomers? A concept called chirality signature was introduced, which manifests as an infinite-dimensional pseudovector continuously defined on the set of T-matrices. It is zero if and only if the object is electromagnetically achiral, and any two versions of a chiral object have opposite chiral signatures. The proposed quantity provides a complete description of electromagnetic chirality, capturing its entire infinite-dimensional nature and allowing to consistently distinguish each member in any pair of enantiomers. It has been proven that the chirality signature, alongside complex and scalar electromagnetic chirality measures, remains invariant under the actions of the conformal group. Historically, exploring concepts of invariance and symmetry has been crucial in expanding our understanding of

physics. The chirality signature's complete, continuous, and conformally invariant nature makes it a unique tool for exploring chirality and its practical applications, for example in the dynamics of chirality evolution in chemical reactions.

The practical effectiveness of the chirality signature is limited by the knowledge of the object's T-matrix. Nevertheless, its existence proves that there are more efficient theoretical ways of extracting information about the chirality of objects than approaches that utilize conventional quantities such as optical activity, which may be negligible even for highly chiral materials.

9.3 Scattering function

In Chapter 8, a novel approach to the description of linear light-matter interactions was proposed. It consists in representing the action of a scatterer as a sum of symmetry transformations. The coefficient of this decomposition, named the scattering function, is defined on the symmetry group manifold and is bijectively connected to the T-matrix. It was shown that the values of the scattering function may reflect the positions of the objects inside a cluster. The observation presented in that chapter opens avenues for novel ways of extracting information from objects in light-matter interaction. Currently, two primary directions of development emerge. The first concerns the utilization of the scattering function in imaging and the inverse design of objects. The second promises advances in understanding of the Rayleigh hypothesis, since the scattering function, unlike the T-matrix, is not limited by the sphere circumscribing the object.

9.4 Applicability outside of electromagnetism

It is suitable to discuss the possible extension of all introduced methods to the scattering with other kinds of waves: gravitational waves, and phonons. Application of the methods to the case of gravitational waves of linearized general relativity is straightforward, since gravitational waves are, as electromagnetic waves, massless and possess two polarization modes [57, §35.4, §35.6]. The difference lies in the values of helicity $\lambda = \pm 2$, which assigns them to the massless irreducible representations of the Poincaré group labeled with $\lambda = \pm 2$. Therefore, gravitational scattering admits a similar group-theoretical treatment as the electromagnetic case, up to the change in helicity values.

On the other hand, applying these methods in the context of chiral phonons [58, 59, 60, 61, 62] and mechanical chiral metamaterials [63, 64] is more complicated and warrants additional research. A notable difference to the electromagnetic scattering is the presence of both transverse and longitudinal polarizations. While transverse waves can be associated with positive and negative helicity modes, longitudinal waves have helicity $\lambda = 0$, which is not present in the electromagnetic case. Consequently, an extension of group-theoretical methods in this direction offers promising avenues for future research.

Bibliography

[1] P.C. Waterman. "Matrix formulation of electromagnetic scattering". In: *Proceedings of the IEEE* 53.8 (1965), pp. 805–812. DOI: 10.1109/PROC.1965.4058.

[2] Gérard Gouesbet. "T-matrix methods for electromagnetic structured beams: A commented reference database for the period 2014–2018". In: *Journal of Quantitative Spectroscopy and Radiative Transfer* 230 (2019), pp. 247–281. ISSN: 0022-4073. DOI: https://doi.org/10.1016/j.jqsrt.2019.04.004. URL: https://www.sciencedirect.com/science/article/pii/S0022407319301608.

[3] Michael I. Mishchenko. "Comprehensive thematic T-matrix reference database: a 2017-2019 update". In: *Journal of Quantitative Spectroscopy and Radiative Transfer* 242 (2020), p. 106692. ISSN: 0022-4073. DOI: https://doi.org/10.1016/j.jqsrt.2019.106692. URL: https://www.sciencedirect.com/science/article/pii/S0022407319307381.

[4] Dominik Theobald et al. "Plane-wave coupling formalism for T-matrix simulations of light scattering by nonspherical particles". In: *Phys. Rev. A* 96 (3 Sept. 2017), p. 033822. DOI: 10.1103/PhysRevA.96.033822. URL: https://link.aps.org/doi/10.1103/PhysRevA.96.033822.

[5] Amos Egel et al. "Extending the applicability of the T-matrix method to light scattering by flat particles on a substrate via truncation of sommerfeld integrals". In: *Journal of Quantitative Spectroscopy and Radiative Transfer* 202 (2017), pp. 279–285. ISSN: 0022-4073. DOI: https://doi.org/10.1016/j.jqsrt.2017.08.016. URL: https://www.sciencedirect.com/science/article/pii/S0022407317305939.

[6] Torleif Martin. "T-matrix method for closely adjacent obstacles". In: *Journal of Quantitative Spectroscopy and Radiative Transfer* 234 (2019), pp. 40–46. ISSN: 0022-4073. DOI: https://doi.org/10.1016/j.jqsrt.2019.06.001. URL: https://www.sciencedirect.com/science/article/pii/S002240731930278X.

[7] D. Schebarchov et al. "Mind the gap: testing the Rayleigh hypothesis in T-matrix calculations with adjacent spheroids". In: *Opt. Express* 27.24 (Nov. 2019), pp. 35750–35760. DOI: 10.1364/OE.27.035750. URL: https://opg.optica.org/oe/abstract.cfm?URI=oe-27-24-35750.

[8] Tom Rother and Stuart C. Hawkins. "Notes on Rayleigh's hypothesis and the extended boundary condition method". In: *The Journal of the Acoustical Society of America* 149.4 (Apr. 2021), pp. 2179–2188. ISSN: 0001-4966. DOI: 10.1121/10.0003958. eprint: https://pubs.aip.org/asa/jasa/article-pdf/149/4/2179/13039192/2179_1_online.pdf. URL: https://doi.org/10.1121/10.0003958.

[9] J. Barkhan, M. Ganesh, and S.C. Hawkins. "Approximation of radiating waves in the near-field: Error estimates and application to a class of inverse problems". In: *Journal of Computational and Applied Mathematics* 401 (2022), p. 113769. ISSN: 0377-0427. DOI: https://doi.org/10.1016/j.cam.2021.113769. URL: https://www.sciencedirect.com/science/article/pii/S0377042721003915.

[10] Aristeidis G. Lamprianidis, Carsten Rockstuhl, and Ivan Fernandez-Corbaton. "Transcending the Rayleigh Hypothesis with multipolar sources distributed across the topological skeleton of a scatterer". In: *Journal of Quantitative Spectroscopy and Radiative Transfer* 296 (2023), p. 108455. ISSN: 0022-4073. DOI: https://doi.org/10.1016/j.jqsrt.2022.108455. URL: https://www.sciencedirect.com/science/article/pii/S0022407322003909.

[11] Amol Ashok Ambardekar and Yong-qing Li. "Optical levitation and manipulation of stuck particles with pulsed optical tweezers". In: *Opt. Lett.* 30.14 (July 2005), pp. 1797–1799. DOI: 10.1364/OL.30.001797. URL: https://opg.optica.org/ol/abstract.cfm?URI=ol-30-14-1797.

[12] C. D. Stanciu et al. "All-Optical Magnetic Recording with Circularly Polarized Light". In: *Phys. Rev. Lett.* 99 (4 July 2007), p. 047601. DOI: 10.1103/PhysRevLett.99.047601. URL: https://link.aps.org/doi/10.1103/PhysRevLett.99.047601.

[13] Heinrich Bech and Alfred Leder. "Simultaneous determination of particle size and refractive index by time-resolved Mie scattering". In: *Optik* 121.20 (2010), pp. 1815–1823. ISSN: 0030-4026. DOI: https://doi.org/10.1016/j.ijleo.2009.05.022. URL: https://www.sciencedirect.com/science/article/pii/S0030402609002216.

[14] Wu-Ki Tung. *Group theory in physics*. World Scientific, 1985.

[15] Bo Peterson and Staffan Ström. "T-matrix for electromagnetic scattering from an arbitrary number of scatterers and representations of E(3)". In: *Physical review D* 8.10 (1973), p. 3661.

[16] E. Wigner. "On Unitary Representations of the Inhomogeneous Lorentz Group". In: *Annals of Mathematics* 40.1 (1939), pp. 149–204. ISSN: 0003486X. URL: http://www.jstor.org/stable/1968551 (visited on 05/15/2023).

[17] Leonard Gross. "Norm Invariance of Mass-Zero Equations under the Conformal Group". In: *Journal of Mathematical Physics* 5.5 (1964), pp. 687–695.

[18] Iwo Bialynicki Birula and Zofia Bialynicka Birula. *Quantum Electrodynamics*. Pergamon, Jan. 1975.

[19] Ivan Fernandez-Corbaton and Carsten Rockstuhl. "Unified theory to describe and engineer conservation laws in light-matter interactions". In: *Phys. Rev. A* 95 (5 May 2017), p. 053829. DOI: 10.1103/PhysRevA.95.053829. URL: https://link.aps.org/doi/10.1103/PhysRevA.95.053829.

[20] Harry E. Moses. "Photon Wave Functions and the Exact Electromagnetic Matrix Elements for Hydrogenic Atoms". In: *Phys. Rev. A* 8 (4 Oct. 1973), pp. 1710–1721. DOI: 10.1103/PhysRevA.8.1710. URL: https://link.aps.org/doi/10.1103/PhysRevA.8.1710.

[21] Maxim Vavilin and Ivan Fernandez-Corbaton. “The polychromatic T-matrix”. In: *Journal of Quantitative Spectroscopy and Radiative Transfer* 314 (2024), p. 108853. ISSN: 0022-4073. DOI: https://doi.org/10.1016/j.jqsrt.2023.108853. URL: https://www.sciencedirect.com/science/article/pii/S0022407323003710.

[22] Chintha Chamalie Handapangoda, Malin Premaratne, and Pubudu N. Pathirana. “Plane wave scattering by a spherical di-electric particle in motion: a relativistic extension of the Mie theory”. In: *Progress in Electromagnetics Research-pier* 112 (2011), pp. 349–379. URL: https://api.semanticscholar.org/CorpusID:53382811.

[23] Timothy J. Garner et al. “Time-domain electromagnetic scattering by a sphere in uniform translational motion”. In: *J. Opt. Soc. Am. A* 34.2 (Feb. 2017), pp. 270–279. DOI: 10.1364/JOSAA.34.000270. URL: https://opg.optica.org/josaa/abstract.cfm?URI=josaa-34-2-270.

[24] Gerhard Kristensson. *Scattering of Electromagnetic Waves by Obstacles*. Electromagnetic Waves. Institution of Engineering and Technology, 2016. URL: https://digital-library.theiet.org/content/books/ew/sbew524e.

[25] P. A. Martin. *Time-Domain Scattering*. Encyclopedia of Mathematics and its Applications. Cambridge University Press, 2021. DOI: 10.1017/9781108891066.

[26] Ivan Fernandez-Corbaton, Martin Fruhnert, and Carsten Rockstuhl. “Objects of Maximum Electromagnetic Chirality”. In: *Phys. Rev. X* 6 (3 July 2016), p. 031013. DOI: 10.1103/PhysRevX.6.031013. URL: https://link.aps.org/doi/10.1103/PhysRevX.6.031013.

[27] Noham Weinberg and Kurt Mislow. “On chirality measures and chirality properties”. In: *Canadian Journal of Chemistry* 78.1 (2000), pp. 41–45. DOI: 10.1139/v99-223. eprint: https://doi.org/10.1139/v99-223. URL: https://doi.org/10.1139/v99-223.

[28] D. Avnir Y.Pinto. “A Generalized handedness strategy: addressing latent handedness in chiral structures”. In: *Enantiomer* 6 (2001), pp. 211–217.

[29] Ernst Ruch. “Algebraic aspects of the chirality phenomenon in chemistry”. In: *Accounts of Chemical Research* 5.2 (1972), pp. 49–56. DOI: 10.1021/ar50050a002. eprint: https://doi.org/10.1021/ar50050a002. URL: https://doi.org/10.1021/ar50050a002.

[30] John David Jackson. *Classical Electrodynamics*. New York City: Wiley, 1998.

[31] D. A. Varshalovich, A. N. Moskalev, and V. K. Khersonskii. *Quantum Theory of Angular Momentum*. WORLD SCIENTIFIC, 1988. DOI: 10.1142/0270. eprint: https://www.worldscientific.com/doi/pdf/10.1142/0270. URL: https://www.worldscientific.com/doi/abs/10.1142/0270.

[32] Steven Weinberg. *The Quantum Theory of Fields (Volume 1)*. 1st ed. Cambridge University Press, June 1995. ISBN: 0521550017. URL: http://www.amazon.com/exec/obidos/redirect?tag=citeulike07-20%5C&path=ASIN/0521550017.

[33] Ya. B. Zeldovich. “Number of quanta as an invariant of the classical electromagnetic field”. In: *Dokl. Acad. Sci. USSR* 163 (1965). (in Russian), p. 1359.

[34] H. Bateman. "The Conformal Transformations of a Space of Four Dimensions and Their Applications to Geometrical Optics". In: *Proceedings of the London Mathematical Society* s2-7.1 (1909), pp. 70–89. DOI: https://doi.org/10.1112/plms/s2-7.1.70. URL: https://londmathsoc.onlinelibrary.wiley.com/doi/abs/10.1112/plms/s2-7.1.70.

[35] Claude Cohen-Tannoudji, Jacques Dupont-Roc, and Gilbert Grynberg. *Photons and Atoms: Introduction to Quantum Electrodynamics*. Wiley, 1989.

[36] Rafael de la Madrid. "The role of the rigged Hilbert space in quantum mechanics". In: *European Journal of Physics* 26.2 (Feb. 2005), p. 287. DOI: 10.1088/0143-0807/26/2/008. URL: https://dx.doi.org/10.1088/0143-0807/26/2/008.

[37] H. E. Moses. "Transformation from a Linear Momentum to an Angular Momentum Basis for Particles of Zero Mass and Finite Spin". In: *Journal of Mathematical Physics* 6.6 (1965), pp. 928–940. DOI: 10.1063/1.1704353. eprint: https://doi.org/10.1063/1.1704353. URL: https://doi.org/10.1063/1.1704353.

[38] X. Garcia Santiago et al. "Decomposition of scattered electromagnetic fields into vector spherical wave functions on surfaces with general shapes". In: *Phys. Rev. B* 99 (4 Jan. 2019), p. 045406. DOI: 10.1103/PhysRevB.99.045406. URL: https://link.aps.org/doi/10.1103/PhysRevB.99.045406.

[39] Michael I Mishchenko, Larry D Travis, and Andrew A Lacis. *Scattering, absorption, and emission of light by small particles*. Cambridge university press, 2002.

[40] Maxim Vavilin, Carsten Rockstuhl, and Ivan Fernandez-Corbaton. "The electromagnetic scalar product in spatially-bounded domains". In: *preparation* (2023).

[41] R.C. Wittmann. "Spherical wave operators and the translation formulas". In: *IEEE Transactions on Antennas and Propagation* 36.8 (1988), pp. 1078–1087. DOI: 10.1109/8.7220.

[42] David Colton and Rainer Kress. *Inverse acoustic and electromagnetic scattering theory*. Vol. 93. New York: Springer Science & Business Media, 2012.

[43] Edward D Palik. *Handbook of optical constants of solids*. Academic press, 1998.

[44] Dominik Beutel et al. "Efficient simulation of biperiodic, layered structures based on the T-matrix method". In: *JOSA B* 38.6 (2021), pp. 1782–1791.

[45] Dominik Beutel, Ivan Fernandez-Corbaton, and Carsten Rockstuhl. "Unified lattice sums accommodating multiple sublattices for solutions of the Helmholtz equation in two and three dimensions". In: *Phys. Rev. A* 107 (1 Jan. 2023), p. 013508. DOI: 10.1103/PhysRevA.107.013508. URL: https://link.aps.org/doi/10.1103/PhysRevA.107.013508.

[46] Nathaniel du Preez-Wilkinson et al. "Forces due to pulsed beams in optical tweezers: linear effects". In: *Opt. Express* 23.6 (Mar. 2015), pp. 7190–7208. DOI: 10.1364/OE.23.007190. URL: https://opg.optica.org/oe/abstract.cfm?URI=oe-23-6-7190.

[47] Leonardo A. Ambrosio, Jhonas O. de Sarro, and Gérard Gouesbet. “An approach for a polychromatic generalized Lorenz–Mie theory”. In: *Journal of Quantitative Spectroscopy and Radiative Transfer* 312 (2024), p. 108824. ISSN: 0022-4073. DOI: https://doi.org/10.1016/j.jqsrt.2023.108824. URL: https://www.sciencedirect.com/science/article/pii/S0022407323003424.

[48] Maxim Vavilin and Ivan Fernandez-Corbaton. “Multidimensional measures of electromagnetic chirality and their conformal invariance”. In: *New Journal of Physics* 24.3 (Mar. 2022), p. 033022. DOI: 10.1088/1367-2630/ac57e8. URL: https://dx.doi.org/10.1088/1367-2630/ac57e8.

[49] John C. Gower and Garmt B. Dijksterhuis. *Procrustes problems*. Oxford University Press on Demand, 2004.

[50] Marcus Carlsson. “von Neumann’s trace inequality for Hilbert–Schmidt operators”. In: *Expositiones Mathematicae* 39.1 (2021), pp. 149–157.

[51] Philipp Gutsche et al. “Role of Geometric Shape in Chiral Optics”. In: *Symmetry* 12.1 (2020). ISSN: 2073-8994. DOI: 10.3390/sym12010158. URL: https://www.mdpi.com/2073-8994/12/1/158.

[52] Paul Mezey. “Rules on chiral and achiral molecular transformations”. In: *Journal of Mathematical Chemistry* 17 (June 1995), pp. 185–202. DOI: 10.1007/BF01164847.

[53] Noham Weinberg and Kurt Mislow. “On chiral pathways in E(n): A dimensional analysis”. In: *Theoretica Chimica Acta* 95.3 (1997), pp. 63–65.

[54] Riccardo Sapienza. “Photonic nano materials: anisotropic transport and optical Bloch oscillations”. PhD thesis. Université Pierre et Marie Curie - Paris VI, Feb. 7, 2005. URL: https://tel.archives-ouvertes.fr/tel-00009751/document (visited on 04/09/2015).

[55] Robert Gilmore. *Lie groups, Lie algebras, and some of their applications*. Courier Corporation, 2012.

[56] V. I. Fushchich and A. G. Nikitin. “Conformal invariance of relativistic equations for arbitrary spin particles”. In: *Letters in Mathematical Physics* 2.6 (Nov. 1978), pp. 471–475.

[57] Charles W. Misner, Kip S. Thorne, and John Archibald Wheeler. *Gravitation*. San Francisco: W.H. Freeman, 1973. ISBN: 0716703343 9780716703341 0716703440 9780716703440.

[58] Lifa Zhang and Qian Niu. “Angular Momentum of Phonons and the Einstein–de Haas Effect”. In: *Phys. Rev. Lett.* 112 (8 Feb. 2014), p. 085503. DOI: 10.1103/PhysRevLett.112.085503. URL: https://link.aps.org/doi/10.1103/PhysRevLett.112.085503.

[59] Mengnan Gao, Wei Zhang, and Lifa Zhang. “Nondegenerate Chiral Phonons in Graphene/Hexagonal Boron Nitride Heterostructure from First-Principles Calculations”. In: *Nano Letters* 18.7 (July 2018), pp. 4424–4430. DOI: 10.1021/acs.nanolett.8b01487.

[60] Hanyu Zhu et al. "Observation of chiral phonons". In: *Science* 359.6375 (2018), pp. 579–582. DOI: 10.1126/science.aar2711. eprint: https://www.science.org/doi/pdf/10.1126/science.aar2711. URL: https://www.science.org/doi/abs/10.1126/science.aar2711.

[61] Hao Chen et al. "Propagating Chiral Phonons in Three-Dimensional Materials". In: *Nano Letters* 21.7 (2021). PMID: 33764075, pp. 3060–3065. DOI: 10.1021/acs.nanolett.1c00236. eprint: https://doi.org/10.1021/acs.nanolett.1c00236. URL: https://doi.org/10.1021/acs.nanolett.1c00236.

[62] Yi Chen et al. "Cubic metamaterial crystal supporting broadband isotropic chiral phonons". In: *Phys. Rev. Materials* 5 (2 Feb. 2021), p. 025201. DOI: 10.1103/PhysRevMaterials.5.025201. URL: https://link.aps.org/doi/10.1103/PhysRevMaterials.5.025201.

[63] Muamer Kadic et al. "3D metamaterials". In: *Nature Reviews Physics* 1.3 (Mar. 2019), pp. 198–210.

[64] Yi Chen, Muamer Kadic, and Martin Wegener. "Chiral triclinic metamaterial crystals supporting isotropic acoustical activity and isotropic chiral phonons". In: *Proceedings of the Royal Society A: Mathematical, Physical and Engineering Sciences* 477.2246 (2021), p. 20200764. DOI: 10.1098/rspa.2020.0764. eprint: https://royalsocietypublishing.org/doi/pdf/10.1098/rspa.2020.0764. URL: https://royalsocietypublishing.org/doi/abs/10.1098/rspa.2020.0764.